2011

Characterizing Wireless and Powerline Communication Channels with Applications to Smart Grid Networks

Sabih Guzelgoz
University of South Florida, sguzelgo@mail.usf.edu

Characterizing Wireless and Powerline Communication Channels with Applications to Smart Grid Networks

by

Sabih Güzelgöz

A dissertation submitted in partial fulfillment
of the requirements for the degree of
Doctor of Philosophy
Department of Electrical Engineering
College of Engineering
University of South Florida

Major Professor: Hüseyin Arslan, Ph.D.
Miguel A. Labrador, Ph.D.
Wilfrido Moreno, Ph.D.
Koon H. Teo, Ph.D.
Paris Wiley, Ph.D.

Date of Approval:
April 11, 2011

Keywords: Impulsive Noise, OFDM, Powerline Communication Channel Characterization, Smart Grid Communication Environments, Wireless Communication Channel Characterization

DEDICATION

This dissertation is dedicated to my beloved wife, my sister, and my parents for their constant love and support

ACKNOWLEDGEMENTS

I would like to thank my advisor Dr. Hüseyin Arslan for his guidance, encouragement, and continuous support throughout my Ph.D. studies. It has been a privilege to become a part of Dr. Arslan's research group. I thank Dr. Dr. Miguel A. Labrador, Dr. Wilfrido Moreno, Dr. Koon H. Teo, and Dr. Paris Wiley for serving in my committee and for providing me with their valuable remarks. I also want to thank Dr. Aydın K. Sunol for chairing my defense.

I owe much to my friends and seniors: Dr. Mustafa Emin Şahin, Dr. Hisham Mahmoud, Dr. Serhan Yarkan, Dr. Hasari Çelebi, Dr. Tevfik Yücek, Dr. Ismail Güvenç, Ibrahim Demirdöğen, Hasan Basri Çelebi, Tayyar Güzel, Murad Khalid, Omar Zakaria, Ismail Bütün, Jamal Haque, Sadia Ahmed, Ali Görçin, Evren Terzi, Dr. Bahattin Karakaya, Dr. Celal Çeken, Dr. Bilal Babayiğit, Ali Rıza Ekti, Özgür Yürür, Çağatay Talay, Hazar Akı, Alphan Şahin, Memhet Bahadır Çelebi, Murat Karabacak, Ahmed H. Mehanna, Emre Seyyal, Kosol Son, Lokman Akbay, Salih Erdem, Salim Erdem, Şener Gültekin and Mustafa Cenk Ertürk. I learned so many virtues from them. Sincere friendship to start with, unselfishness, tolerance, and helpfulness.

My sincere appreciation goes to my parents and my younger sister for their sacrifice and unconditional support as well as my parents in law and sisters in law. I will always be indebted to them throughout my life.

Last, but by no means least, my deepest gratitude from my heart goes to my wife, Özden, for her love, all the sacrifices she made, her firm support, her vast patience, and her steady encouragement for almost four years now. Finally, I like to extend my gratitude to my unborn kid for adding excitement to the final year of my PhD program.

TABLE OF CONTENTS

LIST OF TABLES

LIST OF FIGURES

ABSTRACT

Smart grid aims at improving the efficiency, reliability, security, and quality of service (QoS) of the current electricity grid by exploiting the advances in communication and information technology. In parallel to size of the electricity grid, smart grid communication infrastructure should cover a very large geographical area that may extend from remote generation sites to densely populated residential regions and inside buildings, homes, and electricity-power-system environments. In such an extensive communication network, different communication technologies operating on different communication medium are likely to coexist. Among the communication technologies available, wireless and power line communication (PLC) based solutions are comparatively attractive especially considering cost of the initial investment required for the realization of a communication network with such an immense size.

In this dissertation, a detailed investigation of wireless and PLC channel characteristics of the smart grid networks is presented. Among the topics discussed are the time variation characteristics of wireless channels, root-mean-squared (RMS) delay spread and path amplitude statistics of PLC channels, and the impact of impulsive noise on orthogonal frequency division multiplexing (OFDM) systems.

CHAPTER 1

INTRODUCTION

Smart grid aims at improving the efficiency, reliability, security, and quality of service (QoS) of the current electricity grid by exploiting the advances in communication and information technology. Objectives of the smart grid require the establishment of a comprehensive communication infrastructure for collecting various types of information regarding electricity generation, consumption, storage, transmission, and distribution. In parallel to size of the electricity grid, smart grid communication infrastructure should cover a very large geographical area that may extend from remote generation sites to densely populated residential regions and inside buildings, homes, and electricity-power-system environments. In such an extensive communication network, different communication technologies operating on different communication medium are likely to coexist. A variety of candidate technologies such as Ethernet, satellite, fiber optic, terrestrial wireless and power line communication (PLC) is available for the smart grid communication infrastructure. Among these, wireless and PLC based solutions are comparatively attractive especially considering cost of the initial investment required for the realization of a communication network with such an immense size. In the establishment of the smart grid communication infrastructure, two approaches can be followed. One of the approaches is based on employing existing communication standards after some modifications by considering the QoS, security, and latency requirements of the smart grid applications, whereas the other strategy relies upon developing novel communication protocols particularly addressing the smart grid communication needs. Regardless of the approaches to be followed, a deep understanding of the communication channels and signal propagation characteristics in smart grid networks is a must prior to the development of optimal communication solutions. Being more favorable

compared to other technologies, emphasis is to be given on wireless and PLC communication channels and their corresponding signal propagation characteristics in the remaining discussions.

A transmit signal goes through various distortions on its way to receiver in both wireless and PLC channels. A variety of parameters is employed while quantifying these distortions in communication channels. In wireless communications, the concept of path loss is used to capture how the power of the transmit signal varies as a function of distance. It is defined as the dB (decibel) value of the ratio of the transmit power to the received power. Presence of the obstacles between transmitter and receiver gives rise to random fluctuations of path loss called shadowing that is usually defined with log-Normal probability density function (PDF) as verified by measurement campaigns over the years. Since variations due to path loss and shadowing take place over relatively large distances, these two variations are traditionally referred to as large-scale propagation effects by wireless communication community. In addition, the drastic changes in the received signal power for short displacements, which are on the order of few wavelengths, are known to be consequences of small-scale effects. The underlying reason behind these drastic changes, which are captured by the notion of path amplitude statistics, is related to the multipath phenomenon and time variation of the wireless communication channel, due to motion in general. Quantification of the small scale effects is achieved with two different parameters that are closely related to multipath propagation and time variation of the wireless channels: delay spread and Doppler spread. A transmit signal can travel to the receiver by following different paths that may involve a variety of propagation mechanisms such as reflection, diffraction, and scattering. Thus, multiple replicas of the original transmit signal arrive at the receiver with different delays. Delay spread describes the extent of the time dispersion of the wireless channel. In connection with the delay spread parameter in time domain, coherence bandwidth, which is inversely proportional to delay spread, is used to describe the channel in the frequency domain revealing the channel's frequency selectivity characteristics. In this respect, time dispersion and frequency selectivity characteristics of a communication channel are analo-

gous to each other. Time variation is another important characteristic of wireless channels. Time variation stems from either mobility of the transmitter-receiver pairs or motion of the reflectors along the propagation path of the transmit signal. Time variation manifests itself in frequency domain as a spectral broadening and Doppler spread is used as a measure to describe the extent of this broadening. Analogous to Doppler spread in frequency domain, coherence time, which is inversely proportional to Doppler spread, describes the time duration over which the wireless channel can be considered time invariant.

In PLC domain, a slightly different terminology is used for defining communication channel characteristics. The relationship between transmit power and received power is captured through the concept of attenuation. Similar to wireless channels, a transmit signal arrives at the receiver by following different paths leading to time dispersion that are mainly governed by a single propagation mechanism, which is reflection mostly as a result of impedance mismatches in the networks seen by the transmit signal along its propagation path. Delay spread and coherence bandwidth are used to describe the extent of time dispersion and frequency selectivity characteristics of PLC channels, respectively. Time variation is also an important attribute of PLC channels. Unlike wireless channels in which time variation is related to motion in general, time variation in PLC channels is classified as long term and short term variations and stems mainly from the varying impedance conditions in the power line network (PLN). Long term variation is related to the continuously varying impedance conditions at termination points as the devices connected to the PLN are switched on/off, whereas short term time variation of the PLC channel stems from the fact that impedance of most electrical loads is dependent on Alternating Current (AC) mains cycle.

Besides distortions caused by the frequency and time selectivity nature of communication channels, noise characteristics are also of paramount importance considering the performance of communication systems. In wireless communication channels, noise is assumed to be additive white Gaussian with a flat power spectrum mainly due to mathematical tractability. However, interference with impulsive nature which is mostly referred to

as "impulsive noise" is also known to exist in certain wireless propagation environments. Major sources of impulsive noise in wireless channels are some devices that we frequently use in our daily lives such as photocopiers, printers, microwave ovens, hair-dryers and etc. Noise structure in PLC channels is relatively more complicated. Background noise in PLC channels that results from the summation of different noise sources of low power present in the network is characterized with power spectrum decreasing with frequency. In addition to colored background noise, narrow band noise that stems from the activities of radio broadcasters is a part of PLC channels. In PLC channels, impulsive noise is considered to be the main source of data errors and electrical appliances connected to the power network are the main reason behind its presence.

1.1 Dissertation Outline

This dissertation discusses several issues regarding wireless and PLC communication channel characteristics of smart grid environments as shown in Fig. 1. Following the introduction (Chapter 1), the flow of the dissertation is given as follows:

- A detailed study of both wireless and PLC channel characteristics of smart grid environments from the aspect of several channel parameters (Chapter 2)
- Investigation of time selectivity nature of wireless communication channels through the use of a reverberation chamber (RVC) (Chapter 3)
- Examination of delay spread and path amplitude characteristics of PLC channels (Chapter 4-5)
- Understanding of bursty impulsive noise in wireless and PLC channels and studying techniques for its mitigation in orthogonal frequency division multiplexing (OFDM) based receivers (Chapter 6)

As can be seen from the dissertation structure, some chapters focus solely on either wireless channel or PLC channel (Chapters 3-4-5), whereas discussions in some other chap-

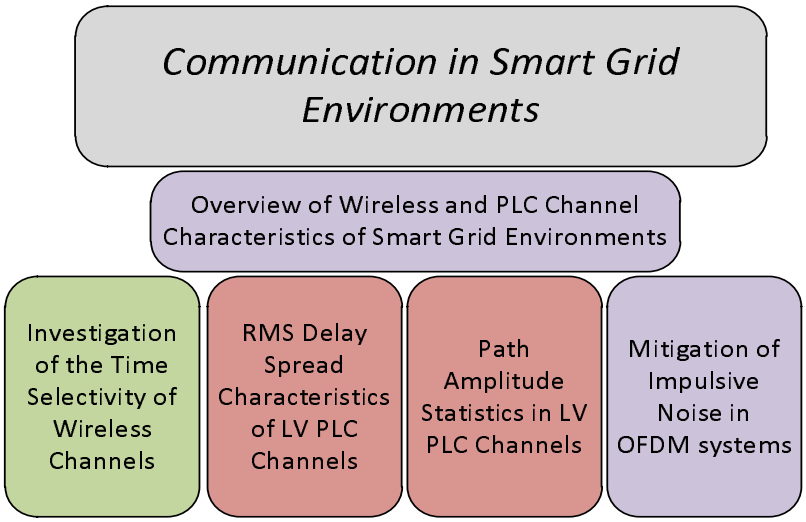

Figure 1.1 Structure of the dissertation.

ters are applicable to both channels (Chapter 2-6). In the remainder of this section, a more detailed outline of each chapter is provided.

1.1.1 Chapter 2: Wireless and PLC Propagation Channel Characteristics for Smart Grid Environments

Wireless, PLC, fiber optic, Ethernet, etc are among the communication technologies on which smart grid communication infrastructure is envisioned to be built as mentioned earlier. Among these, wireless and PLC based solutions are attractive considering the cost of initial deployment. Wireless communication deployment in smart grid covers a variety of environments such as indoor, outdoor, and electric-power-system facilities. Similar diversity is expected in PLC deployment as well covering low voltage (LV), medium voltage (MV), and high voltage (HV) segments of the grid. In spite of being attractive, wireless and PLC channels are very harsh posing great challenges to performance of communication systems. This chapter [1] provides a very detailed description of wireless and PLC channel characteristics of smart grid networks in terms of several parameters such as path loss and

[1] Content of this chapter is published in [1].

attenuation, time dispersion, time selectivity, amplitude statistics, and noise characteristics which are of vital importance considering the communication system performance.

1.1.2 Chapter 3: Investigation of Time Selectivity of Wireless Channels Through the Use of RVC

Smart grid requires a reliable wireless communication infrastructure that should operate in various deployment scenarios either fixed or mobile giving rise to different channel time selectivity characteristics. Expansion of the grid as more renewable energy sources are integrated is likely to lead to unique communication related issues as well. For instance, signal propagation characteristics in renewable energy sites such as wind power generation stations should be studied in depth for either establishing reliable wireless systems in these sites or understanding their impact on existing legacy wireless systems such as radar signals. All of these concerns entail a detailed investigation of the time selectivity characteristics of various propagation environments. This chapter [2] focuses on time selectivity nature of wireless channels by considering two typical mobility scenarios by the use of an RVC: motion of the transmitter or receiver antenna or motion of the surrounding objects both of which are bound to be observed in wireless communication infrastructure of the smart grid networks as will be discussed subsequently. Mobility causes spectral broadening whose impact is generally evaluated through the observation of Doppler spectrum. In this study, investigation of Doppler spectrum characteristics through the use of an RVC and the methods for the purpose of its manipulation are presented. This study verifies that the Doppler spectrum can be manipulated in various ways. However, unless a precise setup is established it is almost impossible to obtain very specific Doppler shapes in RVCs such as widely known Jakes' spectrum. Also, a different interpretation of mobility for wireless channels is given by the use of a new concept called motion intensity. This concept is elaborated in terms of both its technical aspects and its impact on wireless channel characterization.

[2] Content of this chapter is published in [2].

1.1.3 Chapter 4: Articulating Factors Defining RMS Delay Spread in LV PLC Networks

PLC along with wireless is considered to be one of the enabler technologies of smart grid. Its use especially in the LV side of the PLN is drawing considerable attention for some certain applications that involve "demand response" and "energy use monitoring" requiring a bidirectional information flow between smart meters and smart devices. In line with the recently emerging interest which envisions conversion of the power transmission network into a communication network, understanding of the root-mean-squared (RMS) delay spread is essential for multipath PLC channels for the establishment of reliable communication systems. In this chapter [3], factors that play a role on the RMS delay spread value of LV PLC channels are articulated. Among these factors, dependency of the RMS delay spread on attenuation, loading, and physical characteristics of the PLNs is investigated.

1.1.4 Chapter 5: Statistical Characterization of the Paths in Multipath PLC Channels

Following up with Chapter 4, multipath phenomenon lies in the heart of PLC and leads to the reception of multiple replicas of the transmit signal at the receiver through various paths. Statistical knowledge of arriving paths is essential in order to evaluate performance of communication systems. First arriving path is distinguishable from the other paths in the sense that it experiences less reflection and less attenuation along its propagation path, giving it a favorable position regarding detectability. In this chapter [4], statistics of the first arriving path are initially investigated. It is shown that the first arriving path can be defined with log-Normal probability density function. It is seen that the mean of the approximating log-Normal variable decreases with an increasing number of branches between transmitter and receiver while its variance increases. The same finding is also observed when the maximum number of branches that extend out a branching node is increased. Although statistics of the first arriving path are emphasized more, statistical characterization of the

[3] Content of this chapter is published in [3].
[4] Content of this chapter is published in [4].

other paths is discussed as well. Infinite bandwidth assumption in which all paths arriving at the receiver can be resolved is considered in the analysis. However, a brief discussion on the impact of finite bandwidth is given.

1.1.5 Chapter 6: Handling Bursty Impulsive Noise in OFDM

OFDM is recently gaining popularity among both wireless and PLC based smart grid standards such as IEEE 802.15.4g and HomePlug Green. Impulsive noise could be widely available in smart grid networks for both wireless and PLC based deployment options. As a result of the recent technology trend which favors the use of OFDM modulation for a variety of smart grid communication standards, analytical evaluation and mitigation of bursty impulsive noise effects on OFDM signals under the influence of frequency selective communication channel is studied in this chapter [5]. At the first stage of the receiver, samples corrupted with impulsive noise are nulled so that impulsive noise power being spread over the entire OFDM symbol is avoided. Subsequently, two techniques are studied that can be employed in order to further improve the performance of OFDM receiver. First, the performance evaluation of the technique, namely "sample replacement based iterative symbol detection", is given. Next, a technique based on "successive symbol detection" is proposed for mitigating the impact of nulling as a result of bursty impulsive noise. For the cases in which these two techniques may fail to provide sufficient bit error rate (BER) performance, a transmission scheme is introduced. Numerical results show that the proposed algorithms eliminate the impact of bursty impulsive noise successfully.

1.1.6 Other Works Done

Besides the work discussed above, outcomes of some other research and teaching related projects are excluded from the dissertation considering its flow and integrity. Some of these projects are outlined in the following paragraph.

As a part of wireless communication channel characterization efforts, radio propagation characteristics of underground mines are discussed in [6–8]. In line with PLC channel char-

[5] Content of this chapter is published in [5].

acterization efforts, time frequency analysis of noise emitted by electrical devices connected to the PLN is investigated in [9, 10]. Analysis of a multi-channel receiver that is capable of accessing both wireless and PLC channels is given in [11]. Teaching certain courses such as wireless communications or digital communications might be very challenging unless the theoretical materials covered are supported with a practical experience. This is mainly due to the fact that immediate relationship between cause and effect can not be easily seen by the study of pure theory. In this respect, a wireless communication systems laboratory course is discussed in [12–14] along with the experiments designed to teach various wireless communication concepts to the students on a weekly basis, as well as interesting projects and other course requirements. Subsequently, some of these completed (or continuing) works are to be discussed in detail.

1.1.6.1 Analysis of a Multi-Channel Receiver: Wireless and PLC Reception

This study investigates the mutual use of wireless and PLC technologies by employing diversity and its impact on the performance of communication systems. Mutual use of these two technologies has been previously the topic of not many but several publications in the literature. Several scenarios that are based on the convergence of wireless and PLC technologies are considered and analyzed mostly through experimental and measurement based analysis [15–19].

Scarcity of spectrum and interference along with the new concepts introduced such as cognitive radio (CR) [20] are the main motivations behind this study. For instance, CRs are supposed to sense the spectrum and detect white spaces before commencing transmission in order to make sure that they do not cause any harmful interference to primary users. Considering scarcity of available white spaces and the abundance of secondary users for both wireless and PLC environments for future communication applications, the capability of accessing both medium could be of great value for the continuity of reliable communication. In case of the suitability of both mediums for communication, CRs may change their strategies and start using both communication channels in order to become more robust to

fading. In this way, radios also reduce the level of interference to the other radios operating in their vicinity in either wireless or PLC environments by dividing the total power available among the channels. In our analysis, both links are assumed to be available. With the use of both channels, performance of selection combining (SC) and maximal ratio combining (MRC) schemes for an ideal multi-channel receiver is analyzed.

1.1.6.2 Time Frequency Analysis of Noise Generated by Electrical Loads in PLC

Unpredictable characteristics of PLC channels seriously affect the performance of the communication systems. Among these unpredictable characteristics, noise is considered to be the main source of errors in data transmission in PLC systems. Unlike conventional communication systems in which noise is usually modeled as additive white Gaussian noise (AWGN), its definition in PLC channels has a more complicated form. In order to design reliable PLC systems, it is essential to understand the features of noise in PLNs. Since the impulsive noise generated by electrical house appliances is one of the most significant noise types in PLC channel, it is very important to analyze these electrical devices with respect to their noise characteristics. In this study, impulsive noise characteristics of various house appliances are analyzed over the frequency range of 30kHz-50MHz. For instance, Fig. 1.2 shows time-frequency, frequency, and time characteristics of the impulsive noise emitted by a dimmer and a drill into the PLN, respectively.

Each device connected to the PLN has a unique noise structure. This uniqueness can be employed for several smart grid applications. For example, providing statistics of the devices to household is very crucial from the perspective of energy monitoring. In this sense, a smart meter that is designed to process these noise signatures and map them into corresponding device type might be of great help while informing the users about their energy use statistics.

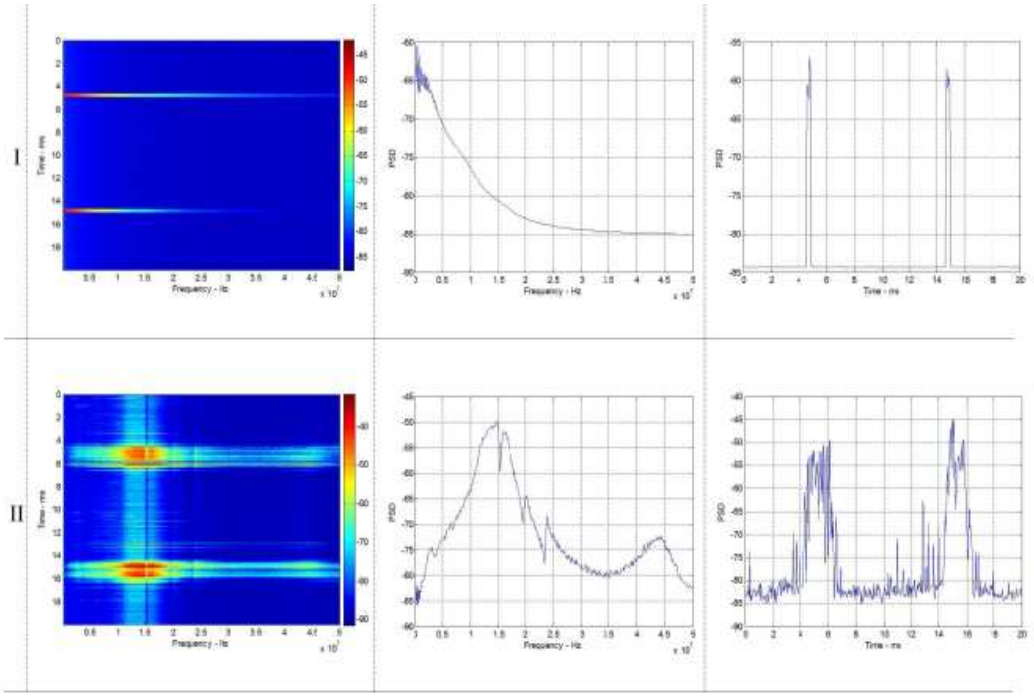

Figure 1.2 Measurement results: I-dimmer and II-drill.

1.1.6.3 Demand Characterization and Estimation for Electric Vehicle Charging Stations

In a power grid that is fitted with additional electrical vehicle (EV) charging stations (CSs), reliability becomes more of a concern since the introduction of EVs could add to the burden of the grid significantly. In order to take preemptive actions to avoid unpredictable power outages or to take corrective actions within the grid itself such as use of renewable energy sources when required, accurate prediction algorithms of power demand should be established. Establishment of the prediction algorithms may only be achieved after understanding the statistical characteristics of the power demand. This study focuses solely on the power demand characteristics of the CSs.

Articulation of statistical characteristics of power demand at the CSs is based on understanding the activities of the EVs at the CSs. Each EV is likely to occupy a CS for a certain duration of time. EVs may continuously draw power from the grid over the entire duration of their parking time or they might be idle (stop drawing power from the grid) for a certain

fraction of time when the batteries are fully charged. In this respect, defining these time related statistics are of paramount importance as the initial step of the investigation. The extent of these durations depend on various factors such as user behavior, battery type, battery size, CS regulations, power supplied at the CS (120V or 240V), floating energy prices, etc. Manipulating these factors in order to shape the power demand and avoid power outages at peak hours or to enhance the performance of power demand prediction algorithms is another objective of the study.

CHAPTER 2

WIRELESS AND PLC PROPAGATION CHANNEL CHARACTERISTICS FOR SMART GRID ENVIRONMENTS

2.1 Introduction

Design principles of the current electricity utility system can be traced back to the late $1800s$ without any fundamental change since then. Utility industry has not been able to sufficiently exploit the advances in communication and information technology so far to improve the electricity grid's efficiency, reliability, security, and quality of service (QoS). Smart grid addresses all of these desired features and more by modernizing the grid with the incorporation of communication and information technologies.

Understanding of the smartness in the term "smart grid" has been rapidly expanded by the industry from smart metering that is more focused on advanced metering infrastructure (AMI)[1] to true smart grid [21]. With this recently endorsed definition, objectives of the smart grid can be summarized as follows [22]:

- achieving active participation of the consumers in the operations of the grid with the support of AMI
- taking advantage of all generation and storage options
- enabling the network with self–healing capability to minimize the impact of power outages on consumers
- achieving resiliency against physical and cyber attacks
- providing good quality of power considering needs of the 21st century

[1] This is sometimes referred to as Smart Grid 1.0.

- enabling new products, services, and markets
- optimizing assets and operating efficiently by minimizing operations and maintenance expenses

Objectives of the smart grid require the collection of various types of information regarding electricity generation, consumption, storage, transmission, and distribution through its communication infrastructure. Considering this requirement, smart grid communication infrastructure should cover a very large geographical area that may extend from remote generation sites to densely populated residential regions and inside buildings, homes, and electricity-power-system environments. Indeed, supervisory control and data acquisition (SCADA) systems have been implemented to monitor and control electricity grid to some extent for some time [23]. However, definition of smart grid clearly necessitates the development of a more complicated two-way communication architecture beyond currently employed relatively insecure SCADA systems for a larger scale monitoring and control.

In order to better understand the communication needs of the smart grid, it might be a good strategy to narrow down the scope and focus only on one of its objectives "integrating customers into the grid" which receives the most attention in terms of planning and investment. The underlying reason for customer integration is to maximize the efficiency of the distribution network by encouraging the customer to react to some type of stimuli coming from the utility. The opportunities with the customer integration includes: 1. providing customers with new pricing options, 2. detecting power outages with automatic verification of restoration, 3. enabling customers to respond to pricing and load control signals, 4. enabling customers to monitor, control, and schedule local energy consumption for maximizing the benefits regarding cost of electricity usage and utilization of the distribution network.

It is obvious that communication in a broader perspective lies in the core of the customer integration. First, a communication infrastructure between home devices and "smart meter" should be set up so that "smart meter" can collect information from the devices and take initiative to adjust the local consumption considering the customer preferences. Second, a communication link between "smart meters" and the utility should be established so

that customers and utility can be bidirectionally notified regarding the real time electricity prices, customer behavior, and power outages. In this respect, the communication environment for the customer integration can be decomposed into three distinct communication networks as illustrated in Fig.2.1: home area network (HAN) for defining the interconnections between devices and the "smart meters", neighborhood area network (NAN) for referring to the interconnections between "smart meters" and "data collection points", wide area network (WAN) for describing the interconnections between "data collection points" and the utility. In all of these networks, a different communication technology based on a different communication medium such as Ethernet, fiber optic, wireless, power line, satellites, etc. can be selected [21, 24–28]. In addition to the selection of a single communication medium, hybrid solutions[2] can also be employed [29]. Focusing only one aspect of smart grid led us to the design of communication systems operating in three different networks most probably with different channel characteristics. Combining other aspects of the smart grid[3] with its complexity and size[4], it is not very difficult to estimate the volume of information flow and the underlying communication infrastructure for its successful realization. Similar diversity is likely to be observed in the communication applications as well with different QoS, latency, and reliability requirements ranging from simple control commands requiring low bandwidth to the transmission of video signals for the surveillance of physical assets requiring relatively larger bandwidth.

Wireless and power line communication (PLC) based solutions are very promising and attractive compared to the other options considering the cost of initial investment required for the smart grid communication infrastructure [27]. While addressing the communication needs of smart grid, two strategies can be followed. One of the approaches is based on integrating existing communication standards (e.g. IEEE 802.11, IEEE 802.15.1, IEEE

[2] "Hybrid" in this context does not mean the use of different technologies within different network segments, rather it refers to the use of different communication technologies within the same network segment when necessary depending upon communication channel characteristics.

[3] For instance, consider communication needs for plugin electric vehicles (PEVs) or in electric-power-system environments, such as transformation substations, power control rooms, bulk generation plants, etc.

[4] The current electricity grid in the U.S. has more than ten thousand transmission substations, two thousand distribution stations, 130 million customers, and 5600 distributed energy facilities [30].

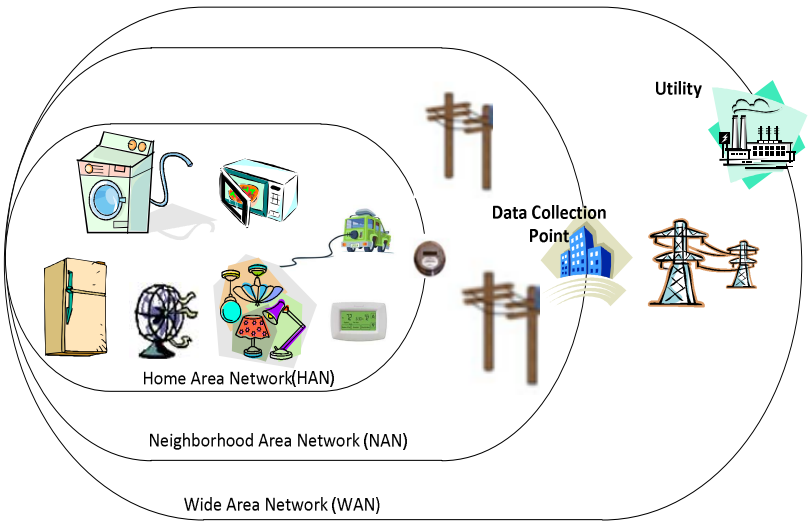

Figure 2.1 Integrating customer with smart grid.

802.15.4, IEEE 802.16, IEEE 802.20, IEEE 1901, HomePlug, etc[5]) into current electricity grid with some modifications regarding QoS, latency, reliability, and power consumption [32–35], whereas the other strategy relies upon developing novel communication protocols particularly addressing the smart grid communication needs based upon the fact that integration of existing communication standards could lead to a performance far below the expectations in a network with such heterogeneity [27, 29, 36]. Some efforts for modifying existing standards considering the requirements of smart grid are already noticeable leading to the emergence of IEEE 802.15.4g [37–39] and HomePlug Green [40][6]. No matter what strategy is followed, channel characteristics of the communication environments in smart grid should be well-known since they are the main determining factor in the ultimate performance of any communication system that is to be deployed. In addition, smart grid may need technologies over time requiring different attributes from today such as larger bandwidth paving the way to the emergence of new communication protocols [41]. It must

[5]Full list of smart grid related standards can be found in [31].

[6]IEEE 802.15.4g defines three physical layer technologies based on frequency shift keying (FSK), offset quadrature phase shift keying (OQPSK), and orthogonal frequency division multiplexing (OFDM) to address different system demands and market segments as well as some medium access control (MAC) layer modifications for lower power consumption. Similarly, HomePlug Green is based on OFDM technology with quadrature phase shift keying (QPSK) modulation for reduced cost of chip design unlike HomePlug AV which supports several modulation schemes up to 1024-quadrature amplitude modulation (QAM) as well as some other modifications for achieving lower power consumption.

also be noted that smart grid communication infrastructure can not be isolated from the advances in the wireless or PLC based communication technologies while seeking communication solutions. Indeed, discussions regarding the use of white spaces in the TV spectrum that advance the state of the art in smart grid communications in a way that requires the design of smart meters with cognitive radio (CR) features already support this provision [42]. Deep understanding of the characteristics of the communication channel is a must prior to developing optimal communication solutions yet again.

In spite of being cost effective solutions for smart grid applications, wireless and PLC environments are very harsh posing great challenges to reliability and performance of communication systems. In this respect, objective of this study is to articulate the channel characteristics of both wireless and PLC channels in smart grid environments in terms of several factors including:

- path loss (or attenuation[7])
- multipath characteristics
  - time dispersion
  - time selectivity
  - channel amplitude statistics
- noise

The remainder of the chapter is organized as follows. Section 2.2 provides a review of propagation mechanisms effective in wireless and PLC environments. Section 2.3 gives the details of wireless communication characteristics of smart grid environments. Details regarding PLC channels are discussed in Section 2.4. Finally, the concluding remarks are given in Section 2.5.

[7] "Attenuation" is a more frequently used term than "path loss" in PLC community.

2.2 Propagation Mechanism

Our discussion starts with the definition of mechanisms that govern the signal propagation within wireless and PLC channels since these propagation mechanisms form the fundamental platform for understanding the channel attributes that are to be discussed subsequently. Although propagation mechanism in wireless communication channels is relatively complex it can still be classified into three categories: *reflection, diffraction, and scattering*. *Reflection* occurs when the propagating wave impinges upon an object whose dimensions are very large compared to the wavelength of the propagating signal. *Diffraction* that explains the non-line-of-sight (NLOS) communication in wireless channels occurs when signal encounters an object with sharp edges in its path to the receiver. *Scattering*, which is the most difficult one among the others to predict, occurs when the propagating wave impinges upon an object whose dimensions are very small compared to the wavelength of the propagating signal.

The propagation in PLC channels is mostly governed by *reflections*. In PLC systems, a transmit signal propagating from one location to another suffers from *reflections* at impedance discontinuities along its path. Branching and impedance appearing at the termination points are the main source of impedance discontinuity in power line networks (PLNs) giving rise to *reflections*. These mechanisms are illustrated in Fig. 2.2.

Due to the propagation mechanisms effective in both environments, when a signal is emitted by a transmitter, the signal received at the receiver consists of attenuated, delayed, and phase-shifted replicas of the transmit signal leading to time dispersion. In communications community, significance of time dispersion is quantified by a parameter called root-mean-squared (RMS) delay spread. RMS delay spread for both communication mediums is to be discussed in a more detailed way in the subsequent sections. Besides time dispersion characteristic, both wireless and PLC channels are time selective as well. Mobility (or relative motion between transmitter and receiver from a broader perspective) is the main reason behind time selectivity of wireless channels, whereas the reason for time selectivity in PLC channels is related to the varying impedance conditions in the PLN espe-

cially at the termination points. Time selectivity is another aspect that is to focused in this study. For digital communication systems, the most common figure of merit is the bit bit error rate (BER) which is directly related to signal-to-noise ratio (SNR). Being a function of SNR, BER can be computed by only having information regarding amplitude statistics of the received signal and the noise characteristics in the communication channel. In this respect, amplitude statistics and the noise characteristics of wireless and PLC channels are among the issues that are touched upon.

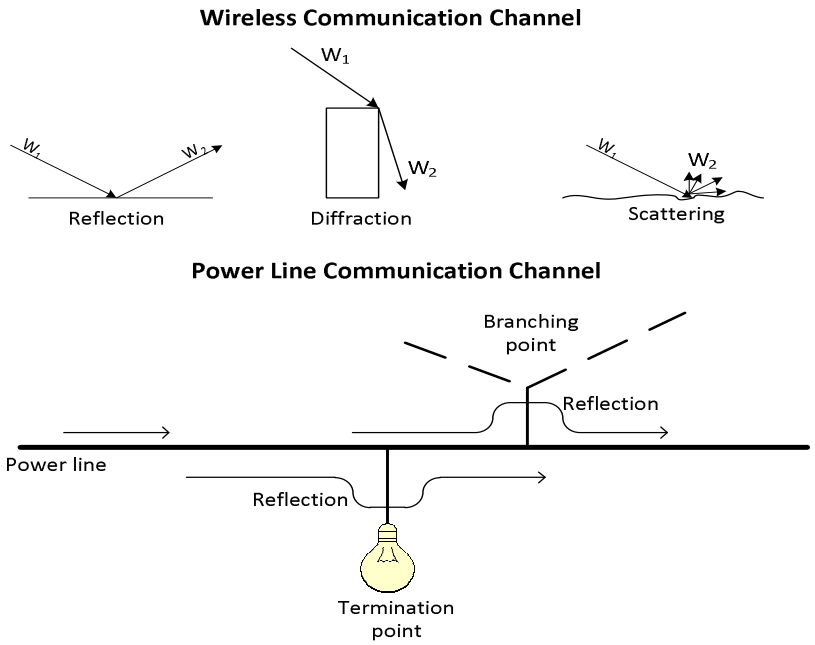

Figure 2.2 Propagation mechanisms for wireless and PLC channels.

2.3 Wireless Channel Characteristics

Large-scale and small–scale fading are the two phenomena that determine the quality of received signal in wireless communication channels. Large-scale fading explains the variation in the received signal due to the motion over large areas, whereas small-scale fading is helpful in understanding the received signal characteristics as a result of small changes (as small as a half wavelength) in the spatial domain. In explaining the large-scale fading characteristics, path loss is used for relating the transmit power to the received power in the logarithmic

scale. At a particular distance d from the transmitter, path loss is expressed as

$$PL(d) = PL(d_0) + 10nlog(d/d_0) + X_\sigma, \tag{2.1}$$

where d_0 is the reference distance in the far field of the transmit antenna, n is the path loss exponent, and X_σ denotes a real zero mean Gaussian random variable (RV) with a particular standard deviation σ. X_σ is referred to as shadowing and accounts for the impact of the terrain profile on the transmit signal. Note that possession of knowledge regarding two parameters, which are n and σ, while characterizing (2.1) is essential. Both n and σ are environmental dependent parameters and may change significantly depending upon communication medium profile. Smart grid communication infrastructure is likely to be deployed in a variety of communication environments. Among these deployment options are:

- Indoor deployment: homes, offices, etc
- Outdoor deployment: rural, urban, suburban areas and so on
- Electric-power-system facility deployment: electric–power–system environments such as transmission, distribution, and transformation substations, power control rooms, etc.

Note that a distinction between indoor and electric-power-system facility has been made in the classification given above. This is due to the fact that electric-power-system environments have very discriminative features compared to regular indoor environments such as prevalence of metallic structure, different noise characteristics that may stem from corona effect or switching operations, hostility in terms of temperature and humidity, etc. Stemming from these differences, further discussion is built upon the classification given above.

Most of the results reported in the literature regarding indoor communication environments are based on measurements carried out at around 900MHz and 1.9GHz. Path loss exponent (n) for a variety of indoor propagation environments range from 1.2 to 6 [43–46].

Values smaller than 2 can be attributed to the waveguide effect present in the environment, whereas higher values are likely due to large attenuations introduced on the transmit signal by walls, ceilings, floors, etc. Regarding the standard deviation of shadowing σ in (2.1), typical values are in the range of 3dB to 14dB [47, 48]. In addition to the model given by (2.1), indoor path loss expressions that consider some other indoor environmental features such as number of walls, number of floors penetrated by the transmit signal are available in the literature as well [46, 47, 49, 50]. For instance, International Telecommunication Union (ITU) recommends a shadowing σ value of 12dB for office environments along with a modified indoor path loss expression that considers transmitter–receiver separation distance and number of floors in the transmit signal path [49].

The typical values for path loss exponent (n) for outdoor environments ranges from 2.7 to 6.5 depending upon the environmental characteristics [50]. For instance, recommended value of path loss exponent by ITU is 4 for both urban and suburban areas [49]. It is also worth mentioning that rural areas with flat terrain should assume lower values of n. Shadowing σ for urban environments is typically $8 - 10$dB [51]. ITU considers a standard deviation value of 10dB as appropriate for both urban and suburban areas [49].

The number of studies for characterizing the radio propagation medium within electric-power-system environments is very limited in the literature. An experimental study in different electric–power–system environments including a 500kV substation, an industrial power control room, and an underground network transformer vault reports that path loss exponent n varies from 1.45 to 3.55 depending upon line-of-sight (LOS) and (NLOS) conditions between transmitter and receiver [52]. Shadowing σ values in these environments are found to be between 2.25dB and 3.29dB.

2.3.1 Multipath Characteristics

A complete multipath characterization of the wireless channel can be given by its complex baseband impulse response as follows [47]:

$$h(t,\tau) = \sum_{r=1}^{N(t)} a_r(t) e^{j\theta_r(t)} \delta(\tau - \tau_r(t)), \tag{2.2}$$

where $N(t)$ represents the number of resolvable multipath components at time t, $a_r(t)$ is the amplitude of the r-th multipath component, $\theta_r(t)$ denotes the phase, $\tau_r(t)$ represents the arrival time, and $\delta(\cdot)$ is the Dirac delta function.

2.3.1.1 Time Dispersion

RMS delay spread is highly dependent on the wireless communication medium characteristics. A large number of studies is available in the literature for the characterization of RMS delay spread in various environments. The most straightforward conclusion that can be drawn from these studies is that the RMS delay spread values of indoor environments are smaller that those of outdoor environments [53, Chapter 2]. Typical values of RMS delay spread for residential buildings are within the range of 5ns to 10ns with some exceptional reported values up to 30ns. Office environments tend to have larger values within the range of 10ns to 100ns. RMS delay spread values of typical urban and suburban environments are usually between 100ns and 800ns with some reported values up to 3μs. Bad urban and hilly terrain environments have much larger RMS delay spread values than these previously mentioned ones up to 18μs. Similar to the other propagation related parameters, the number of studies performed in electric-power-system environments is very limited. A measurement campaign carried out in a distribution transformer revealed that the mean RMS delay spread in this environment is 85ns [54].

2.3.1.2 Time Selectivity

Time selectivity in wireless channels manifests itself in transform domain as a spectral broadening which is known as Doppler spread. Impact of the spread is generally evaluated through the observation of Doppler spectrum. In (3.1), the impact of the mobility, hence the consequence of time selectivity is observed in the phase term, namely $\theta_r(t)$, for each tap (delay). Doppler spread in the received waveforms is caused by the instantaneous changes in $\theta_r(t)$ stemming from the differences in the path distance between receiver and transmitter antennas over a very small duration of time. Doppler spectrum depends on several parameters such as operating frequency, speed, and angle of arrival (AOA) statistics at the receiver. AOA statistics are mostly define the shape of the Doppler spectrum. When 3-D propagation environment is considered, shape of the Doppler spectrum may vary from classical Jakes' bath-tube like shape to flat depending upon the AOA statistics in both azimuth and elevation planes [55, 56]. Besides these parameters, motion scenario between transmitter and receiver is another factor that defines the Doppler spectrum. In wireless communication applications, two categories can be identified to define motion scenarios: mobile receiver and fixed receiver with moving surrounding objects. It must be noted that different motion scenarios in the wireless channel lead to different Doppler spectra. Jakes' classical spectrum is commonly used in scenarios which consider the motion of the receiver antenna [51]. If transmitter is fixed and channel variation stems only from the motion of surrounding objects, then the Doppler spectrum takes a different shape from that of Jakes' with a power spectral density (PSD) approaching zero with increasing frequency [2, 57, 58]. These differences between Doppler spectra are also considered in many standards and recommendations. For instance, a flat Doppler spectrum and Classical Jakes' spectrum are recommended by ITU for indoor and outdoor propagation environments, respectively [49]. Smart grid communication infrastructure is likely to cover both mobile and fixed wireless scenarios. Wireless voice and video communication with the maintenance team in the field may correspond to the mobile receiver case, whereas the wireless communication between smart meters and home devices or within the electric-power-system facilities for monitoring

and control applications may refer to the fixed receiver scenario. In this sense, the Doppler spectrum should be carefully thought for truly characterizing the communication channel. Although there is no specific study for characterizing the Doppler spread or AOA statistics within electric-power-system environments, a very rough classification can be applied and Jakes' classical spectrum for mobile receiver case and the spectrum with a PSD approaching zero with increasing frequency for fixed receiver case is considered to be appropriate. However, it is also worth mentioning that electric-power-system environments might be located in regions or positions entirely isolated from the outside effects (e.g. underground transformer stations). Such a condition may lead to time invariance of the wireless communication channel for fixed receiver-transmitter case unlike the situation observed in indoor and outdoor communication environments in which motion of the surrounding objects such as pedestrians and vehicles results in wireless channel variation.

2.3.1.3 Amplitude Statistics

Rayleigh and Ricean probability density functions (PDFs) are widely used to describe the small scale statistics of the amplitude ($a_r(t)$ in (2.2)) in wireless communication channels for NLOS and LOS conditions, respectively [47, 59]. This stems from the fact that a very large number of multipath components falls into each tap in (2.2) leading to the realization of complex Gaussian process as a result of central limit theorem. Besides Rayleigh and Ricean, Nakagami fading is also commonly used in oder to model more variety of fading conditions. One of the interesting properties of Nakagami PDF is that it can closely approximate Rayleigh and Ricean PDF through very simple parameter manipulations [59, 60]. Finally, some other fading distributions such as Weibull are also used while defining the amplitude statistics of received signal in the literature [61].

2.3.2 Noise Characteristics

In conventional wireless communication systems, thermal noise is usually modeled as stationary additive white Gaussian noise (AWGN). In spite of being an accurate model

for most of the time, wireless communication systems are subject to impulsive noise in certain indoor and outdoor environments [62, 63]. Major sources of impulsive noise in indoor wireless channels are some devices that we frequently use in our daily lives such as photocopiers, printers, microwave ovens, hair-dryers and etc. Impulsive noise in outdoor environments may result from some other effects such as vehicle ignition. Besides these regular environments, noise characteristics of electric-power-system environments may be dominated by the presence of impulsive noise as well [64, 65]. For instance, gap breakdown discharge phenomenon that is mainly caused by circuit breaker opening may result in a very strong impulsive noise in a transformer substation.

In the literature, time domain samples of the entire noise process (background noise corrupted with impulsive noise) is very frequently represented by a mixture of zero mean complex Gaussian variables with different variances and occurrence probabilities as follows:

$$f(n) = \sum_{l=0}^{L} p_I g(n|\sigma_I^2), \tag{2.3}$$

where p_I's denote model parameters whose sum should equal unity and $g(n|\sigma_I^2)$ is the PDF of the complex Gaussian variable with zero mean and σ_I^2 variance. Note that (2.3) is a generalization of Bernoulli–Gaussian and Middleton Class-A models as noted in [66]. In spite of being widely used for the purpose of analysis, this model is memoryless and lacks representing the bursty nature of impulsive noise [67]. In order to incorporate its bursty nature into analysis, Markov model is commonly employed [67, 68]. Employing Markov model along with a persistence parameter which signifies memory of the channel may turn this memoryless model into a bursty model forming a more realistic analysis platform.

2.4 PLC Channel Characteristics

Based on extensive measurements, frequency–distance dependent attenuation in low voltage (LV) PLC networks is defined as [69]

$$A(f,d) = \exp\big((-a_0 - a_1 f^k)d\big), \tag{2.4}$$

where f and d correspond to frequency of the signal and the distance covered, respectively. a_0, a_1, and k are all cable dependent parameters and are mostly extracted by empirical measurements [69].

2.4.1 Multipath Characteristics

If the total number of replicas received at the receiver is considered to be limited to N, a complete characterization of the PLC channel can be given by its channel frequency response (CFR) as follows: [69]

$$H(f) = \sum_{i=0}^{N} \Big[\prod_{k=1}^{K} \Gamma_{ik} \prod_{m=1}^{M} T_{im} \Big] A(f,d_i) exp(-j2\pi f \tau_i), \tag{2.5}$$

where Γ and T correspond to the reflection and transmission coefficients along the propagation path, respectively, $A(f,d_i)$ means the frequency–and–distance dependent attenuation stemming from the physical characteristics of the cable, and $exp(-j2\pi f\tau_i)$ refers to the phase of the ith component due to the time delay. K and M represent the number of reflection and transmission coefficients experienced by the propagating signal along a particular path denoted by the subscript i. Finally, it is worth mentioning that multiplication of Γ's and T's in (2.5) is referred as the reflection factor ($|r_i|e^{j\theta_i}$) of a particular propagation path. Note that τ_i, the time delay, is related to the speed of propagation within the communication medium, power line cables in our consideration as follows:

$$\tau_i = \frac{d_i\sqrt{\epsilon_r}}{c_0} \tag{2.6}$$

where ϵ_r is the dielectric constant of the insulation material and c_0 is the speed of light in vacuum.

2.4.1.1 Time Dispersion

Our discussion starts with the articulation of factors that define RMS delay spread in PLC channels and extends into more specific values based on measurement campaigns. One of the factors on which RMS delay spread depends in PLNs is the impedance status at the termination points. Studies show that low impedance or high impedance values at the termination points yield the worst case scenario from the aspect of RMS delay spread [70–72]. Another factor is the physical attributes of the PLC medium [3]. Number of branching nodes between transmitter and receiver, distance between transmitter and receiver as well as the length statistics of the branches are among these attributes.

In spite of confusion and unclarity in RMS delay spread computation in PLC literature, values reported in [73, 74] show that it is mostly on the order of $2-3\mu s$ with a few exceptions as high as $5-6\mu s$ for a frequency range up to 30MHz. Another very extensive study that considers the site measurements of 120 channels in the $1.8-30$MHz range reveals that the RMS delay spread is mostly below $1.31\mu s$ with only two exceptions of channel responses that exhibit a higher value $1.73\mu s$ and $1.81\mu s$ [75]. Similarly, RMS delay spread values reported over the same frequency range reveals that it is smaller than $0.5\mu s$ for 99% of the studied channels [76]. Also, a similar study conducted over a frequency range up to 30MHz reports that 95% of the channels have an RMS delay spread value between $240ns$ and $2.5\mu s$ [77]. Another study which considers a larger frequency band up to 100MHz finds out that 80% of the channels exhibit RMS delay spread values between $0.06\mu s$ and $0.78\mu s$ with a mean value of $0.413\mu s$ upon conducting extensive measurement campaigns by obtaining 144 transfer functions collected from 7 sites [78]. In conclusion, typical RMS delay spread values in LV PLC channels are on the order of few microseconds.

2.4.1.2 Time Selectivity

Even for a fixed PLN topology, response of the PLC channels can not be considered as time invariant. Time variation of the PLC channels is attributed to the change in the reflection factors ($|r_i|e^{j\theta_i}$) of the propagation paths. It can be examined in two main categories: long term and short term. Long term variation stems from the fact that impedance status of the termination points constantly changes as the devices connected to the PLN are switched on/off. Change in the impedances seen at the termination points leads to a change in the reflection and transmission coefficients of some paths giving rise to the variation of the channel response. It is worth mentioning that the impedance values seen at the termination points are also dependent on the state of the connected electrical load: unplugged, plugged but inactive, and plugged and active [79]. In addition to this long term change in the impedance status of the termination points, impedance of most of the electrical loads is dependent on the Alternating Current (AC) mains cycle giving rise to a cyclic short term variation in the channel response [80]. Coherence time[8] of the LV PLC channel due to the short-term impedance variations in the PLN is reported to be no smaller than 600μs [80]. It is worth mentioning that studies show that separation distance between transmitter and receiver plays a important role in the significance of the channel variation due to the impedance dependency of the electrical loads on the mains AC cycle [81]. It is also shown that if a certain feature is always present in the PLN, then the PLC channel becomes a more deterministic medium than commonly believed [82].

2.4.1.3 Amplitude Statistics

Studies show that path amplitudes in LV PLC networks can be characterized with log-normal PDF merely resembling the shadow fading in wireless channels [4, 72, 75, 83, 84]. Besides frequently used log-normal distribution, use of some other PDFs such as Rayleigh and Rician is also recommended for defining path amplitudes in PL channels [73, 85, 86].

[8]Coherence time refers to the duration of time over which channel can be considered invariant

Statistics of signal amplitude in PLC environments are not well-established compared to the wireless communication case and need further investigation and verification.

2.4.2 Noise Characteristics

Noise in PLC channels is classified into three main categories that are colored background noise, narrow band noise, and impulsive noise. Colored background noise results from the summation of different noise sources of low power present in the network and is usually characterized with a PSD decreasing with the frequency. Narrow band noise stems from the existence of radio broadcasters in long, middle, and short wave ranges. Colored background noise and narrow band noise are mainly considered to constitute the background noise since their amplitudes vary very slowly over the time. In addition to the background noise, impulsive noise, generated mostly by electrical appliances, is the most significant among the noise types present in PLC networks. It is considered to be the main reason behind the errors in the data transmission over the PLC channels. Analysis of the impulsive noise proposes that it can be further categorized into three categories as follows:

- Periodic impulsive noise asynchronous to the mains AC cycle, which is generated mostly by switched-mode power supplies.
- Periodic impulsive noise synchronous to the mains AC cycle, which is caused by rectifier diodes used in some of the electrical appliances.
- Asynchronous impulsive noise, which results from the electrical motors, drills, and on/off switching transients present in the network.

Models proposed regarding the noise categories mentioned above are all based on empirical measurement campaigns. The main approach undertaken while modeling the background noise is based on its frequency domain characterization. One of the methods to characterize the background noise is to express it as a function of frequency by using its fitted PSD [87]. The major downside of this approach is that the random behavior of the noise process is not considered at all. In order to incorporate its random nature into anal-

ysis, background noise variation at a particular frequency value should be characterized by a certain PDF. Among these PDFs proposed in the literature are sum of two Rayleigh PDFs [88], log-normal [89], and Nakagami-m [90]. With regards to impulsive noise, common methodology is based on characterizing it in time domain in terms of several parameters such as impulse amplitude, impulse width, and impulse interarrival times [68, 91, 92]. In spite of the fact that impulsive noise results from entirely different sources in wireless and PLC channels, models employed in the literature are very similar to each other. Hence, the model given by (2.3) is widely employed in PLC community as well for the purpose of communication system analysis.

As a final note, notice that most of the preceding discussions are dedicated to the LV PLC channels. However, this does not necessarily imply that other segments of the PLN can not be considered for the purpose of communication in spite of some reliability related concerns[9] [93–95]. However, although HV power lines serve as a communication medium for voice for a long time dating back to 1920s [96], the literature defining its channel characteristics is almost inexistent. Regarding the communication channel characteristics of MV channels, although there is not much study in the literature, some general conclusions can still be drawn. Similar to LV PLC channels, MV lines exhibit time dispersion. RMS delay spread values of MV PLC channels are on the order of 10μs. Time variation of the channel is very weak and the amplitude statistics obey Nakagami-m distribution [97]. In addition to these multipath related parameters, noise components of MV power lines are usually very similar to those of LV power lines with some discriminative features such as the dominance of corona discharges in the background noise [98].

2.5 Concluding Remarks

Smart grid is a challenging project that requires the establishment of a very extensive communication infrastructure. PLC and wireless based solutions seem very attractive con-

[9]Ensuring the continuation of power line cable in medium voltage (MV) and high voltage (HV) segments for end-to-end communication is a relatively more difficult issue than in LV segment.

Table 2.1 Outline of wireless and PLC channel characteristics

Channel Param.	**Wireless**	**Powerline**
Path Loss / Attenuation	Highly dependent on the propagation environment of interests with extensive results reported in the literature	Dependent on the characteristics of cable used in the PLN
Time dispersion / Freq. selectivity	Governed by reflection, diffraction, and scattering	Governed by reflections mainly due to impedance discontinuities along the propagation path
Time selectivity / Freq. dispersion	Mobility of transmitter/ receiver pairs or motion of surrounding objects	Impedance variations over both long and short term
Path Amplitudes	Mostly assumed Rayleigh or Ricean depending on NLOS/LOS condition	Merely resembles shadowing effect in wireless channels and mostly assumed to obey log-Normal PDF
Noise	Mostly assumed AWGN, presence of impulsive noise in certain environments	More complicated noise structure: colored background noise, narrow band noise and impulsive noise very effective

sidering the cost of initial investment. Being cost effective solutions, two approaches are likely to emerge: integration of already existing PLC and wireless technologies into the grid with some modifications regarding QoS, latency, reliability, power consumption, etc or developing novel communication protocols particularly addressing the smart grid communication needs. No matter what approach is taken, a deep understanding of the communication channel characteristics of smart grid environments is essential. In this study, communication characteristics of both PLC and wireless environments were discussed in detail. Smart grid wireless deployment options were classified roughly as indoor, outdoor and electric-power-system environments. Similar methodology was followed in PLC environments as well by classifying them as LV, MV, and HV.

Among the communication channel characteristics discussed were path loss and attenuation, time dispersion, time selectivity, path amplitudes and noise characteristics as outlined

in Table 2.1. These parameters are of great importance from the perspective of communication system design for smart grid communication infrastructure. To sum up these characteristics, path loss and attenuation profile of wireless and PLC channels significantly vary with respect to communication environment and several model parameters are available in the literature for different environment types. RMS delay spread which indicates the significance of time dispersion of a communication channel is on the order of a few microseconds in LV PLC channels. MV lines exhibit a larger RMS delay spread values on the order of 10μs. Similarly, typical values of RMS delay spread for indoor wireless environments are usually less than 100ns, whereas outdoor wireless propagation environments have larger values on the order of microseconds. Regarding electric-power-system environments, RMS delay spread of wireless propagation channel in a distribution transformer is found to be 85ns. Both wireless and PLC channels are time variant. Doppler spread is observed in order to evaluate the consequences of time selectivity in wireless channels. While discussing the Doppler spectra of different wireless communication environments, a rough classification with respect to motion scenarios was performed. Jakes' classical spectrum seems to be a suitable model for mobile receiver scenarios, whereas the spectrum with a PSD approaching zero with increasing frequency is considered to be appropriate for fixed receiver case. However, time variation of the wireless communication channel in certain electric–power–system environments could be very insignificant since these environments might be completely isolated from the outside effects. Although no specific model is available regarding the time selectivity of PLC channels, time selectivity is related to the long and short term varying impedance conditions in the PLN. Coherence time of the LV PLC channel is no less than 600μs in the short term. Log-normal distribution is widely used while defining amplitude statistics in LV PLC channels, whereas Rayleigh and Rician PDFs are commonly employed in wireless channels for NLOS and LOS conditions, respectively. Structure of the noise in PLC channels is relatively more complex than that of wireless channels. Impulsive noise stemming from electrical loads connected to the PLN is the major source of data errors in PLC channels. Impulsive noise is observed in certain wireless

indoor, outdoor, and electric-power-system environments as well. Photocopiers, printers, microwave ovens, hair-dryers, vehicle ignition are some of the sources of impulsive noise in indoor and outdoor environments. In electrical–power–system environments especially in transformer substations, impulsive noise as a result of gap breakdown discharge phenomenon could significantly impact wireless communication.

It is worth mentioning that some aspects of the smart grid needs further investigation in terms of communication channel characteristics. For instance, a more in-depth understanding of the radio propagation characteristics in electric-power-system environments is essential for the design of reliable wireless communication systems in the smart grid. Similarly, most of the research efforts in PLC channels are dedicated to the LV side of the PLN and lack of literature in MV and HV PLC channels suggests a more comprehensive look at these environments.

CHAPTER 3

INVESTIGATION OF TIME SELECTIVITY OF WIRELESS CHANNELS THROUGH THE USE OF RVC

3.1 Introduction

The most attractive and desired feature of wireless communications is mobility. In wireless communications community, mobility is considered to include the following scenarios: motion of transmitter and/or receiver, motion of surrounding objects, and both. Since all these three scenarios can be unified under the umbrella of motion, a more comprehensive characterization might be more appropriate in terms of analysis by considering the relative motion in general rather than the mobility concept. Thus, motion in general leads to several consequences from the perspective of wireless propagation channel and plays a crucial role on its characterization.

Selectivity is a statistical tool that is used for characterizing wireless channels. Formally, selectivity is defined in both time and frequency domains. Time selectivity is used to characterize the consequences of motion [99]. Time selectivity manifests itself in transform domain as a spectral broadening which is known as Doppler spread. Impact of the spread is generally evaluated through the observation of Doppler spectrum.

It is known that different propagation environments and motion behaviors lead to different Doppler spectrum characteristics. In order to achieve a reliable wireless communications system, it is required that all sorts of propagation characteristics should be well understood. Furthermore, the entire communication system must be evaluated under various transmission conditions whose characteristics have been derived based on arduous experimental field tests. Among these propagation characteristics, Doppler phenomenon is one of the most

prominent one considering the motion aspect of wireless communications systems. In this respect, reverberation chambers (RVCs) can be considered as a potential test environment to emulate different Doppler characteristics without going through time-consuming and expensive field tests.

The RVC is a closed cavity which is generally of metallic structure. When it is excited empty, it has many well-behaved propagation modes which lead to great electromagnetic (EM) field variations [100]. A stirrer is rotated to randomize the maxima and minima locations of the EM field magnitudes giving rise to a more uniform field magnitude distribution throughout the chamber. Rotation of the stirrer inside the RVC causes also Doppler spread in the received signal. Although there are not many Doppler related RVC studies in the literature, some research can still be found in the framework of a broader perspective. In [101] which can be considered to relate Doppler directly to RVC, the authors derive a relation between the speed of stirrer and maximum observed Doppler frequency. Another Doppler related study for RVCs can be found in [102] which compares the experimental results with the Jakes spectrum. The authors claim that there is a discrepancy between the model and the experimental results stemming from the dimensional assumptions in signal propagation. In contrast to the previous studies, an indirect relation between Doppler and RVC is established in [103] from the time domain perspective. Similarly, in [104], multiple-input multiple-output (MIMO) performance analysis for nonisotropic propagation environments is performed in an RVC. However, as concluded by the authors, nonisotropic propagation environments need to be further investigated especially in terms of motion related parameters.

The study presents the findings of the measurement campaigns within an RVC that are performed to make a complete characterization of the Doppler behavior. The objectives can be summarized as follows:

- Having a better understanding of Doppler spectrum characteristics as well as the factors which define its behavior through the use of an RVC. Some of the factors that are studied are operating frequency, speed, angle of arrival (AOA). In conjunction

with these factors, a new perspective of mobility in wireless channels is also given by proposing a concept called motion intensity.

- Comparing experimental results with some vastly used theoretical models and elaborating the reasons of discrepancies between the models and the results. In addition, steps for the accurate realization of the theoretical models such as Jakes in RVCs are given.

The remainder of the chapter is organized as follows. Section 3.2 gives the analytical background for wireless channel model and Doppler spectrum in the light of specific motion scenarios. Section 3.3 provides the details of measurement system and procedure employed in the study. Section 3.4 elaborates the outcomes of the experiments conducted. Section 3.5 discusses the effective factors on Doppler spectrum and the realization of theoretical Doppler spectra in RVCs such as Jakes' model. Finally, the concluding remarks are given in Section 3.6.

3.2 Wireless Channel Model, Doppler Spectrum, and Motion Scenarios

In this section, first fundamental characteristics of wireless channel and its relation to Doppler spectrum is given. Next, motion scenarios are analyzed and discussed from the perspective of Doppler spectrum.

3.2.1 Wireless Channel Model and Doppler Spectrum

When a wireless signal is transmitted, the signal received at the receiver consists of attenuated, delayed, and phase-shifted replicas of the transmitted signal. Therefore, a complete characterization of the wireless channel can be given by its complex baseband impulse response as follows:

$$h(t,\tau) = \sum_{r=1}^{N(t)} a_r(t) e^{j\theta_r(t)} \delta(\tau - \tau_r(t)), \tag{3.1}$$

where $N(t)$ represents the number of resolvable multipath components at time t, $a_r(t)$ is the amplitude of the r-th multipath component, $\theta_r(t)$ denotes the phase, $\tau_r(t)$ represents the arrival time, and $\delta(\cdot)$ is the Dirac delta function [61].

In (3.1), the impact of the mobility manifests itself in the phase term, namely $\theta_r(t)$, for each tap (delay). Doppler spread in the received waveforms is caused by the instantaneous changes in $\theta_r(t)$ stemming from the differences in the path distance between receiver and transmitter antennas over a very small duration of time. In order to characterize the propagation channel, the statistical behavior of the taps (delays) in (3.1) over time should be investigated. Channel correlation function is used as a tool in order to evaluate this statistical behavior. Transform domain counterpart of channel correlation function is known as Doppler spectrum. Since different motion scenarios lead to different Doppler spectra, it is appropriate to investigate them individually. Subsequently, the following fundamental motion scenarios will be the focus: motion of transmitter/receiver and motion of surrounding objects.

3.2.2 Motion Scenarios

3.2.2.1 Motion of Transmitter/Receiver

This subsection details a scenario in which one of the nodes in transmitter/receiver pairs is considered to be moving and the other to be fixed. The key factor in Doppler phenomenon is the relative motion between transmitter and receiver. Stemming from this fact, analysis is independent of mobility status of the nodes as long as the relative motion is maintained. Note that, in a traditional cellular system, such a scenario corresponds to uplink/downlink communication between a mobile node and a fixed base station. Therefore, for the sake of brevity, only the moving receiver-fixed transmitter case will be investigated.

A receiver moving with a particular speed of v is considered in the analysis as depicted in Figure 3.1. Although the receiver travels very short distance over the interval of Δt, phases of the rays arriving the receiver from different angles change drastically. The assumptions

related to angle of ray arrivals, their power levels as well as the gain pattern of the antenna are of utmost importance for the statistical characterization of the propagation channel.

For the sake of simplicity and ease of analysis, milder assumptions can be employed such as constant arriving ray power levels, uniformly distributed ray arrival angles, omni-directional antenna pattern, and so on. Note that all these simplified assumptions can be formally expressed by the following zeroth order Bessel function of the first kind when the channel correlation function is considered for the rth tap:

$$E\left\{h(t,\tau_r)h^*(t+\Delta t,\tau_r)\right\} = R_h(\Delta t) = J_0(2\pi f_D \Delta t), \tag{3.2}$$

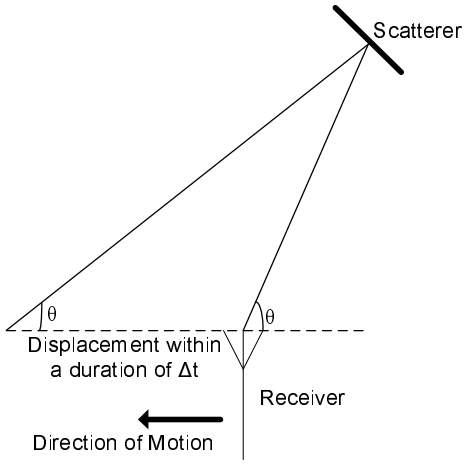

Figure 3.1 Geometry of moving receiver case.

where $E\{\cdot\}$ is the statistical expectation operator, $(\cdot)^*$ denotes the complex conjugate of its input, Δt is the time shift in the correlation operation, and f_D is maximum Doppler frequency. Maximum Doppler frequency, namely f_D, is related to the carrier frequency of the transmit signal and to the speed of the mobile as $(v f_c)/c$ where c is the speed of light. The Fourier transform of (3.2) which corresponds to Doppler spectrum is known as Jakes'

model and takes the following form [51]:

$$R_H(f) = \begin{cases} \dfrac{1}{\pi\sqrt{f_D^2 - f^2}} & , |f| \leq f_D \\ 0 & , \text{otherwise} \end{cases} \tag{3.3}$$

When a particular receiver velocity is assumed, graphical representation of the Doppler spectrum reminds of the famous bathtub-like shape as depicted in Figure 3.2. Note that frequency axis is normalized by the maximum Doppler frequency f_D where the carrier frequency f_c is represented with $f = 0$. In the literature, several measurements performed with this transmitter-receiver configuration approximate this Doppler behavior [56, 105]. It is worth mentioning that the assumptions considered in the analysis of Jakes' model are very strong and not applicable in most of the propagation environments. However, Jakes' Doppler spectrum is vastly used in the literature for comparison purposes of the experimental data or of some other theoretical models [102].

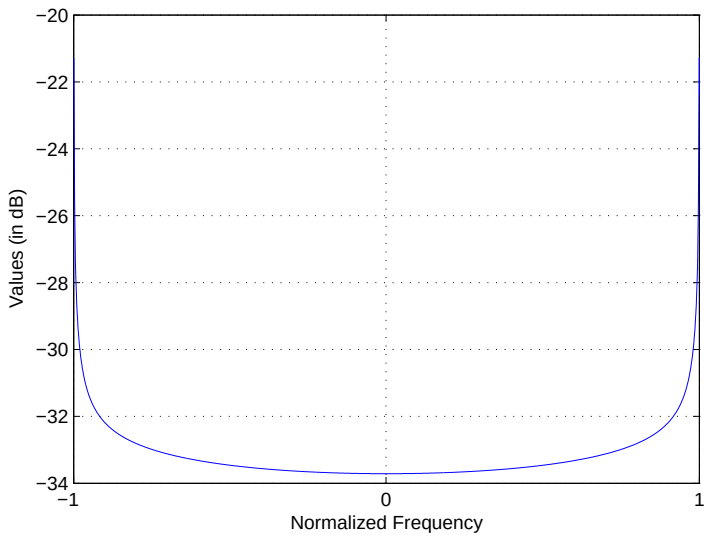

Figure 3.2 Doppler spectrum for moving receiver case.

3.2.2.2 Motion of Surrounding Objects

The scenario, in which motion of the surrounding objects is considered, is shown in Figure 3.3. Such a scenario is vastly encountered in typical indoor wireless communication applications. As can be clearly seen in Figure 3.3, the phase change of the received signal is due to the movement of the surrounding scatterers and depends on the movement direction of the object as well as on the incident angle of the arriving ray on the scatterer. If the arrival angle θ and the motion angle β are considered to be uniformly distributed over (-π,π], channel correlation as a function of Δt can be derived as follows [58]:

$$R_h(\Delta t) = J_0^2(2\pi f_D \Delta t) \tag{3.4}$$

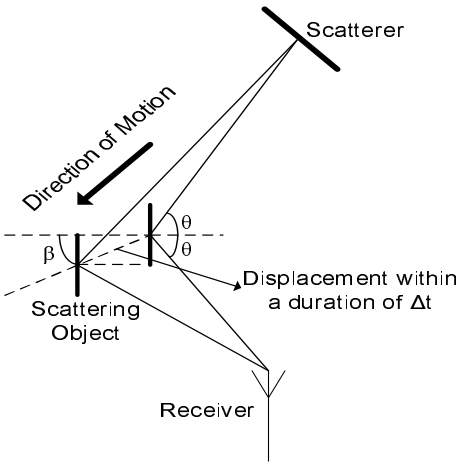

Figure 3.3 Geometry for moving objects case.

Corresponding Doppler spectrum which is the Fourier transform of (3.4) can be computed as:

$$R_H(f) = \begin{cases} \dfrac{2}{\pi^2\sqrt{4f_D^2 - f^2}} K\left(\dfrac{2f_D}{\sqrt{4f_D^2 - f^2}}\right) & , \ |f| \leq 2f_D \\ 0 & , \ \text{otherwise} \end{cases} \tag{3.5}$$

where $K(\cdot)$ implies the complete elliptic integral. Doppler spectrum indicated by (3.5) is valid if all the rays come across a moving object before arriving the receiver. This is not

a valid assumption considering the possibility that some percentage of the rays arriving the receiver is reflected from the stationary sources such as walls, doors, windows and so on. This fact favors the idea of distinguishing propagation environments with respect to their motion characteristics. In this respect, a formal tool is required to identify distinct motion characteristics. For instance, if a ratio which articulates the relation between rays coming from stationary objects and moving objects is introduced, such a formal distinction is achieved to some extent.

The above-mentioned idea can directly be incorporated into the channel correlation function as well. If a factor, namely m, denotes the rays coming from the moving objects with various velocities that can be defined by a probability density function (PDF) and $1-m$ the rays reflected from stationary objects, the channel correlation function takes the following form [58]:

$$R_h(\Delta t) = (1-m) + mE\{J_0^2(2\pi f_c V \Delta t/c)\} \tag{3.6}$$

Note that (3.6) still includes a statistical expectation taken over V which is the random variable characterizing the speed of surrounding objects. In order to exemplify this, consider a typical residential environment. In such environments, most of the time motion is caused by pedestrians whose speed is of ≈ 3m/s. In order to emphasize the randomness of V and incorporate the effect of the motion of other possible objects, it is reasonable to assume that it has a PDF which is distributed over $(0, 3]$m/s. Note that in (3.6) this randomness is weighted by the factor m which is called motion intensity.

Motion intensity articulates the significance of motion in a particular environment. It forms a platform in which Doppler spectrum characteristics of different motion scenarios can be related to each other. For instance, the scenario given in Section 3.2.2.1 corresponds to the case where motion intensity is equal to unity, whereas the scenario given in Section 3.2.2.2 corresponds to a motion intensity factor of lower than unity. This reasoning stems from the fact that $m = 1$ represents absolute motion which can be interpreted as each ray arrives at the receiver from a source in motion. Furthermore, the case where $m = 0$ implies an absolute stationary environment in which there exists no motion at all.

Evidently, $0 < m < 1$ refers to the case in which surrounding objects are in motion with fixed transmitter-receiver pair.

Different Doppler spectrum shapes stemming from different motion intensity factors m are given in Figure 3.4. While deriving the plot in Figure 3.4, the speed of the surrounding objects are all assumed to be the same. It can be noticed that as the motion intensity of the operating environment decreases meaning that the less amount of rays being reflected by moving objects, the spectrum significantly changes. Recall that as the motion intensity approaches to zero, the Doppler spectrum converges to a Dirac delta. This is very intuitive since it is expected that no spread is observed in an absolute stationary environment as mentioned earlier.

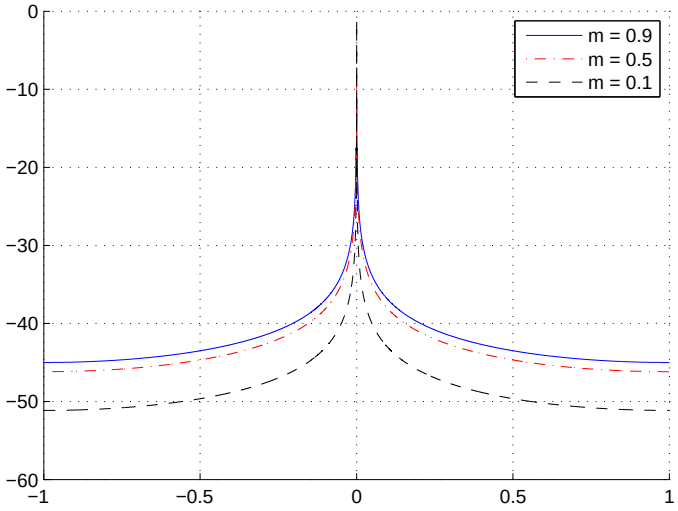

Figure 3.4 Doppler spectrum with moving objects case for different values of m.

Upon introduction on the nature of Doppler spread examined with different scenarios, subsequent sections deal with its characterization in the RVCs.

3.3 Measurement System and Procedure

A setup in order to conduct the Doppler spread measurements inside the RVC has been established in the Wireless and Microwave Information Systems (WAMI) laboratory

of Electrical Engineering department at the University of South Florida (USF) as shown in Figure 3.5. List of the equipment used in the measurements is as follows:

- Agilent E4438C ESG vector signal generator (VSG)
- Agilent E4440A PSA series vector signal analyzer (VSA)
- Omnidirectional Anritsu 2000-1035 and HyperLink Technologies HyperGain RE07U antennas for 910 MHz and 2410MHz measurements, respectively
- Pyramidal Radio Frequency (RF) absorbers in order to control the shape of the Doppler spectrum
- Speed controllable stirrer

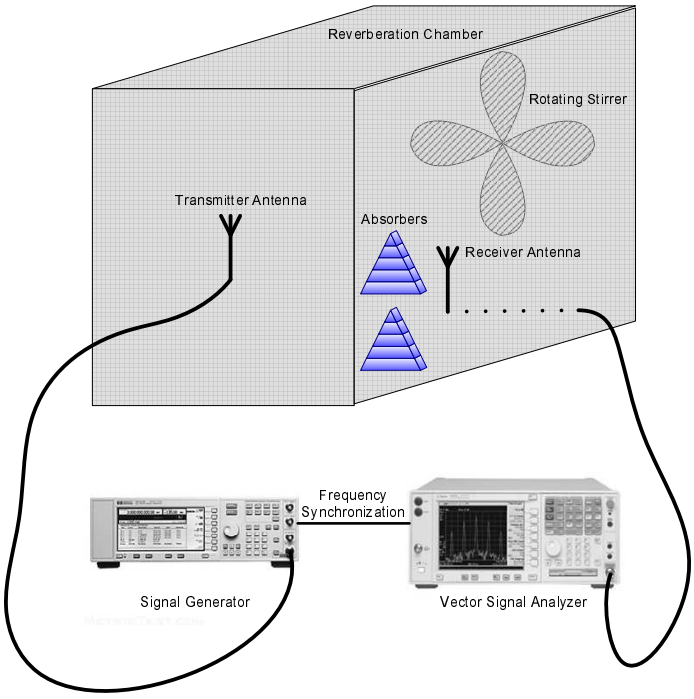

Figure 3.5 Pictorial description of the measurement setup.

In order to extract the Doppler characteristics of the wireless propagation channel between transmitter and receiver antennas within the RVC, two tones at 910 MHz and 2410MHz were transmitted via Agilent E4438C ESG VSG. Agilent E4440A PSA series VSA

was used in order to record the transmitted waveform. In every measurement, data with a duration of 20 seconds was captured to obtain sufficient statistics at the post-processing stage. Caution must be taken while adjusting the span of the spectrum analyzer so as to ensure that the Nyquist sampling criterion is not violated when Doppler affects the transmitted tone. The relation between the span of Agilent E4440A PSA series VSA and a particular target value of sampling rate can be formulated as follows:

$$f_s = \Delta W * 1.28 \tag{3.7}$$

where ΔW denotes the span of the bandwidth to be captured by the device and f_s corresponds to the desired sampling rate. In all of the measurements, the span of the VSA was set to $\Delta W = 8$kHz corresponding to $f_s = 10.24$kHz of sampling rate.

Captured waveform which is provided by Agilent E4440A PSA series VSA as I/Q complex data samples needs to be processed so that the Doppler spectrum is revealed. The post-processing stage steps are as follows:

- *Correction of frequency offset:* The first step of the processing is to make sure that the frequency offset between transmitter and receiver is handled properly. Frequency offset is observed due to the mismatches between transmitter and receiver local oscillators and causes time-dependent phase shifts in the received symbols. Its effect must be corrected before handling the data. However, it is also possible to frequency-synchronize the transmitter and receiver by physically connecting them through their proper ports via a piece of cable depending upon the flexibility of the measurement setup. In all the measurement results presented in this chapter, this impairment was overcome by a direct cable connection between transmitter and receiver as shown in Fig. 3.5. The overhead of correcting the effect of frequency offset in the post-processing is avoided by this way.

- *Calculation of channel correlation function:* After the compensation of frequency offset, channel correlation function needs to be computed. For this purpose, autocorrelation of the I/Q complex data array is calculated.

- *Obtaining Doppler Spectrum:* At this point, Doppler spectrum is obtained by applying fast Fourier transform (FFT) to the channel correlation function which is calculated in the previous step.

3.4 Measurement Results

Considering the scenarios described in Section 3.2, factors that define the Doppler spectrum characteristics can be itemized as follows: (F.1) frequency of operation, (F.2) speed of the receiver terminal or the surrounding objects, (F.3) AOA statistics of the incoming rays, and (F.4) motion intensity. Beside these factors, antenna gain pattern is another parameter affecting the Doppler spectrum; however, it is outside the scope of this study. Considering the fact that physical propagation environment can be emulated by RVC to some extent, all these factors can be mapped into RVC experiments by introducing different stimuli conditions. For example, (F.1) corresponds to the frequencies used in the experiments; (F.2) implies the stirrer speed located inside the RVC; (F.3) is manipulated by changing the number/location of absorbers; and (F.4) is adjusted by changing the number of stirrers rotating inside the RVC. An illustrative schematic representation of this mapping is given in Figure 3.6. As can be seen in Figure 3.6, characteristics of Doppler spectrum are altered by different stimuli introduced into the RVC.

3.4.1 Impact of Frequency of Operation and Speed

As mentioned in Section 3.3, two different frequencies are investigated to see the impact of operating frequency on Doppler spectrum. In addition, the speed aspect of motion is manipulated by changing the speed of stirrer and the results are observed.[1]

[1]It is worth mentioning that different parts of the stirrer moves with different speed due to the rotational movement. Therefore, speed inside the RVC must be treated as a random variable with a particular distribution rather than a single value.

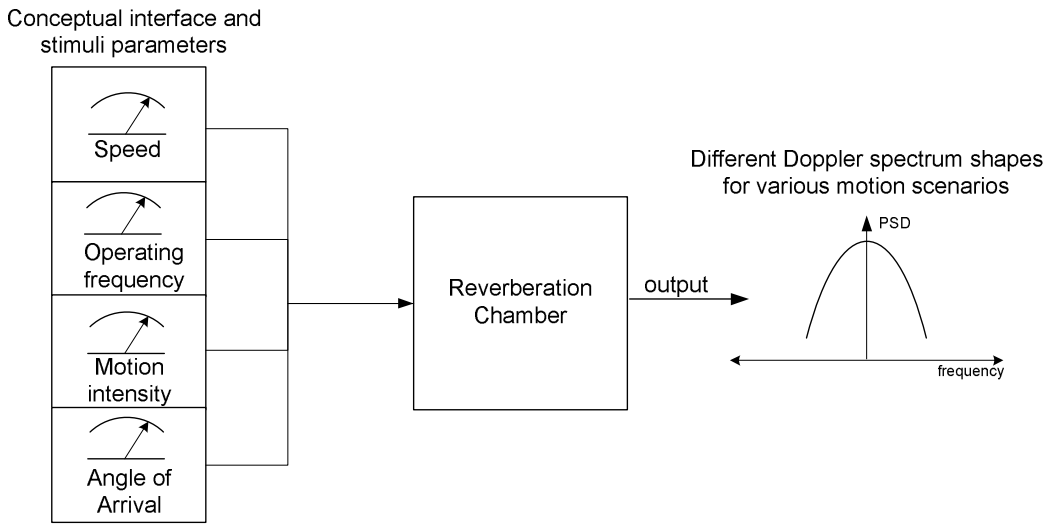

Figure 3.6 Mapping between factors affecting Doppler in physical environment and stimuli conditions for RVC experiments.

The effect of operating frequency and the speed of the stirrer on Doppler spectrum can be seen by observing the spectrogram of the received signal as shown in Figure 3.7, namely through (a)-(d). If the figure is investigated either along the horizontal axis or along the vertical axis, it is clear that an expansion occurs in the frequency spectrum of transmitted signal. This expansion is emphasized by the dashed rectangular boxes placed on the right-hand side of each subfigure.[2] Note that, the size of each rectangular box expands both in the direction of operating frequency and in the direction of stirrer speed. This shows that an increase in operating frequency or stirrer speed gives rise to an expansion in Doppler spectrum. Note also that the amount of expansion caused either by the operating frequency or by the stirrer speed evolves linearly. This is not surprising since the very well-known Doppler shift equation $(vf_c)/c$ is a linear function of both operating frequency and speed.

In order to better see the effect of speed, timefrequency analysis (TFA) can be projected onto solely frequency domain yielding the Doppler spectrum. Figure 3.8(a) and 3.8(b) plot the results for 910MHz and 2410MHz of two different stirrer speeds, respectively. As can be clearly seen from the figures, the tendency of the curves indicates that the energy spreads

[2]The Doppler spectra observed in Figure 3.7 yield a symmetric output in each spectrogram since the transmitted signal is real (*i.e.*. a single tone); therefore, only the right-hand side of the expansion is delineated representing the main lobe of the spread.

to a larger bandwidth with the higher value of stirrer speed. These results are in conformity with the spectrogram plots given in Figure 3.7.

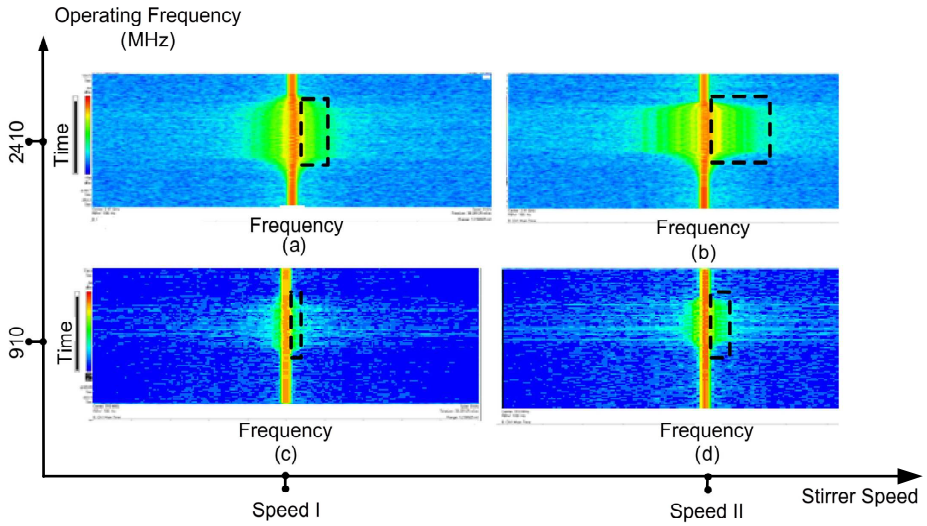

Figure 3.7 Doppler spectrogram of the measurements.

In light of the measurement results presented in this section, it is concluded that the environment inside an RVC is seen to yield a Doppler spectrum that is similar to the motion scenario outlined in 3.2.2.2.

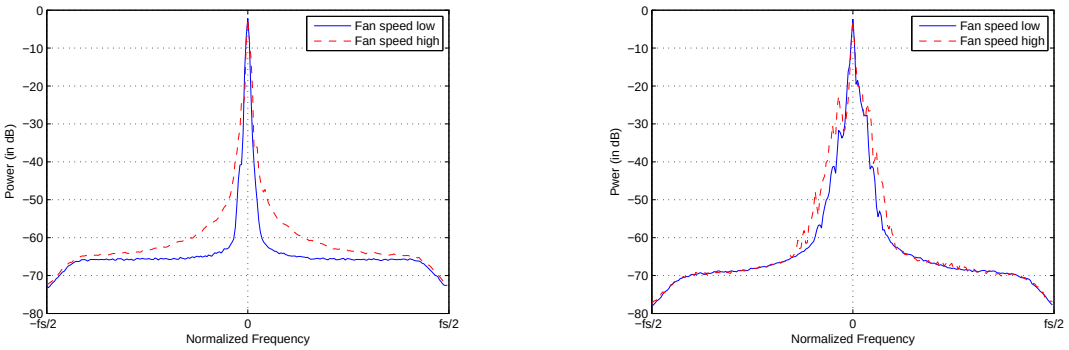

(a) f=910MHz (b) f=2410MHz

Figure 3.8 Impact of operating frequency and speed on Doppler spectrum.

3.4.2 Impact of Motion Intensity on Doppler Spectrum

Motion intensity implies the ratio between the percentage of rays coming from stationary and moving objects. Its value can be altered by changing the probability that the rays come across a moving object within a particular volume in which the wireless signal propagates. In the experiments, the value of motion intensity was increased by introducing another identical stirrer inside the RVC having the same speed statistics. In this experiment, it must be mentioned that the speed of the stirrers was adjusted to their highest values. Placing more stirrers within the same volume is expected to increase the motion intensity of the propagation environment, *i.e.*, RVC in this particular case. Increase in the motion intensity (*i.e.*, $m \rightarrow 1$) was expected to cause a rise in the spectrum curve along the power axis as shown in Figure 3.4. Experimental results which plot the effect of changing the motion intensity at two different operating frequencies are given in Figures 3.9(a) and 3.9(b). Note that each figure bears the combined impact of two factors, namely change in the operating frequency and change in the motion intensity. As explained earlier, change in the operating frequency provides an expansion along the frequency axis. An increase in motion intensity factor m is expected to cause a rise along the power axis. Hence, the comparison of these two figures highlights the combined impact of the two factors. Finally, manipulating Rician K-factor of the wireless communication channel within the RVC can be considered as an alternative to the technique presented above as described by [106]. This is due to the fact that all direct rays contribute to $1 - m$, whereas most of the reflected rays are expected to interact with the stirrer contributing to m factor of (3.6).

3.4.3 Impact of AOA Statistics on Doppler Spectrum

Use of RF absorbers in order to manipulate AOA statistics within RVC is common in the literature [106, 107]. The idea behind the use of absorbers to generate different Doppler behavior is very straightforward. Absorbers intentionally placed around the receiver antenna block some of the rays arriving from particular angles. The composite signal at

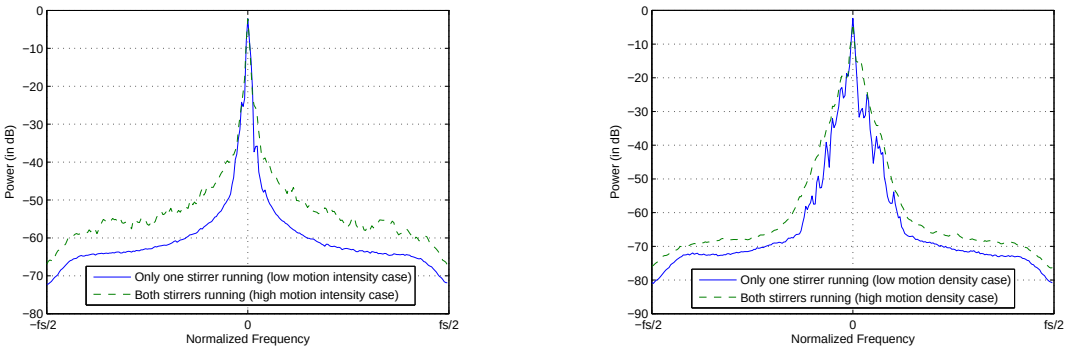

(a) f=910MHz (b) f=2410MHz

Figure 3.9 Impact of motion intensity on Doppler spectrum.

the receiver having contributions only from some particular angles is expected to yield a different Doppler spectrum (usually more asymmetric) from the traditional ones.

It is worth mentioning that the speed of the stirrer is set to its highest value during the experiments presented in this subsection since the purpose is only to see the change in the Doppler spectrum with regard to the AOA. Doppler spectrum was analyzed before and after the introduction of the absorbers so that their effect could be comparatively seen. In the experiments, absorbers were located around the receiver antenna in a way that it reminds a cubic shape. Only one side of the cubic shape was open inside the RVC allowing the wireless signal to arrive at the receiver antenna from this particular angle.

The result of the experiment at 910MHz is shown in Figure 3.10. It is seen that the Doppler spectrum appears to have a more symmetric structure prior to placing the absorbers. Note that the figure has been zoomed in so that the asymmetry can be observed in a clearer way. Introducing the absorbers in order to block wireless signal propagating from certain angles destroyed the symmetric structure of the spectrum to some extent. At this point, it is essential to mention that use of the absorbers to have asymmetric Doppler spectrum does not seem to be the only solution. Based upon the experience of the authors, it was seen that the location of the antenna and the stirrer within the RVC play a role

in shaping the Doppler spectrum as well. Changing the location of the antenna or the stirrer may lead to different Doppler spectrum shapes; however, the use of absorbers may be considered as an option if the measurement setup is not flexible enough allowing such a modification within the RVC. Another important observation of the authors in this section was that the absorbers affect the motion intensity of the environment as well. This may happen if the rays coming from stationary objects and the moving objects are not equally absorbed. Similar results were obtained for 2410MHz case; however, these results are not presented due to space considerations. As a final note, it must be also kept in mind that loading the chamber with lossy materials such as absorbers gives rise to a reduction in its quality factor (Q) increasing Rician K-factor of the wireless communication channel within the RVC [106]. This could also be considered as one of the causes of the change in motion intensity of the environment related to the placement of absorbers within RVC.

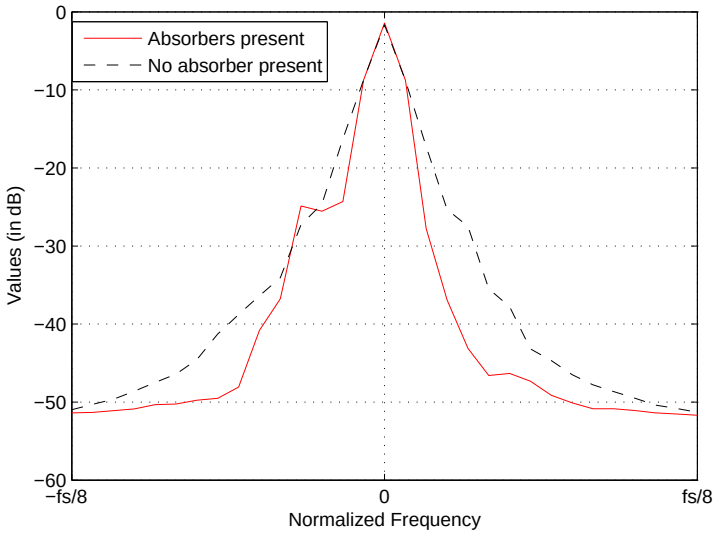

Figure 3.10 Impact of absorbers on Doppler spectrum at 910MHz.

3.5 Discussion

In this section, some main points in the light of the numerical results and of the aforementioned issues will be given.

3.5.1 Effective Factors on Doppler Spectrum

As depicted in Figure 3.6, Doppler can be manipulated by changing several parameters. However, measurement results show that some of these parameters do not yield drastic change in the Doppler behavior. Among these four factors, the operating frequency seems to yield the most drastic change in the Doppler behavior in RVC followed by motion intensity and speed. However, the impact of AOA is not as drastic as those of the remaining three. Furthermore, manipulation of AOA in RVCs requires extra effort with special attention. Note that such an extra effort is not required for the other three factors. This difference between impact of factors is not surprising when the well-known Doppler shift equation $(vf_c)/c$ and (3.6) are considered. Operating frequency, speed, and motion intensity are the direct parameters affecting these two equations. However, AOA is not such a parameter since it rather refers to a statistics whose effect becomes clearer after additional mathematical operations such as averaging and integration over its PDF. Therefore, change in AOA statistics may not yield an impact as conspicuous as the other aforementioned factors.

3.5.2 Realization of Theoretical Doppler Spectrum in RVCs

The result of the experiments has showed that the Doppler spectrum inside an RVC has a good agreement with the motion scenario presented in Section 3.2.2.2. At this point, it would be very interesting to investigate the feasibility of generating Jakes' classical Doppler spectrum that is frequently referred in the literature within RVCs with a rotating stirrer and fixed receiver configuration. Consider the scenario illustrated in Figure 3.11. A scatterer moves along an elliptic path and receiver-transmitter antenna pairs are located at the focal point of this elliptic movement. Since the transmission path from transmitter to receiver does not change instantaneously keeping the phase of the receiver signal the same all the time due to the geometric property of an ellipse, no Doppler is observed at the receiver terminal. This fact suggests that it is possible to control the Doppler behavior by intel-

ligently manipulating the location of transmitter-receiver pairs and the motion pattern of the scatterer.

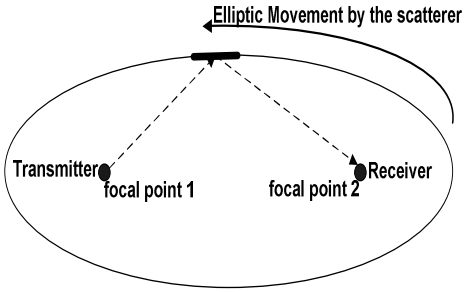

Figure 3.11 Elliptic motion of a scatterer.

Consider the case in which a scattering object is moving in a particular direction as shown in Figure 3.12. If an analysis similar to the one presented in Section 3.2.2.2 is performed, it is seen that the delay on a particular propagation path due to the movement of the reflector, and the corresponding phase change become $2V\Delta t\cos\theta/c$ and $4\pi f_c V\Delta t\cos\theta/c$, respectively. Assuming that the receiver antenna is omnidirectional and θ is uniformly distributed over $(-\pi,\pi]$, the following channel correlation is obtained as a function of time offset Δt:

$$R_h(\Delta t) = \frac{1}{2\pi}\int_{-\pi}^{\pi} e^{j4\pi f_c V\Delta t\cos\theta/c} = J_0(4\pi f_D\Delta t) \tag{3.8}$$

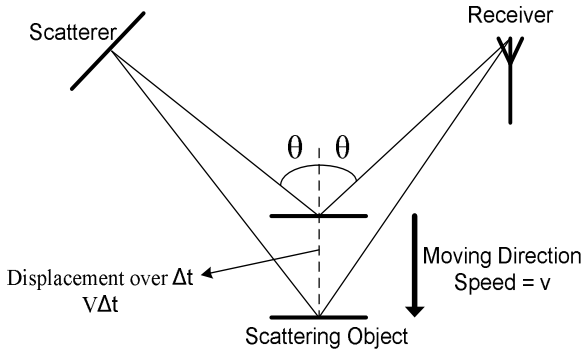

Figure 3.12 Theoretical approximation of classical Jakes' Doppler spectrum within RVCs.

Note that this is very similar to the channel correlation function obtained in Jakes' model given by (3.2). However, it is worth mentioning that the speed of mobile must be halved in order to achieve the same maximum Doppler frequency as the classical Jakes' model. This

channel correlation function is obtained if all the incoming rays arriving at the receiver come from moving objects. This case implies the maximum motion intensity condition in which m is equal to one. Taking m into account in order to consider a ratio between the rays coming from stationary objects and moving objects, the channel correlation function takes the following form:

$$R_h(\Delta t) = (1-m) + m\frac{1}{2\pi}\int_{-\pi}^{\pi} e^{j4\pi f_c V \Delta t \cos\theta/c} = (1-m) + mJ_0(4\pi f_D \Delta t) \tag{3.9}$$

It is practically very difficult to design an environment with m equals one with fixed receiver and surrounding objects in motion. However, the motion intensity of the wireless propagation environment within the RVC can be increased by placing more moving objects inside as shown in Section 3.4.2.

Figure 3.13 shows the classical Doppler spectrum and the Doppler spectrum which is obtained from the model depicted in Figure 3.12 with the same constant speed value. It is seen that by intentionally aligning the direction of the moving objects with respect to the transmit and receiver antennas, classical Jakes' spectrum may be approximated. However, an impulse at the zero frequency is always observed due to the rays coming from stationary objects. The power of this impulse may be reduced by increasing the motion intensity of the environment, i.e. introducing more moving objects. It is also seen that the maximum Doppler frequency obtained due to the motion of the surrounding objects is twice the classical Jakes' shape with the same speed value.

It is theoretically shown that it is possible to approximate classical Jakes' spectrum; however, the practical verification needs some technical capability. In summary, it is concluded that the classical Jakes' spectrum can be generated within an RVC by intelligently adjusting the motion pattern as well as the location of the transmitter-receiver antenna pairs.[3]

[3]It must be kept in mind that this may even require a change in the movement pattern of the stirrer from circular to linear motion.

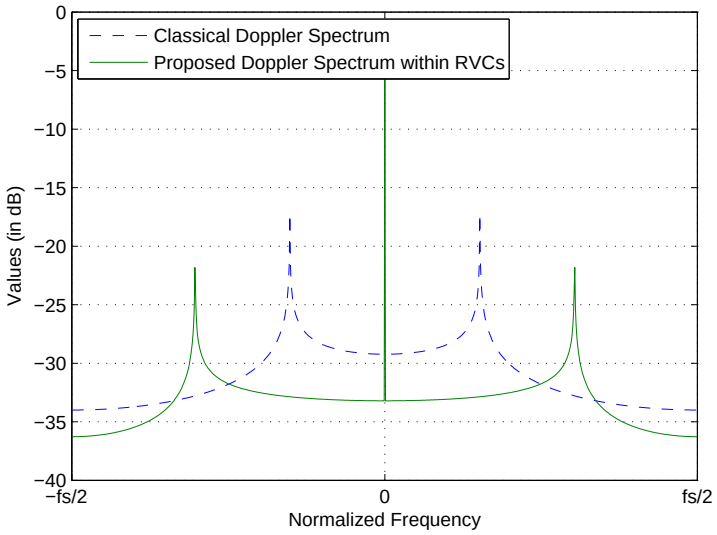

Figure 3.13 Obtaining Jakes' classical Doppler spectrum with fixed receiver configuration.

3.6 Concluding Remarks

It is known that characterization of wireless propagation channel is key to a successful wireless communication system design and implementation. Since mobility lies in the heart of the wireless communications, mobility related parameters should be well understood. For this purpose, further investigation on mobility by performing various experiments and field tests is essential. From these perspectives, RVCs seem to be a promising test bed due to its experiment related flexibilities. In wireless community, the word "mobility" is generally interpreted as the displacement of either receiver or transmitter. However, this study shows that a more comprehensive characterization is possible by considering the motion in a particular environment including the transmitter and receiver within.

In this study, Doppler phenomenon caused by motion is investigated in RVCs by elaborating the key factors such as operating frequency, speed, AOA. In addition, motion intensity which can be considered as a formal generalization of wireless channel mobility characteristics is introduced and its consequences are discussed.

Also, a very well-known Jakes' Doppler model is compared with the experimental findings. It is observed that there is a significant discrepancy between Jakes' model and the

experimental results obtained. It is shown and theoretically explained that the main reason for this discrepancy is not the dimensional assumptions in signal propagation as reported in the earlier studies in the literature. It is found out that the discrepancy is more related to the motion scenario in the propagation environment. Although the analysis of an RVC with fixed transmitter-receiver pair has shown that the realization of Jakes' spectrum is difficult to achieve, it can still be approximated under certain conditions when motion of the scatters is controlled in a specific way.

Although it is obvious that the field tests yield the most reliable results regarding the performance of wireless communication systems, concerns including cost and time consumption while performing these tests force to have alternative approaches. RVCs are promising candidates in this aspect. However, the main hurdle for RVCs to be a reliable replacement to field tests lies in their design. Therefore, RVC design should be improved in a sense that it is capable of emulating various motion scenarios with minor modifications.

CHAPTER 4

ARTICULATING FACTORS DEFINING RMS DELAY SPREAD IN LV PLC NETWORKS

4.1 Introduction

Communication over the power line network (PLN) referred as power line communication (PLC) is recently gaining significant momentum for various communication applications such as smart grid, Internet, data and voice transmission [108]. PLC is very promising for many communication applications in the sense that the communication medium is based on the use of an existing infrastructure in a very extensive network that virtually reaches anywhere in the world. Design purpose of the PLNs is the transmission of power from one point to another and conveying the high frequency communication signals is not the actual reason behind its existence. Therefore, PLN is considered to be a very harsh communication medium such that PLC systems must tackle various challenges such as noise and multipath in order to ensure reliable communication.

Future PLC based systems are envisioned to provide very high data rates requiring wideband to support high–quality multimedia. The popularity of wideband PLC especially in low voltage (LV) networks for last–inch applications is growing [109, 110]. In wideband communication channels, multipath induced inter-symbol interference (ISI) is one of the phenomena that leads to performance degradation. In communications community, significance of ISI is quantified by a parameter called root-mean-squared (RMS) delay spread. In a nutshell, the RMS delay spread indicates the capability of the communication channel of supporting high data rate communications by implying the probability of performance degradation which may occur due to the ISI as a result of multipath signal propagation.

Understanding the RMS delay spread in PLC channels is crucial from many aspects. For instance, the driving technology in PLC applications requiring wideband is overwhelmingly considered to be orthogonal frequency division multiplexing (OFDM) due to its inherent advantages [108]. Cyclic prefix is employed in OFDM systems in order to combat multipath related ISI and RMS delay spread of the communication channel is considered while determining the duration of the cyclic prefix [111]. The apparent relation between RMS delay spread and the cyclic prefix in OFDM systems is one of the considerations that favors the idea of looking into RMS delay spread of LV PLC channels in a more detailed way. In PLC systems, the RMS delay spread depends on the following factors:

- frequency-distance dependent cable attenuation
- loading condition, that is the impedances of the electrical loads appearing at termination points
- physical characteristics of the operating PLC medium

The aim of this chapter is to investigate and explain statistically the impact of these factors on the RMS delay spread value of LV PLC networks.

Based on extensive measurements, frequency–distance dependent attenuation in LV PLC networks is defined as [69]

$$A(f,d) = \exp\big((-a_0 - a_1 f^k)d\big), \tag{4.1}$$

where f and d correspond to frequency of the signal and the distance covered, respectively. a_0, a_1, and k are all cable dependent parameters and are mostly extracted by empirical measurements [69]. a_0, a_1, and k are considered to be time invariant, *i.e.* fixed parameters for a PLC network. Hence, attenuation defined by (4.1) does not cause any time variation in the RMS delay spread for a given topology. Unlike the first factor listed above, loading in LV PLC networks is time varying. Branches in the network are terminated with various electrical loads with different impedance characteristics. The loading condition of

the network may change throughout the day. Hence, RMS delay spread of the LV PLC networks may change significantly as the impedances seen at the termination points change even the considered network topology is fixed. In addition, even if the loading condition is not altered, the dependency of the load impedances on the Alternating Current (AC) mains cycle [80] gives rise to a cyclic change in the RMS delay spread of PLC channels. Indeed, several studies performed earlier noticed this relation between RMS delay spread and loading by considering some specific topologies [70, 71]. An excerpt taken from [71] says:

"It has been shown the maximum delay spread occurs for cases when the channel is terminated either in low impedances or high impedances"

Some other studies available in the literature implicitly express this fact by calling the open circuit condition at termination points as the worst case scenario [72]. Findings of this study will naturally shed some light on these statements extensively encountered in the PLC community through the establishment of a mathematical background while the impact of loading is examined. In addition, PLC systems are deployed on PLNs possessing different physical characteristics. Number of branching nodes between transmitter and receiver, length statistics of branches, and statistics regarding the number of branches extending from each branching node are some of the characteristics which may significantly differ from network to network. Depending upon the communication application and deployment condition, distance between transmitter and receiver is another parameter which may also change. These different attributes of the PLNs give rise to a change in the multipath profile of the communication channel between transmitter and receiver leading to a change in the RMS delay spread values. Revealing the relation between these physical characteristics of PLNs and the RMS delay spread is another objective of this study.

The remainder of the chapter is organized as follows. Section 4.2 gives the analytical background for the multipath propagation model in PLC channels and defines RMS delay spread. Section 4.3 discuses impact of attenuation and loading on the RMS delay spread in PLC channels. Section 4.4 provides the details on the relation between the physical

characteristics of PLC channels and RMS delay spread. Finally, the concluding remarks are given in Section 4.5.

4.2 PLC Multipath Channel Model and RMS Delay Spread

When a signal is transmitted on the power line conductors, the signal received at the receiver consists of attenuated, delayed, and phase-shifted replicas of the transmitted signal. If the total number of received signal replicas are considered to be limited to N, a complete characterization of the PLC channel can be given by its channel frequency response (CFR) as follows: [69]

$$H(f) = \sum_{i=0}^{N} \Big[\prod_{k=1}^{K} \Gamma_{ik} \prod_{m=1}^{M} T_{im} \Big] A(f, d_i) \exp(-j2\pi f \tau_i), \tag{4.2}$$

where Γ and T correspond to the reflection and transmission coefficients along the propagation path, respectively, $A(f, d_i)$ means the frequency–distance dependent attenuation stemming from the physical characteristics of the cable used in the network and given by (4.1), and $\exp(-j2\pi f \tau_i)$ refers to the phase of the ith component due to the time delay. Finally, K and M represent the number of reflection and transmission coefficients experienced by a propagating signal along a particular path denoted by the subscript i. Multiplication of reflection (Γ) and transmission (T) coefficients leads to a parameter which is called reflection factor in the literature. Reflection factor, denoted as $|r_i|exp(j\theta_i)$ for a certain path implied by the subscript i, is usually but not necessarily a complex number. It accounts for the losses inflicted upon the transmit signal due to physical characteristics of the PLC environment. It is clear from (4.2) that the accurate computation of the reflection factors (reflection and transmission coefficients) is essential for a true characterization of the PLC channel. In PLC systems, a transmit signal propagating from one location to another suffers reflections at impedance discontinuities along its path to the receiver. Due to these impedance mismatches, some part of the signal is reflected back towards the source, whereas some proceeds to the destination. Reflection coefficient Γ articulates the amplitude/phase ratio between the reflected signal and the incident signal, whereas transmission coefficient T

implies the amplitude/phase relation between the proceeding signal and the incident signal. Reflection and transmission coefficients at a particular impedance discontinuity for a cable with characteristic impedance Z_0 is given by the following equations [112]:

$$\Gamma = \frac{Z_L - Z_0}{Z_L + Z_0} \text{ and } T = 1 + \Gamma, \tag{4.3}$$

where Z_L refers to the impedance that the signal sees at a discontinuity. Since branching and impedance appearing at the termination points are the main reason behind the impedance discontinuity for homogeneous PLNs which are to be considered in our study, it is worth taking a closer look at the calculation of the reflection and transmission coefficients at these instants as illustrated in Fig. 4.1.

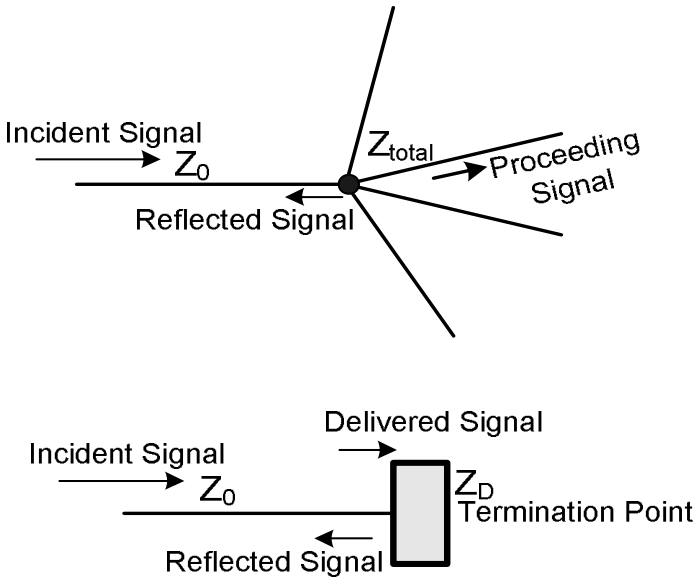

Figure 4.1 Reflection/Transmission coefficients at branching and termination.

4.2.1 Reflection/Transmission Coefficient at Branching

At a branching node, calculation of reflection/transmission coefficient is based on treating each branch extending from the node as parallel connection. If a homogeneous network with a particular cable impedance Z_0 is assumed, it is easy to show that the impedance seen

by the incident signal arriving at a branching node is given by the following expression:

$$Z_{total} = \frac{Z_0}{n-1}, \tag{4.4}$$

where n is the total number of branches extending from a node including the branch on which the incident signal propagates. [1] By using (4.3), it can be easily shown that reflection and transmission coefficients are given by,

$$\Gamma = \frac{Z_{total} - Z_0}{Z_{total} + Z_0} = \frac{2-n}{n} \text{ and } T = \Gamma + 1 = \frac{2}{n}, \tag{4.5}$$

4.2.2 Reflection/Transmission Coefficient at Termination Points

In a similar fashion, reflection/transmission coefficient at a termination node can be computed as follows:

$$\Gamma = \frac{Z_D - Z_0}{Z_D + Z_0} \text{ and } T = \Gamma + 1 = \frac{2Z_D}{Z_D + Z_0}, \tag{4.6}$$

where Z_D denotes the impedance seen by the incident signal at the termination point. Note that the incident wave is fully reflected in case the termination point is open or short with the same amplitude but 180° of phase difference. In case a device is connected to the termination point, then impedance of the corresponding device must be taken into consideration while computing reflection/transmission coefficients. Signal passes through many impedance discontinues and experiences multiple reflections on its way to the receiver in a PLC network. Reflection factor, that was previously mentioned while introducing the multipath characteristics of PLC channels, represents the total effect of all these reflection/transmission coefficients on the propagating signal.

[1] Note that 3 is the minimum value that n can assume to ensure branching keeping in mind that a node should have at least one branch for arriving signal and one branch for proceeding signal.

If inverse fast Fourier transform (IFFT) operation is applied on CFR given by (4.2), channel impulse response (CIR) is obtained as follows:

$$h(\tau) = \sum_{j=0}^{R} h_j \delta(t - \tau_j), \tag{4.7}$$

RMS delay spread is derived from the CIR and defined as: [47]

$$\tau_{rms} = \sqrt{\frac{\sum_{j=0}^{R} \tau_j^2 |h_j|^2}{\sum_{j=0}^{R} |h_j|^2} - \Big(\frac{\sum_{j=0}^{R} \tau_j |h_j|^2}{\sum_{j=0}^{R} |h_j|^2}\Big)^2}, \tag{4.8}$$

where R is the number of paths considered in the calculation and usually determined by thresholding as will be clear in the forthcoming sections. It is worth mentioning that delay of the first arriving path, which is denoted as τ_0, is aligned to zero before computation.

So far, signal propagation and multipath characteristics of PLC channels as well as the computation of the RMS delay spread are elaborated. These concepts are important in a sense that they form a basis for our future discussions. From this point on, our discussion will be extended to the RMS delay spread and the factors that characterize it in PLNs.

4.3 Impact of Attenuation and Loading on RMS Delay Spread

Our initial objective is to understand the impact of attenuation and loading on the RMS delay spread. T-network is the main PLC topology in LV PLC networks that is usually taken into consideration. Multipath phenomenon was first elaborated by considering a T-network topology in [69]. Similarly, signal reflections are analyzed by considering this fundamental topology structure in [113]. Its popularity in PLC channel analysis stems from the fact that it forms a basis for more complex LV networks in a way that these complex networks can be decomposed into different connections of T-network structure [69, 113]. Stemming from the fact that our initial objective is to investigate the impact of attenuation and loading on the RMS delay spread, physical characteristics of PLC channels will be isolated from our

analysis and popularly used T-network topology, being a more controlled environment, will be utilized in line with the previous studies.

T-network topology is depicted in Fig. 4.2. It is composed of three branches connected to node B with the length of d_1, d_2, and d_3. A denotes the point where the signal is injected into the network, and D is the point where the signal is received. Consideration of the homogeneous network structure in which all the branches have the same characteristic impedance Z_0 is one of the assumptions made for the ease of analysis. In addition, A and D are assumed to be matched to Z_0 for the sake of simplicity, hence B and C are the only sources of reflection in the topology.

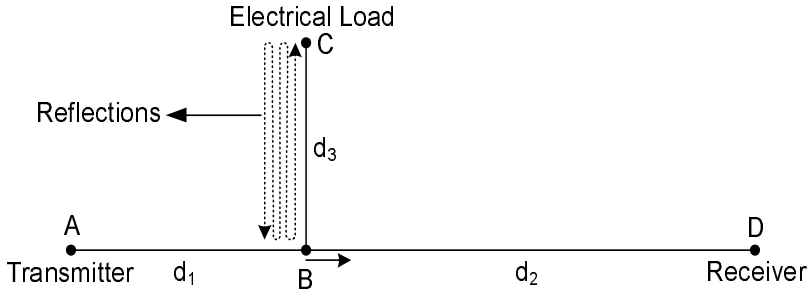

Figure 4.2 T-network topology.

Reflection and transmission coefficients at node B (Γ_b, T_b) and C (Γ_c, T_c) for this particular network topology are given by (4.5) and (4.6) for $n = 3$. Note that Z_D in (4.6) refers to impedance of the electrical load connected to node C.

Following the discussion on PLC channel and RMS delay spread given in Section 4.2, it is now convenient to articulate why the first two factors (attenuation and loading) that are listed in the beginning of the chapter play a role in the RMS delay spread of PLC channels. Recall that the RMS delay spread of a communication channel is computed by aligning the first arriving path to zero delay. Upon this alignment, the number of paths to be included in the RMS delay spread computation, which is R as can be seen in (4.8), is determined by applying a threshold considering the maximum power value in the delay profile. With this threshold so determined, the paths with the power values below are considered to be noise and excluded from the analysis. With the explanation given, the impact of attenuation on

RMS delay spread can be explained by an example. Considering the T-network topology given in Fig. 4.2, assume that only two paths satisfy the threshold condition. So, these paths should naturally follow the following paths: A-B-D (at τ_0) and A-B-C-B-D (at τ_1). Assume that d_3 is slowly increased. Note that this change in the topology does not lead to any change in either τ_0 or in the power of the first arriving path since $d_1 + d_2$ stays the same. However, this affects the second arriving path in a way that it arrives at a later delay with a smaller value of power due to the attenuation which increases with distance. The attenuation may reach at a point (as $d_3 \rightarrow \infty$) at which the threshold condition is not satisfied even for the second arriving path leading us to consider it as a part of background noise in the computation of RMS delay spread. Disappearance of a particular path from delay profile (or arriving at a larger delay) leads to a change in the RMS delay spread value as can be clearly seen from (4.8).

The second factor given in the beginning of the chapter, which is the loading, determines Γ's and T's in (4.2). Therefore, any change in the loading condition leads to a change in Γ's and T's in the network and results in a change in the RMS delay spread. Recall also that even if the loading condition is not altered, the dependency of the load impedances on the AC mains cycle [80] gives rise to a cyclic change in the RMS delay spread of PLC channels. If the term, $A(f, d)$ in (4.2) is ignored in order to isolate ourselves from the effect of attenuation and solely focus on the impact of loading, (4.2) reduces to the following form:

$$H(f) = \sum_{i=0}^{N} \Big[\prod_{k=1}^{K} \Gamma_{ik} \prod_{m=1}^{M} T_{im} \Big] \exp(-j2\pi f \tau_i), \tag{4.9}$$

If IFFT operation is applied to the CFR, CIR is obtained as follows:

$$h(\tau) = \sum_{i=0}^{N} \Big[\prod_{k=1}^{K} \Gamma_{ik} \prod_{m=1}^{M} T_{im} \Big] \delta(t - \tau_i), \tag{4.10}$$

Note that the reflection factor of the direct path (A-B-D) is composed of only one term which is the transmission coefficient at B, namely T_b. The reflection factors of other paths consist of Γ_c, Γ_b, and T_b. Based upon this observation, the CIR of T-network topology

assumes the following form:

$$h(\tau) = T_b\delta(\tau - \tau_0) + \sum_{j=1}^{R} T_b\{\frac{2}{n}\}^j\{\frac{2-n}{n}\}^{j-1}(\Gamma_c)^j\delta(\tau - \tau_j), \tag{4.11}$$

where R refers to the number of reflections considered between B and C.

The graphical illustration of the amplitude of (4.11) is given in Fig. 4.3. As can be seen, amplitude of the signal components decreases with increasing delay. This is due to the fact that power of the signal reduces as it passes through more reflection points on its way to the receiver even though the attenuation effect is not accounted for. Taking the attenuation into consideration, amplitude of each component should be even smaller. Therefore, the RMS delay spread values obtained from Fig. 4.3 are pessimistic since the effect of attenuation especially for late arriving paths is not accounted for. However, this will not affect our conclusions since our focus is on the impact of loading rather than attenuation.

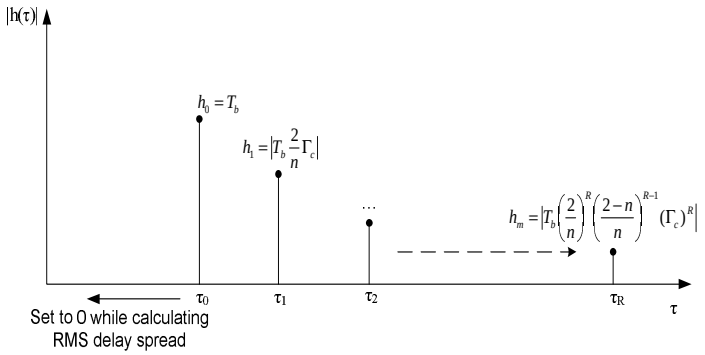

Figure 4.3 Graphical representation of the CIR for T-network topology.

For the purpose of mathematical tractability, if two of the delays (τ_0 and τ_1) along the delay axis are considered ($R = 1$) in Fig. 4.3, using (4.8) and (4.11) the RMS delay spread τ_{rms} takes the following form:

$$\tau_{rms} = \tau_1\frac{2n|\Gamma_c|}{n^2 + 4(\Gamma_c)^2} = \tau_1\frac{6|\Gamma_c|}{9 + 4(\Gamma_c)^2}, \tag{4.12}$$

Note that (4.12) depends on two parameters which are τ_1 and the reflection coefficient Γ_c. When τ_0 is set to 0, time delay τ_1 for the second arriving path is expressed as

$$\tau_1 = \frac{2d_3}{v} = \frac{2d_3\sqrt{\epsilon_r}}{c_0}, \tag{4.13}$$

where ϵ_r is the dielectric constant of the insulation material and c_0 is the speed of light in vacuum.

Referring back to (4.3), Γ_c being the reflection coefficient at node C depends on the impedance of the electrical device Z_D connected to the network which is regarded as a random variable (RV) in this study for generalization so that various loading conditions can be taken into account. If C is assumed to be left open ($Z_D = \infty$), Γ_c becomes 1. Γ_c becomes -1 if a short circuit assumption ($Z_D = 0$) is considered at node C. These two scenarios correspond to two extreme cases. Therefore, it is expected that any electrical device connected to node C yields a reflection coefficient between the values generated by these extreme cases, -1 and 1. These two values are also the maximum and minimum values of Γ_c during an AC cycle duration even if the electrical load connected to node C is unchanged.

In order to understand the impact of loading on the RMS delay spread τ_{rms}, we have to derive the probability density function (PDF) of the variable

$$\psi = \frac{6|\Gamma_c|}{9 + 4(\Gamma_c)^2}, \tag{4.14}$$

Before proceeding with the statistical characterization of ψ, some important observations should be made regarding its behavior. ψ has the following characteristics:

- monotonically increasing for $0 < \Gamma_c \leq 1$
- monotonically decreasing for $-1 \leq \Gamma_c < 0$
- has a critical point at $\Gamma_c = 0$

Proof of these observations can be given as follows. ψ takes the following form within this interval $0 < \Gamma_c \leq 1$

$$\psi = \frac{6\Gamma_c}{9 + 4(\Gamma_c)^2}, \tag{4.15}$$

The derivative of ψ with respect to Γ_c is given by

$$\frac{d\psi}{d\Gamma_c} = \frac{54 - 24(\Gamma_c)^2}{(9 + 4(\Gamma_c)^2)^2}, \tag{4.16}$$

Since $\frac{d\psi}{d\Gamma_c} > 0$ for $0 < \Gamma_c \leq 1$, ψ is a monotonically increasing function within this interval.

Similarly, the derivative of ψ with respect to Γ_c within the interval $-1 \leq \Gamma_c < 0$ is given by

$$\frac{d\psi}{d\Gamma_c} = \frac{-54 + 24(\Gamma_c)^2}{(9 + 4(\Gamma_c)^2)^2}, \tag{4.17}$$

Since $\frac{d\psi}{d\Gamma_c} < 0$ for $-1 \leq \Gamma_c < 0$, ψ is a monotonically decreasing function within this interval.

Equating (4.16) and (4.17) shows that ψ has a critical point at $\Gamma_c = 0$ where the function may have a minimum or maximum. However, it is easily seen from the first and second claims that $\Gamma_c = 0$ minimizes ψ. It is also worth mentioning that $|\Gamma_c| = 1$ maximizes ψ considering its behavior on the intervals analyzed.

An alternative insight into the observations presented above can be given in this way. $\Gamma_c = 0$ corresponds to the case in which the impedance of the electrical device connected at node C matches the impedance of the cable Z_0. This case implies that no reflection occurs at C leaving only one propagation path between A and D. Disappearance of the other signal components along the delay axis in Fig.4.3 gives rise to minimum value of the RMS delay spread, hence ψ. Other values of $\Gamma_c \neq 0$ lead to the reception of several signal components from other propagation paths along with the direct path. This phenomenon leads to an increase in the value of the RMS delay spread, hence ψ. First and the second claims are details of this observation. Claims derived from our analytical analysis also shed

some light on the statements that are encountered frequently in the literature as mentioned in the beginning of the chapter. As empirically concluded in the previous studies and mathematically shown here, open/short circuit condition at the termination point leads to the maximum value of RMS delay spread, whereas its minimum value is obtained if the termination points are matched to the network cable impedance. This also validates the reason why open/short circuit condition at termination points of LV PLC channels is considered as the worst case scenario from the perspective of multipath signal propagation.

Referring back to the statistics of ψ, several PDFs can be offered in order to characterize the statistical behavior of Γ_c. Extracting the statistics of device impedances that are widely used in LV networks and building a statistical model would be very desirable. Since no such a study is available in the literature, Γ_c is assumed to be uniformly distributed over [−1,1]. By using the fundamental theorem for functions of one random variable [114] and employing change of variables $Y = |\Gamma_c|$, the PDF of (4.14) can be expressed as follows:

$$f_\psi(\psi) = \frac{\Big(36\psi^2 + (3 - 3\sqrt{1-4\psi^2})^2\Big)^2}{24\psi^2\Big(36\psi^2 - (3 - 3\sqrt{1-4\psi^2})^2\Big)}, \quad 0 < \psi < \frac{6}{13} \tag{4.18}$$

Integrating (4.18) leads to the cumulative distribution functions (CDF) of ψ. CDF can be calculated by changing the variable $cos(\theta) = \sqrt{1-4\psi^2}$. After a series of cumbersome mathematical operations that are skipped here for the sake of brevity, CDF is computed as

$$F_\psi(\psi) = \frac{3}{2} tan\Big(\frac{arcsin(2\psi)}{2}\Big), \quad 0 < \psi < \frac{6}{13} \tag{4.19}$$

Figures 4.4 and 4.5 show the PDF and CDF of ψ. It is clearly seen that analytical derivations and simulation results are in good agreement. Curves are also seen to be in good agreement with the lemma provided. For instance, plugging $|\Gamma_c| = 1$ into (4.14) for the purpose of maximization yields 6/13. Due to the maximization, ψ must never exceed 6/13 and it is seen from Fig. 4.5 that this observation is satisfied.

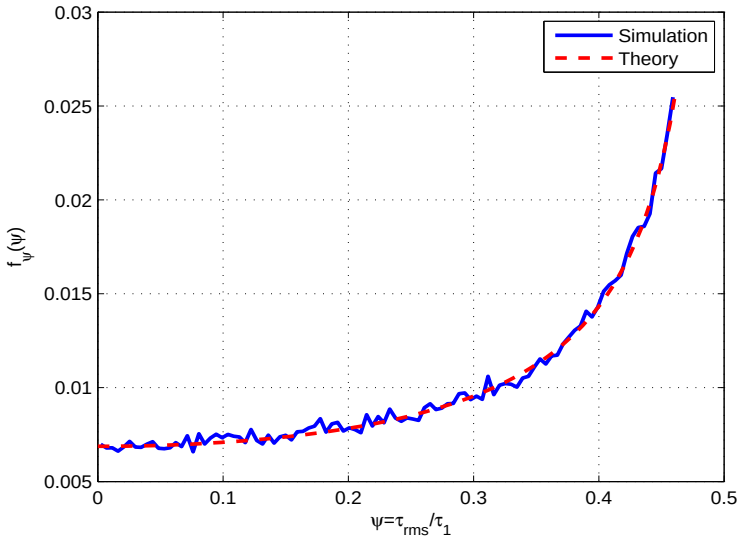

Figure 4.4 PDF of the RMS delay spread of T-network topology when node C is randomly loaded.

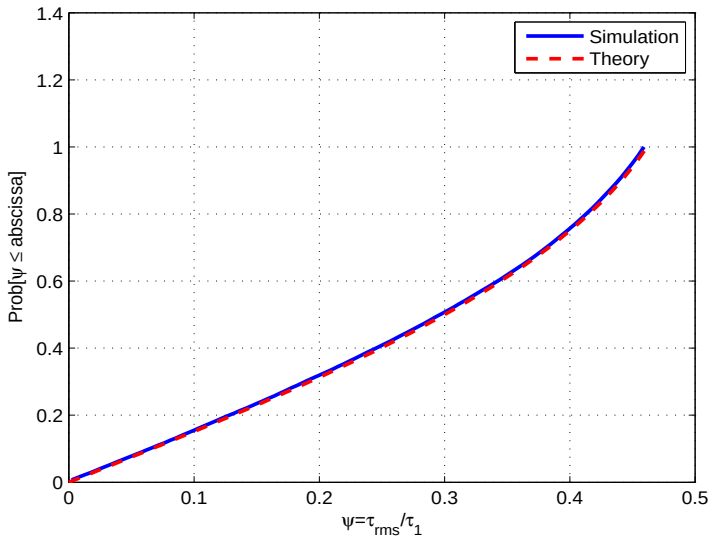

Figure 4.5 CDF of the RMS delay spread of T-network topology when node C is randomly loaded.

Impact of attenuation and loading on the RMS delay spread is detailed in this section. Subsequently, impact of the physical characteristics of the PLC operating environment will be our focus.

4.4 Impact of the Physical Characteristics of the PLC Channel on RMS Delay Spread

PLC systems may be deployed on LV PLC environments having entirely different physical characteristics. Among these characteristics, impact of the following items on the RMS delay spread will be addressed in this section:

- number of branching nodes between transmitter and receiver
- distance between transmitter and receiver
- length statistics of branches

It is obvious that the analysis that we plan to perform in this section requires the establishment of more complicated PLC networks than the T-network topology utilized in Section 4.3. Modeling PLC systems and building simulation techniques for them have been the focus of several studies earlier in the literature. The model which considers the PLC channel as a multipath communication environment was first introduced in [69] as mentioned earlier. Based upon this multipath consideration, analytical calculation of the multipath components by describing the PLC channel via a set of matrices is proposed in [115, 116]. PLC models that are based on treating the transmission line as a two-port device are available in the literature as well [117, 118]. A channel model and a simulation platform along with the results of various channel measurement campaigns are discussed in [79, 119]. A statistical PLC channel characterization regarding attenuation, multipath related parameters, etc. is presented in [78, 120]. In our analysis, the matrix based PLC simulation technique proposed in [115] will be considered as the basis. However, matrices introduced in [115] are to be modified in a way that the simulation module lets us easily generate PLC networks with different physical characteristics. In line with the procedure described in [115], generated PLC network topology, which is illustrated in Fig. 4.6, is

mapped into a single matrix as follows:

$$\mathbf{C}_{[(\mathrm{t+b})\mathrm{x}(\mathrm{t+b})]} = \begin{bmatrix} 0_{[txt]} & CT_{[txb]} \\ CT^{T}_{[bxt]} & CC_{[bxb]} \end{bmatrix}, \tag{4.20}$$

where t and b correspond to the number of termination points and branching points (referred to as internal nodes in [115]), respectively. CC is the submatrix which describes the interconnections among branching nodes. CT shows the connections between branching nodes and termination points. The corresponding length of each interconnection and impedances at termination points are kept in separate matrices. In order to isolate our analysis from the impact of impedance variation that was discussed in Section 4.3 and focus solely on the impact of physical characteristics of the environment, it is assumed that the termination points are open circuit. In addition, number of branches extending from each branching node is considered to be uniformly distributed over [3,6] in the simulations. Similar to the analysis performed in Section 4.3, transmitter and receiver are also assumed to be matched to the characteristic impedance of the homogeneous PLC network. Impact of physical attributes is statistically investigated by generating 20000 realizations of PLC network for each case taken into consideration. PLC topologies with different physical attributes are generated by manipulating the values of t, b, and the length matrix whose elements are composed of the values l_{ij} shown in Fig. 4.6. Note that a change in the topology gives rise to a change in the values of t and b which results in a change in the dimensions of the submatrices denoted as CC and CT. For each realization, CIR was calculated by taking the IFFT of CFR given by (4.2). After CIR is obtained, procedure described in Section 4.2 is followed with the threshold value of 20dB while computing the RMS delay spread.

The impact of number of nodes between transmitter and receiver on the RMS delay spread can be seen in Fig. 4.7. While deriving this figure, transmitter–receiver separation distance and length statistics of the branches are considered to be 150m and U[10m-30m][2], respectively. Upon the analysis performed, it is concluded that an increase in the number

[2]U refers to uniform distribution.

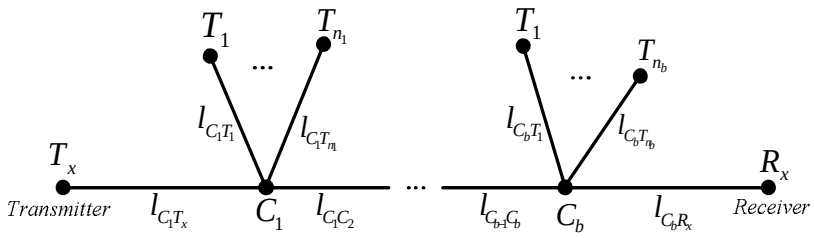

Figure 4.6 Graphical illustration of the PLC network topology considered in the study.

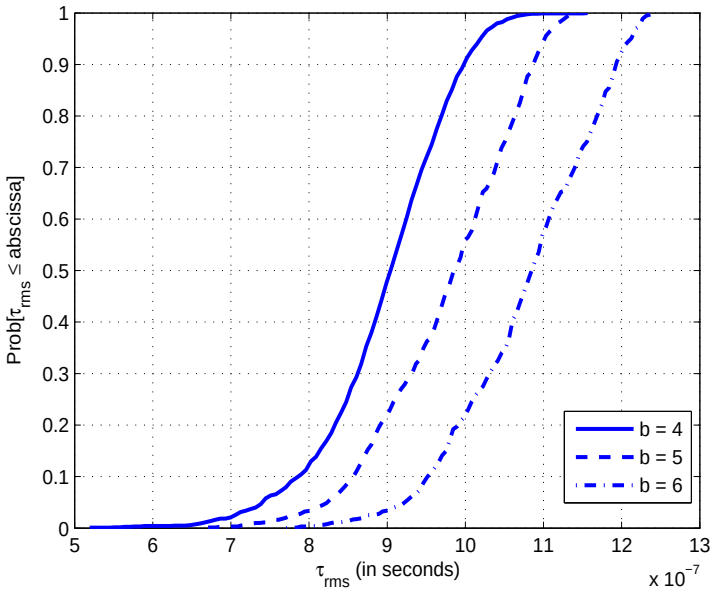

Figure 4.7 Dependency of RMS delay spread (τ_{rms}) on the number of nodes (b) between transmitter and receiver when separation distance between transmitter and receiver is 150m and branch lengths are assumed to be uniformly distributed over [10m-30m].

of nodes while keeping all the other effective physical attributes of the PLC network the same gives rise to an increase in its RMS delay spread value. This behavior can be related to the multipath components arriving at larger delays as b is increased. This relation was previously noticed in [70] by considering some specific PLC network topologies. Our findings verify the results of this earlier study by taking more general PLC network scenarios into account. Fig. 4.8 shows the impact of transmitter–receiver separation distance on τ_{rms}. Similar to the previous case analyzed, increasing separation distance between transmitter and receiver leads to the reception of multipath components at larger delays leading to an

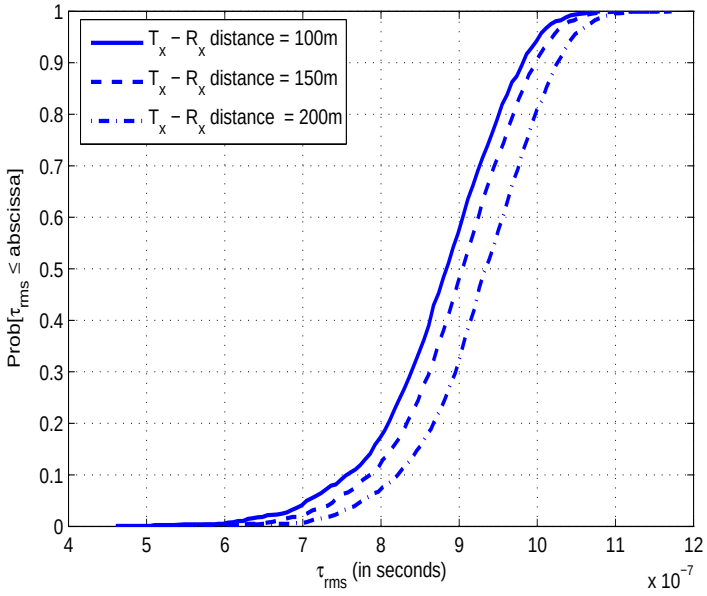

Figure 4.8 Dependency of RMS delay spread (τ_{rms}) on the separation distance (d) between transmitter and receiver when number of nodes between transmitter and receiver is 4 and branch lengths are assumed to be uniformly distributed over [10m-30m].

increase in τ_{rms} values. Finally, the impact of branch length statistics is seen in Fig. 4.9. Among all of these aforementioned factors, change in the length statistics of branches seems to yield the most drastic change in τ_{rms} values. This is expected since expanding the range of values that branch lengths may assume increases the probability that some multipath components arrive at larger delays. If the effect of attenuation is not significant within the length range considered, it should naturally result in higher τ_{rms} values as can be seen in the figure.

4.5 Concluding Remarks

Trend in PLC indicates that the future applications will need more bandwidth and higher data rates to address user requirements. This growing interest into PLC entails a good understanding of its channel characteristics. RMS delay spread which is frequently used in communications community while quantifying multipath characteristics of communication channels was the focus of this study. Factors, which have a significant impact on

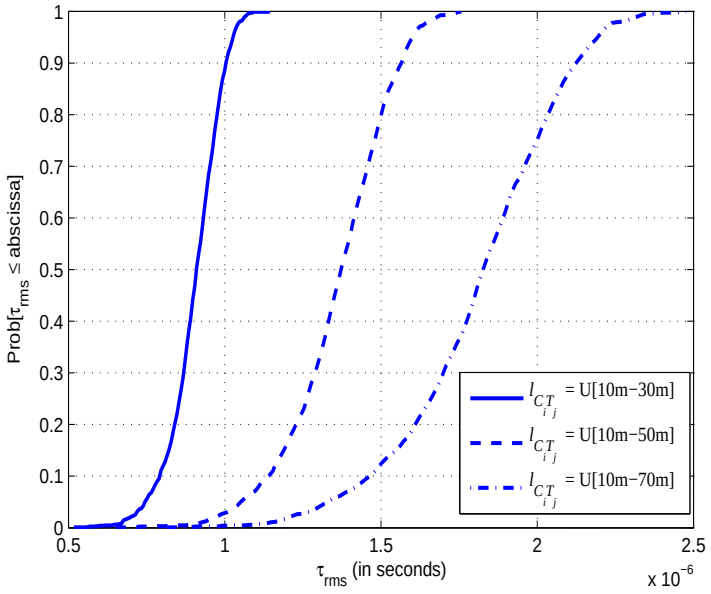

Figure 4.9 Dependency of RMS delay spread (τ_{rms}) on the length statistics of branches when number of nodes between transmitter and receiver is 4 and separation distance between transmitter and receiver is 150m.

the RMS delay spread, peculiar to PLC channels were elaborated in a detailed way. Among these factors, impact of attenuation and loading was discussed by exploiting T–network being the most fundamental LV PLC topology that is frequently used in the literature. The relation between attenuation and loading to the RMS delay spread was explicitly demonstrated and compared with the results already present in the literature. Next, impact of the physical characteristics of PLC channels on the RMS delay spread was studied. Number of nodes between transmitter and receiver, transmitter–receiver separation distance, and length statistics of branches are identified as the physical characteristics which may significantly change from one PLC network to another. A matrix based simulation technique was employed while generating PLC network topologies with distinct physical characteristics. For each attribute examined, statistics regarding the RMS delay spread were presented by observing corresponding CDF curves. Based upon the results of extensive simulations, important conclusions regarding the relation between these attributes and the RMS delay spread were drawn.

CHAPTER 5

STATISTICAL CHARACTERIZATION OF THE PATHS IN MULTIPATH PLC CHANNELS

5.1 Introduction

Multipath propagation and the noise are the two factors that play an important role in the quality of received signal in power line communication (PLC) systems. The former is related to the impedance discontinuities and corresponding reflections in the PLC network, whereas the latter stems from the presence of undesired disturbances in the communication medium. Both of these subjects drew considerable attention from the researchers especially after the promising features of power line networks (PLNs) for communication purposes are recently rediscovered. The focus of this study among these two topics will be on the multipath phenomenon in PLC channels.

The multipath characteristics of the PLC communication environment have been the focus of several publications earlier in the literature. Multipath model for PLC channels is first elaborated in [69]. A matrix based algorithm for the calculation of multipath components in PLC networks is given in [115, 121, 122]. Channel characterization of indoor PLNs with various loading conditions is investigated in [70]. Similarly, the impact of load impedances which are classified as high resistive, low resistive, and inductive, line length and branching to the multipath characteristics of the PLC channel is analyzed in [123, 124] by studying certain scenarios. PLC channel models that are based on treating the transmission line as a two-port network are available in the literature as well [117, 118, 125, 126]. All of these studies presented as the prior art form an analysis platform for PLC environments with exactly known characteristics leading to site-specific information. Our

aim in this chapter will be the establishment of a statistical model for the behavior of the received signal in PLC environments in order to avoid this site-specific information and to draw more general conclusions. In order to do that, the PLC network will be treated as an unknown communication environment except for some high-level attributes. The fact that no communication system can be built based upon site-specific information is the main motivation behind this study.

In line with our objective, although not so many papers are available in the literature, some other studies aim at modeling the PLC channels statistically based upon the results derived from measurement campaigns [78]. Path arrival times and amplitudes are investigated particularly for narrow band channels in [72]. The authors approach is based on defining the path arrival times as Normally distributed. This definition for path arrival times leads to the characterization of path amplitudes as log-Normally distributed although its relation to the PLC network topology is not articulated.

As stated earlier, impedance discontinuities in the PLNs lead to the multipath propagation phenomenon. Impedance of the electrical loads and the branching are the main causes of impedance discontinuities in PLC networks. The significance of the impact of the impedance discontinuity on the transmit signal may only be revealed by having an exact knowledge of the impedances at the corresponding discontinuity locations. Possession of this information is very unlikely considering the variety of electrical loads with different impedance characteristics that can be connected to the medium as well as the differences in PLC network topologies leading to different branching structures. Therefore, considering these two parameters as the high-level attributes of the PLC communication medium and approaching the problem by employing statistical tools seem to be appropriate. As mentioned earlier, this will help us reach more general conclusions regarding the performance of communication systems by avoiding network-specific analysis.

As a result of the multipath propagation, received signal in power line communication systems consists of the replicas of the transmit signal. Among these received replicas, knowledge on the first arriving path behavior is important since it reaches the receiver with

the highest power level making it more detectable for receivers. This basically results from the relatively low frequency-and-distance dependent attenuation and the less number of reflections experienced along the propagation path in comparison with the other arriving paths. Stemming from this fact, first arriving path will be considered as the case study and most of the analysis will be focused on its statistics. However, other path statistics as well as some considerations will be touched upon towards end of the section. To sum up, objectives of the study can be listed as follows:

- Understanding the statistics of the paths in PLC networks with a particular emphasis on the first arriving path as well as discussing the impact of finite bandwidth on these statistics.

- Articulating the impact of PLC network attributes on path statistics. Number of branches between transmitter and receiver and number of branches that extend out a branching node are among these network attributes.

5.2 Multipath Propagation and Analysis of the First Arriving Path

In this section, first some mathematical background on the multipath propagation in PLC channels will be given. Next, the discussion will be extended to the analysis of the first arriving path.

5.2.1 Multipath in PLC Channels

When a signal is transmitted on power line conductors, the signal at the receiver consists of attenuated, delayed, and phase-shifted replicas of the transmit signal. If the total number of replicas is considered to be limited to N, a complete characterization of the PLC channel can be given by its channel frequency response (CFR) as follows: [69]

$$H(f) = \sum_{i=0}^{N} \Big[\prod_{k=1}^{K} \Gamma_{ik} \prod_{m=1}^{M} T_{im} \Big] A(f, d_i) exp(-j2\pi f \tau_i), \tag{5.1}$$

where Γ and T correspond to the reflection and transmission coefficients along the propagation path, respectively, $A(f, d_i)$ means the frequency-and-distance dependent path loss stemming from the physical characteristics of the cable, and $exp(-j2\pi f\tau_i)$ refers to the phase of the ith component due to the time delay. Finally, K and M represent the number of reflection and transmission coefficients experienced by the propagating signal along a particular path denoted by the subscript i.

If the term $A(f, d)$ is ignored in order to solely focus on the characteristics of the physical operating environment of the PLC systems, (5.1) reduces to the following form:

$$H(f) = \sum_{i=0}^{N} \Big[\prod_{k=1}^{K} \Gamma_{ik} \prod_{m=1}^{M} T_{im} \Big] exp(-j2\pi f\tau_i), \tag{5.2}$$

If fast Fourier transform (FFT) operation is applied to the CFR, channel impulse response (CIR) is obtained as follows:

$$h(\tau) = \sum_{i=0}^{N} \Big[\prod_{k=1}^{K} \Gamma_{ik} \prod_{m=1}^{M} T_{im} \Big] \delta(t - \tau_i), \tag{5.3}$$

where multiplication of Γ and T in (5.3) is referred as the reflection factor ($|r_i|e^{j\theta_i}$) of a particular propagation path. As can be seen clearly, computation of reflection factor plays an important role in the characterization of PLC channels. With this observation, its characterization along the direct path ($i = 0$) is essential for understanding the first arriving path. A more detailed look at the reflection factor in PLNs can be found in [113].

5.2.2 Analysis of the First Arriving Path

Analysis of the first arriving path starts by having a closer look at the PLC network structure. A more detailed look into this structure, characterized with some highlevel attributes, is given in Fig. 5.1.

As can be seen, the direct propagation path between transmitter and receiver operating on a PLC system consists of several branching nodes that are represented by the letter n in

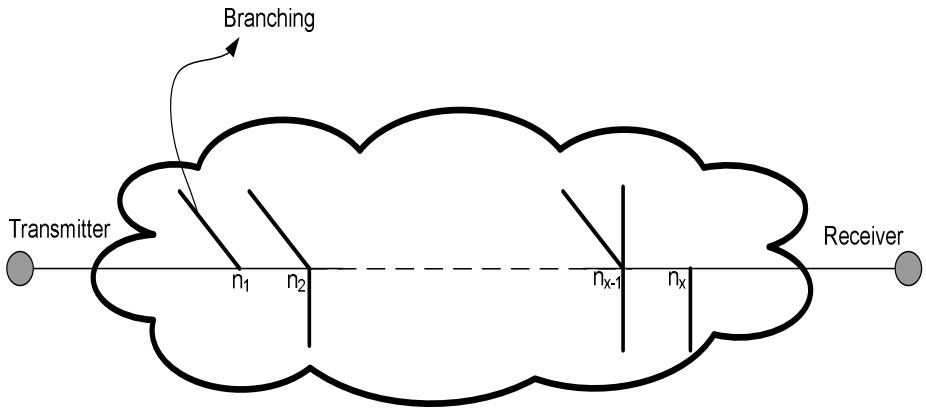

Figure 5.1 Analysis of the first arriving path.

the figure. These branches extending from each branching node (n) may be terminated by an electrical load or lead to another branching node depending upon the network structure.

Note that the reflection factor of the first arriving path ($|r_0|e^{j\theta_0}$) is composed of only the transmission coefficients ($T's$) experienced along the direct path stemming from the impedance discontinuities at the branching nodes. So, calculating $T's$ is sufficient in order to characterize the reflection factor of the first arriving path.

A branching node is depicted in Fig. 5.2 in which the characteristic impedance of the branches are labeled with the letter $Z's$. According to transmission line theory, reflection and transmission coefficients at a branching node are expressed by considering parallel connections of extended branches as follows [112]:

$$\Gamma = \frac{(Z_1//Z_2//...//Z_z) - Z_0}{(Z_1//Z_2//...//Z_z) + Z_0} \text{ and } T = \Gamma + 1, \tag{5.4}$$

In case the impedance of all the branches are equal to each other (Z_0), then (5.4) becomes

$$\Gamma = \frac{2 - z}{z} \text{ and } T = \frac{2}{z}, \tag{5.5}$$

where z refers to the total number of branches extending from a particular branching node.

Referring back to Fig. 5.1, assuming that the transmitter and receiver are matched to the impedance of the corresponding characteristic impedance of the cable for the sake of

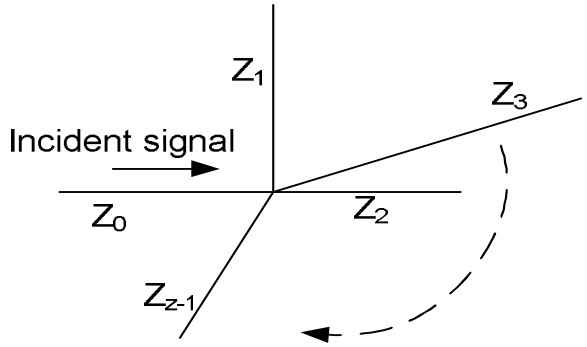

Figure 5.2 Reflection at a branching node.

simplicity, $|r_0|e^{j\theta_0}$ is composed of multiplication of x transmission coefficients as follows:

$$|r_0|e^{j\theta_0} = \frac{2}{n_1}\frac{2}{n_2}...\frac{2}{n_x} = \frac{2^x}{n_1 * n_2 * ... * n_x} \tag{5.6}$$

where n_i $(i = 1, 2, ..., x)$[1] is the number of paths extending from a branching node including the path on which the incident signal propagates. Note that the phase term θ of the reflection factor is 0 for this particular case since n_i can not be a complex number, i.e. $|r_0|e^{j\theta_0} = |r_0|$.

In light of the discussion presented in the beginning of the chapter, n_i's and x can be considered as the two of the high-level attributes of the PLC channel. Stemming from this fact, $|r_0|$ given by (5.6) is indeed a random variable (RV). Our initial observations will be on the first and second order statistics of this RV. If the natural logarithm of both sides of (5.6) is considered

$$Y = ln(|r_0|) = x \ln 2 - \sum_{i=1}^{x} \ln n_i \tag{5.7}$$

Upon this mathematical manipulation, it is easy to see that Y is an RV with the following mean, μ and variance, σ^2:

$$\mu = x \ln 2 - \sum_{i=1}^{x} E[\ln(n_i)] \text{ and } \sigma^2 = \sum_{i=1}^{x} Var[\ln(n_i)] \tag{5.8}$$

[1]Note that the letter n is used for referring both the branching node itself and the number of branches extending from it.

Several probability density functions (PDFs) can considered in order to characterize the randomness in n_i's. If n_i's are assumed to be identically uniformly distributed discrete RV denoted by n dropping the subscript i over [a,b] [2], then

$$\begin{aligned} \mu &= x \ln 2 - xE[\ln(n)] \\ &= \frac{-x}{b-a+1} \ln\left(\frac{b!}{(a-1)!}\right) + x \ln 2 \end{aligned} \tag{5.9}$$

$$\begin{aligned} \sigma^2 &= xVar[\ln(n)] \\ &= xE[(\ln(n))^2] - xE[(\ln(n))]^2 \end{aligned} \tag{5.10}$$

Some important observations can be made regarding μ and σ^2 at this point.

μ and σ^2 has the following characteristics:

- μ is monotonically decreasing function of x for $a, b \geq 3$
- σ^2 is monotonically increasing function of x for $a, b \geq 3$

Proof of the observations can be given as follows. The derivative of μ with respect to x is given by

$$\frac{d\mu}{dx} = \frac{-1}{b-a+1} \ln\left(\frac{b!}{(a-1)!}\right) + \ln 2 \tag{5.11}$$

In order to make sure that a branching exists at a branching node a and b must be equal to or greater than 3. Considering this fact it is easy to see that

$$\left(\frac{b!}{(a-1)!}\right)^{\frac{1}{b-a+1}} > 2 \tag{5.12}$$

Reasoning in (5.12) naturally proposes that (5.11) must be negative. Since $\frac{d\mu}{dx} < 0$ for $a, b \geq 3$, μ is a monotonically decreasing function of x.

[2] This is also denoted as U[a,b] where U means uniform distribution. Note also that 3 is the minimum number that n, hence a and b can assume in order to make sure that a branching in a branching node takes place.

In a similar fashion, the derivative of σ^2 with respect to x is given by

$$\frac{d\sigma^2}{dx} = E[(\ln(n))^2] - E[(\ln(n))]^2 \tag{5.13}$$

(5.13) is equal to the variance of the RV $\ln(n)$. Variance of an RV is always positive. Since $\frac{d\sigma^2}{dx} > 0$ for $a, b \geq 3$, σ^2 is a monotonically increasing function of x.

Mean and variance values of Y which were obtained through simulation and analytical derivation are presented in Figures 5.3 and 5.4 if n is assumed to be uniformly distributed over [3,6]. As can be seen clearly, the mean value of Y decreases with increasing x, whereas its variance increases as x is increased which is in good agreement with the claims proposed above.

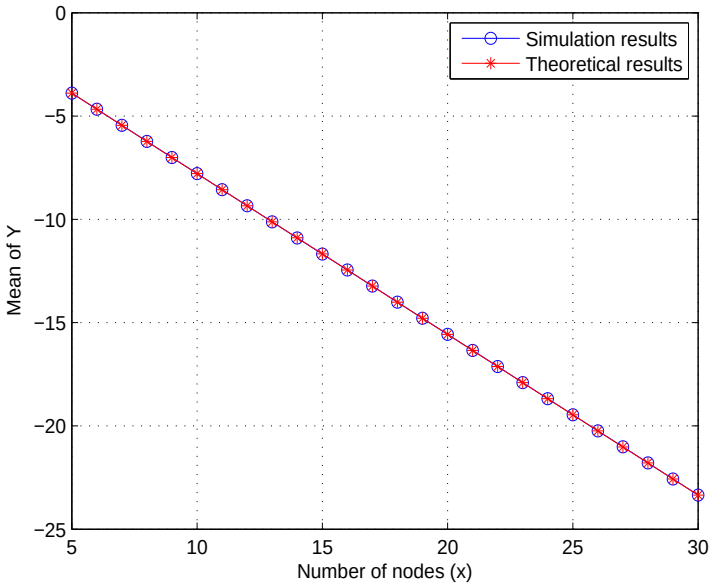

Figure 5.3 Mean of Y with different values of x.

Note that the denominator of (5.6) is composed of the multiplication of RVs. Multiplication of RVs can be approximated with log-Normal PDF according to the central limit theorem for products of RVs [114]. However, each of the n_i's appearing in the denominator can only take discrete values coming from a discrete distribution due to the homogeneous network structure assumption. The log-Normal approximation, hence the use of central

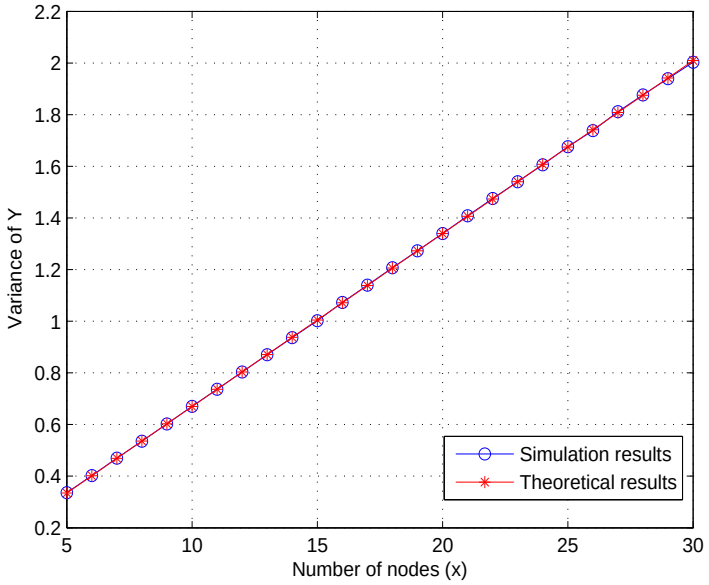

Figure 5.4 Variance of Y with different values of x.

limit theorem for discrete type of RVs should be carefully thought. Although the cumulative distribution function (CDF) of the logarithm of (5.6) is supposed to appear as a staircase function approaching the CDF of a Normal distribution, the probabilities in general are unrelated to the Normal density with some exceptions for some particular type of RVs [114]. Subsequently, our objective will be the investigation of the conditions in which the log-Normal approximation as a result of the central limit theorem for the product of RVs can be employed. Note that the log-Normal approximation, if validated, considerably simplifies the analysis of PLC networks.

Having a homogeneous PLC medium is physically very difficult even though the same type of cable is used throughout the network due to the variety of factors that affect the characteristic impedance. If we were to continue with the homogeneity assumption, a deviation term which implies the minor changes of impedances across the branching nodes can be considered to be more practical. This way, the impedance of a branch which was assumed to equal Z_0 can now be assumed to be $Z_0 + d_e$, where d_e denotes the deviation from Z_0. Similar to the previous case, several assumptions can be made regarding the

characteristics of d_e. Treating d_e as a uniformly distributed RV over a range which can be considered as a very small fraction of Z_0 guarantees reflection factor $|r_0|$ to be a continuous RV. However, the expression for $|r_0|$ can not be simplified as (5.6) since the impedances appearing at the branches extending from a particular branching node are different from each other by a value d_e characterized as a uniformly distributed RV. Similarly, its first and second order statistics will not be as straightforward as it used to be in (5.9) and (5.10) since it includes averaging over a more complicated mathematical expression stemming from the parallel connection consideration of the branches as outlined by (5.4). However, they can be obtained through simulations. To summarize, we will be investigating if the following approximation is valid or not

$$|r_0| = T_1 * T_2 * ... * T_x \approx e^Y \tag{5.14}$$

where recall that T_i's are the transmission coefficients at corresponding branching nodes and Y is an RV characterized with the Normal PDF.

Prior to the investigation of the first and second order statistics of $|r_0|$, KolmogorovSmirnov (KS) test will be performed in order to verify the Gaussianity assumption presented in (5.14). In order to verify this assumption, a simulation has been performed by assuming Z_0 and d_e to be 50Ω and a uniformly distributed RV over $[-1\Omega,1\Omega]$, respectively. In KS goodness-of-fit test, the following distance measure is taken into consideration

$$D = max_x|F(x) - F_N(x)| \tag{5.15}$$

where $F(x)$ and $F_N(x)$ are the CDF of the empirical data and the CDF of the theoretical Normal distribution, respectively.

In order to quantify the statistics of the underlying process, the following hypotheses test was performed:

$$H_1 : Y \text{ is a Normal RV}$$

and

$H_2 : Y$ is *not* a Normal RV

recall that Y is defined as the logarithm of the multiplication of the corresponding transmission coefficients T_i's as outlined by (4.7) and (5.14)

$$Y = \ln(|r_0|) = \ln(\prod_{i=1}^{x} T_i) \tag{5.16}$$

Results of the KS goodness-of-fit for Y are shown in Fig. 5.5 with the significance level α equals 0.05. Note that the vertical and horizontal axes refer to the p-value obtained from the test and the number of branching nodes (x), respectively. The values of p shown in Fig. 5.5 were obtained by averaging the results of 100 trails, each with 10000 samples.

Being a two-tailed test, the following condition $p > \alpha/2$ must be satisfied in order to accept H_1. As can be clearly seen from the figure, x as low as 7 is sufficient for the acceptance of H_1.

As mentioned previously, theoretical derivation of the mean and variance of Y for networks whose cable impedance is defined as $Z_0 + d_e$ is not a simple task. However, Monte Carlo simulations can be employed in order to overcome this difficulty. Indeed, this same reasoning can be applied to networks with heterogeneous structure if the cable impedances can be characterized with a particular PDF. This heterogeneity will be introduced by manipulating the statistics of d_e in this study by assuming it to be uniformly distributed over a larger range than the previous case. Figures 5.6 and 5.7 show the mean and variance of Y (logarithm of the reflection factor) when Z_0 and d_e are assumed to be 50Ω and uniformly distributed over [$-$25Ω,25Ω], respectively. This corresponds to a PLN in which the characteristic impedance of the cables takes some value between 25Ω and 75Ω according to

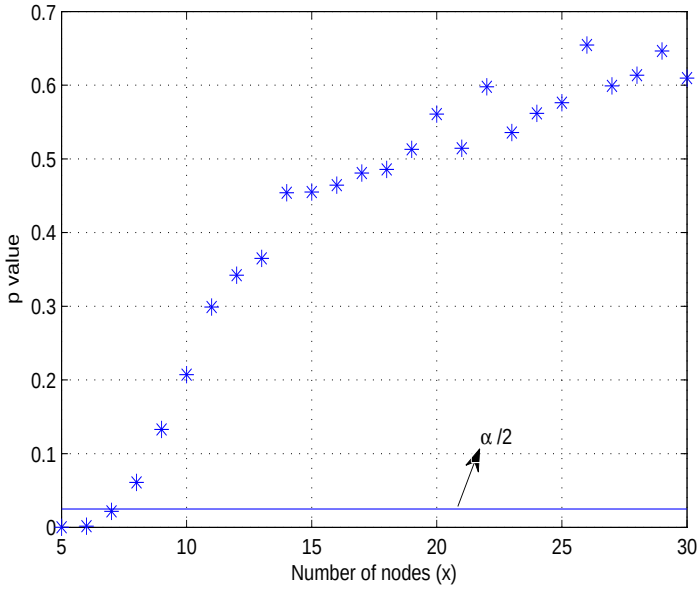

Figure 5.5 Results of KS test for the verification of Gaussianity assumption with Z_0=50Ω and d_e=U[−1Ω,1Ω].

uniform distribution. If least squared error (LSE) based line fitting is adopted, the mean and variance of Y are related to the number of branching nodes x with the following two equations:

$$\mu = -0.822x - 9.23\text{x}10^{-5} \tag{5.17}$$

$$\sigma^2 = 0.086x - 0.00237 \tag{5.18}$$

Although the first and the second order statistics cannot be expressed in the same way as in (5.9) and (5.10), claims presented above regarding μ and σ^2 still hold. Results presented in (5.17) and (5.18) carries significant importance considering the simulation of PLC channels with unknown network structure. If the PLC communication environment is not known except for some high-level attributes, the amplitude of the first arriving path can be characterized with the log-Normal distribution as shown in Fig. 5.5. The mean

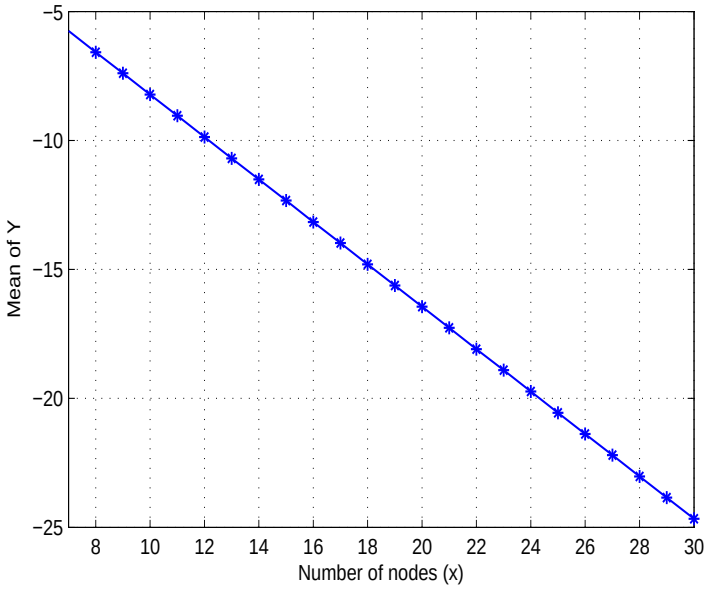

Figure 5.6 Mean of Y with Z_0=50Ω and d_e=U[−25Ω,25Ω].

and variance of the log-Normal distribution can be extracted by adopting Monte Carlo simulations. This simplifies the analysis of the communications systems to be employed on PLC networks since the statistics of the signal is very often used in order to evaluate their efficiency.

In the above example, these two parameters are extracted for a particular case; however, this methodology along with the log-Normal approximation may be easily used for other cases in which characteristic impedances assume different PDFs as well. The most striking outcome of this log-Normal approximation is the avoidance of network specific results. Upon this approximation, all networks whose attributes are defined with the above-mentioned statistics can be incorporated into the performance analysis which can be carried out prior to system deployment process.

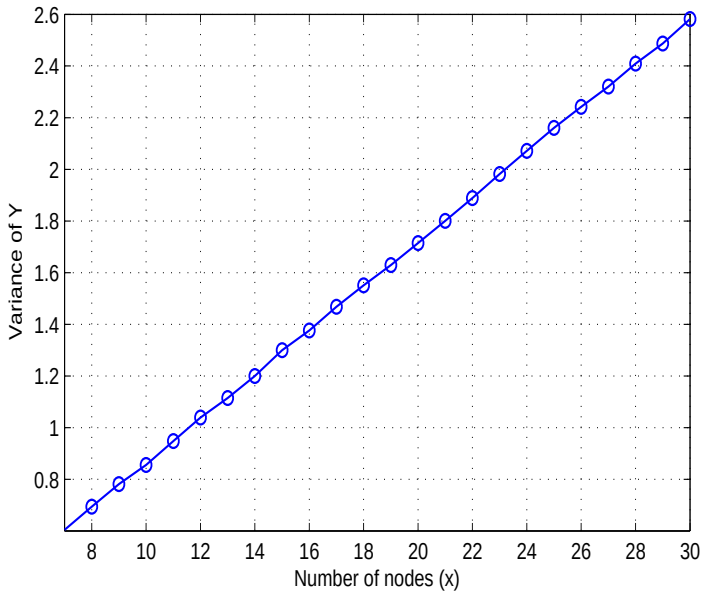

Figure 5.7 Variance of Y with Z_0=50Ω and d_e=U[−25Ω,25Ω].

Our next objective will be investigating the relation between the number of branches extending from a branching node and the mean and variance of Y. This investigation will be based on increasing the maximum number of branch that may extend out a branching node while keeping the number of branching nodes (x) fixed. Recall from (5.9) that this number is denoted as b. The results of the simulations when b is varied from 6 to 10 are shown in Figures 5.8 and 5.9. Similar to x, increase in b gives rise to a decrease in the mean and an increase in the variance of Y. This proposes that when two different PLC environment structures are considered with the same number of branching nodes (x), the environment in which more branches are expected to extend out from each branching nodes yields lower mean and higher variance for the log-Normal approximation.

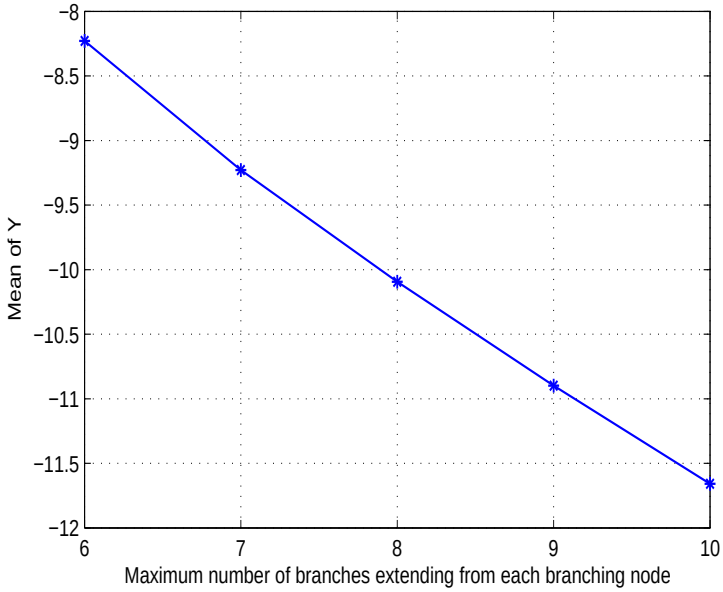

Figure 5.8 Mean of Y with Z_0=50Ω and d_e=U[−25Ω,25Ω] when the number of branches are U[3,$x-axis$] and the number of nodes (x) is assumed to be 10.

Upon articulating the relation between attributes of PLC network topology and statistics of the first arriving path, statistics regarding other paths as well as the assumptions considered in the analysis will be clearly presented in the subsequent section.

5.3 Discussion

In this study, the log-Normal approximation for the statistics of the first arriving path in particular has been tested and validated by employing KS goodness-of-fit test, the impact of the network structure on the first and second order statistics (mean and variance) of this approximation is investigated. To sum up, adopting the log-Normal PDF in order to characterize the statistics of the first arriving path:

- Determine the high-level attributes of the PLC environment. Number of branching nodes between the transmitter-receiver pairs, statistics regarding the number of

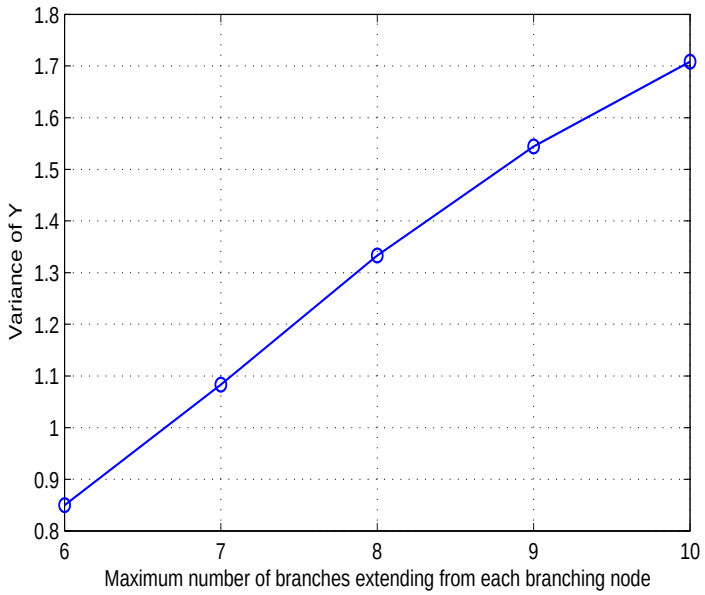

Figure 5.9 Variance of Y with Z_0=50Ω and d_e=U[−25Ω,25Ω] when the number of branches are U[3,$x-axis$] and the number of nodes (x) is assumed to be 10.

branches extending from branching nodes, and statistics of the cable impedances constitute these high level attributes for the first arriving path.

- Determine the mean and variance of the reflection factor $|r_0|$ considering the high-level attributes of the communication medium. This process may include Monte Carlo simulations.

- Approximate $|r_0|$ with the log-Normal PDF having mean and variance obtained from the previous step.

So far, statistics of the strongest path in PLC environment has been the focal point of the discussion. In addition to the reception of the first path, a number of paths from other reflection points is received by the receiver as indicated by (5.3). The log-Normality assumption to define the statistics of these paths should hold as well especially when the

presence of only resistive loads or open circuit condition at the termination points [3] are considered since the reflection factor of each of these paths again include the multiplication of several reflection and transmission coefficients. Although they can be approximated as log-Normal RVs, the correlation between these RVs (amplitudes of the paths arriving at different instances of time) should always be kept in mind. This correlation among the paths results from common impedance discontinuities that are seen while traveling towards the receiver.

The final remark that is worth mentioning at this point is regarding the bandwidth assumption or time resolution of the CIR. It must be noted that in our analysis, the bandwidth was assumed to be infinite which led to the resolution of each and every multipath component individually along the delay axis of CIR. If the symbol duration is considered to be limited with a finite value (finite bandwidth), the receiver observes the vectorial addition of the multipath components that fall into one symbol duration [47]. The number of multipath components that are vectorially added at the receiver depends on both the bandwidth and the network topology. As an extreme case, if the delay of the latest arriving multipath component, which is N in (5.3), is small compared to the duration of a symbol, the resultant received signal is the vectorial combination of N multipath components whose statistics are defined with log-Normal PDFs. Fortunately, some methods are already present in the literature to approximate addition of correlated log-Normal RVs by another log-Normal RV [127, 128].

[3] Note that open circuit assumption corresponds to the worst-case scenario from the perspective of multipath propagation.

5.4 Concluding Remarks

Design and performance evaluation of communication systems are carried out considering the statistics of the arriving paths. In this regard, statistics of the paths in PLC environments defined by some high-level attributes were the focus of this study with a particular emphasis on the first arriving path. Upon investigating the statistical behavior of the first arriving path, the statistical characterization of other paths was discussed briefly. The most significant outcome of this chapter is that the first arriving path as well as the other paths in PLC systems can be approximated with a log-Normal distribution (e^Y where Y is a Normal RV) for both heterogeneous and homogeneous networks upon an introduction of a characteristic impedance deviation parameter, namely d_e. It was proved by employing KS goodness-of-fit test that the number of branching nodes between transmitter-receiver pairs could be as low as 7 with a significance level of α 0.05 for the validity of this approximation.

Mean and variance are the two parameters that are sufficient to characterize a Normal, hence a log-Normal RV. The relation between these two parameters of Y and the high-level attributes of the PLC environment was elaborated by considering the first arriving path as a case study. Upon investigation, following conclusions were reached:

- The mean of Y decreases with increasing number of branching nodes (denoted as x in the simulations) while the variance increases.
- When the maximum number of branches that extend out a branching node, denoted as b in the simulations, is increased, mean of Y decreases while the variance increases.

As a final note, our analysis was performed by assuming the availability of infinite bandwidth. However, it was pointed out that findings concluded with this assumption

can be easily generalized for finite bandwidth case by considering the vectorial addition of individual multipath components.

CHAPTER 6

HANDLING BURSTY IMPULSIVE NOISE IN OFDM

6.1 Introduction

A set of orthogonal subcarriers are transmitted in parallel in orthogonal frequency division multiplexing (OFDM). Simplification of equalization and efficient implementation through fast Fourier transform (FFT) and inverse fast Fourier transform (IFFT) operations are considered to be the primary advantages of OFDM modulation. Combining these advantages with the demand for higher data rates, which requires the design of communication systems that must combat with severe inter-symbol interference (ISI), makes OFDM a very promising technology for a variety of communication media such as wireless and power line. Both wireless and power line communication (PLC) environments are often characterized by a type of interference with impulsive nature which is referred to as "impulsive noise". Photocopiers, printers, microwave ovens, hair dryers , etc. are among the sources of impulsive noise in wireless communication channels [62]. Similarly, electrical devices connected to the power line network are the main reason behind impulsive interference in PLC systems [108]. Each of these aforementioned sources generate impulsive noise with a unique pattern (mostly periodic with Alternating Current (AC) mains cycle) whose statistics have been the subject of several publications [62, 68, 129]. Besides these unintentional sources of impulsive noise, it can be generated intentionally to jam OFDM signals. Bernoulli–Gaussian [130] and Middleton Class-A [131] are the most frequently used models to describe impulsive noise in the literature for analysis purposes. In spite of being frequently used, it should be noted that these models are memoryless and become insufficient in representing the bursty nature of impulsive noise [67]. Gated Gaussian noise model, in which the sum of additive white

Gaussian noise (AWGN) and another Gaussian component with a higher variance is considered, is one of the solutions to take bursty nature of impulsive noise into account [132–134]. Markov model along with a persistence parameter which signifies memory of the channel is another way of taking more realistic impulsive noise structure into account as discussed in [67].

Considering the current communication trend, it is obvious that robustness of OFDM systems against impulsive interference should be maintained. There are several publications in the literature proposing solutions for mitigating impact of impulsive noise on OFDM. A decision directed impulsive noise mitigation technique is proposed in [132]. A compensation technique based on some operations performed in the frequency domain is introduced in [135]. An impulsive noise cancellation technique that exploits the presence of pilot tones is given in [136]. Iterative decoding based solutions are available as well [137–140]. Regardless of the impulsive noise model considered, it is a well-known fact that impact of impulsive noise on OFDM could be detrimental once its power exceeds a certain threshold since FFT operation at the receiver spreads its effect over the entire OFDM symbol block [130]. Detecting and blanking (or nulling) the samples corrupted with impulsive noise at the receiver prior to FFT operation is one of the straightforward solutions to diminish its adverse impact [66, and references therein]. Although this fact is brought to the attention of the reader in most of these aforementioned studies, its relation to the OFDM receiver and algorithm performance is not discussed any further. In addition to this, the emphasis in most of these studies is given on memoryless impulsive noise models.

This chapter deals with the analytical evaluation and mitigation of bursty impulsive noise effects on OFDM signals under the influence of frequency selective communication channel assuming that the receiver performs nulling prior to FFT. Note that nulling procedure implemented at the receiver distorts orthogonality among the subcarriers and gives rise to inter-carrier interference (ICI). In brevity, harmful impact of impulsive noise is avoided at the cost of ICI. Further processing stages may be required in order to cope with the emerging ICI and enhance the OFDM receiver performance. Before these stages, the im-

pact of nulling on OFDM signals as a result of impulsive noise with bursty nature must be understood. Indeed, analysis of the emerging ICI upon nulling in AWGN channels only for memoryless impulsive noise models without any consideration of bursty structure is given earlier in [66, 141]. Analysis given in this chapter is to be applicable to both memoryless and bursty impulsive noise scenarios with the consideration of frequency selective channel.

Sample replacement based iterative technique is one of the proposed solutions for handling impulsive noise in OFDM [138–140]. We analytically analyze this technique in relation to the nulling operation for the first time in the literature. In addition, we present a successive detection technique for compensating the impact of bursty impulsive noise on OFDM signals. Performance of these techniques is to be articulated by observing bit error rate (BER) figures along with their computational complexities. The key contributions and distinctions of this chapter are summarized as follows:

- A detailed analysis of the ICI that emerges upon nulling in OFDM receivers operating in impulsive noise environments under the influence of frequency selective channel is given. The main distinction of our work from [66, 141] is the incorporation of bursty impulsive noise and frequency selective channel model into the analysis. Note also that these previous studies only analyze the impact of nulling on OFDM signals in memoryless impulsive noise environments without touching upon the next stages of the receiver. In this respect, this chapter also studies the subsequent stages of the receiver upon nulling and carries out a detailed performance analysis setting the main distinction of this chapter from other publications available in the literature.

- Mathematical evaluation of the sample replacement based iterative technique proposed in [138–140] in relation to the nulling operation is carried out.

- Alternative to the sample replacement based iterative technique, we apply successive symbol detection technique to our case and demonstrate its superior performance along with relevant discussions.

- In case both techniques fail to provide satisfactory performance, a new transmission scheme that is based on ICI reduction is introduced at the expense of reduced data rate (or spectral underutilization).

This chapter is organized as follows: Section 6.2 gives the system model. Impact of nulling on OFDM signals that suffer from frequency selective communication channel is analyzed in Section 6.3. Section 6.4.1 provides the details of replacement based iterative technique. Successive detection technique is introduced in Section 6.4.2. Section 6.5 presents the numerical results. Finally, the concluding remarks are given in Section 6.6.

6.2 System Model

The system model is illustrated in Fig. 6.1. The baseband OFDM signal can be written as

$$s(n) = \frac{1}{\sqrt{N}} \sum_{k=0}^{N-1} S(k) e^{j2\pi kn/N}, \quad -N_G \leq n \leq N-1 \tag{6.1}$$

where N is the number of subcarriers, N_G is the length of cyclic prefix (CP), $S(k)$ corresponds to the information-bearing symbol on the kth carrier. It is assumed that $S(k)$, $k \in$ [0,N-1], are complex random variables (RVs) with $E[S(k)] = 0$ and $E[S(k)S^{\star}(m)] = \delta(k-m)$. Here $E[\cdot]$ is the expectation operator and $\delta(\cdot)$ denotes the Kronecker's delta function.

Time domain OFDM symbol passes through communication channel and suffers from impulsive noise with bursty nature. Received signal samples, $r(n)$, can be expressed as

$$r(n) = h(l,n) \star s(n) + n(n), \tag{6.2}$$

where $h(l,n)$ is the time varying communication channel impulse response, $n(n)$ corresponds to the impulsive noise process, and $\star$ refers to the convolution process. The same expression

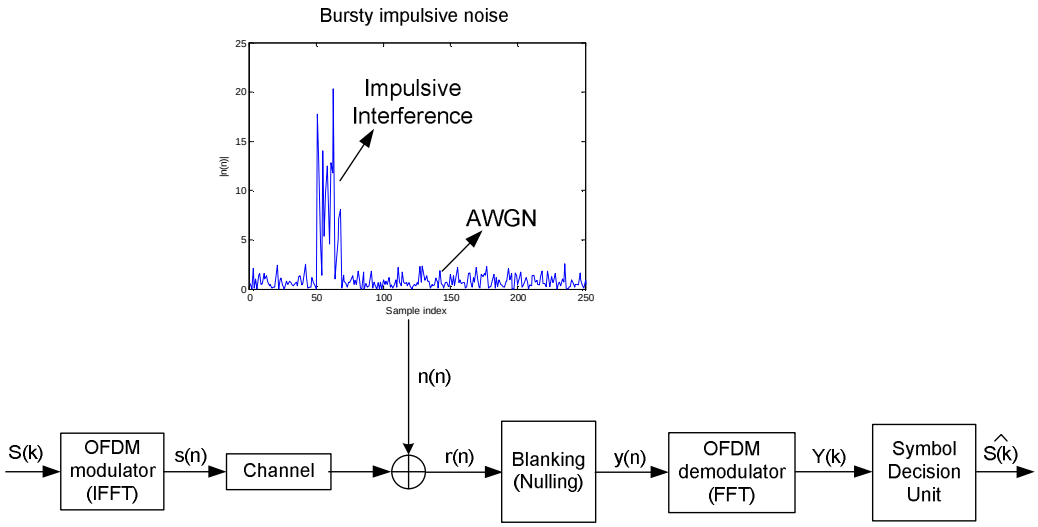

Figure 6.1 OFDM symbol disturbed by bursty impulsive noise.

can be written in a more explicit way as follows:

$$\begin{aligned} r(n) &= \frac{1}{\sqrt{L}} \sum_{l=0}^{L-1} h(l,n)s(n-l) + n(n) \\ &= \frac{1}{\sqrt{N}} \frac{1}{\sqrt{L}} \sum_{k=0}^{N-1} \sum_{l=0}^{L-1} h(l,n)S(k)e^{j2\pi k(n-l)/N} + n(n), \end{aligned} \tag{6.3}$$

where L is the number of channel taps. Samples that are corrupted with the impulsive interference in the received signal, $r(n)$, are detected and nulled before FFT operation at the receiver so that impulsive noise power being spread over all frequency domain symbols is avoided. Assume that $y(n)$ is obtained upon nulling operation,

$$y(n) = \begin{cases} r(n) & n \notin Z \\ 0 & n \in Z \end{cases} \tag{6.4}$$

where Z refers to a set that holds sample indexes corrupted with impulsive noise. As a direct consequence of the IFFT operation at the transmitter, demodulation at the receiver is realized by applying FFT on $y(n)$. Selecting length of the CP, N_G, larger than the maximum excess delay of the communication channel avoids ISI. Assuming perfect time

synchronization, output of the OFDM demodulator upon CP removal can be written as

$$Y(k) = \frac{1}{\sqrt{N}} \sum_{n=0}^{N-1} y(n) e^{-j2\pi kn/N}, \quad 0 \leq k \leq N-1 \tag{6.5}$$

A rough description of the system model is given in this section without going into details of the operations performed at the receiver side in order to avoid the detrimental impact of impulsive noise. These details are to be discussed subsequently.

6.3 Analysis of the Nulling Operation at the Receiver

Since nulling is the first stage of the receiver its impact on OFDM signals must be well understood so that performance enhancement in any subsequent receiver stages can be guaranteed. Stemming from the lack of analysis in the literature of this operation on OFDM systems under the influence of both frequency selective channel and bursty impulsive noise, this section aims at enlightening the outcome of nulling as a result of bursty impulsive noise. In this letter, we assume that samples that are corrupted with the impulsive noise are known, or estimated, by the receiver [1]. If the communication channel is assumed to be time invariant over the duration of OFDM symbol, then $h(l,n) = h(l)$. In the absence of background noise (discussion regarding background noise is to be carried out later), samples that are pushed into FFT block after nulling at the receiver can be represented by

$$y(n) = \frac{1}{\sqrt{N}} \frac{1}{\sqrt{L}} \sum_{k=0}^{N-1} S(k) \Big[\sum_{l=0}^{L-1} h(l) e^{j2\pi k(n-l)/N} - \sum_{i=1}^{K} \sum_{l=0}^{L-1} h(l) e^{j2\pi k(z_i-l)/N} \delta(n-z_i) \Big], \tag{6.6}$$

[1] Estimation of the samples corrupted with impulsive noise (or Z in (6.4)) is out of this chapter's scope. Aim of this section is to enlighten what processing techniques can be employed so as to further enhance the receiver performance after corrupted samples of the OFDM symbol are successfully estimated and nulled. Some estimation techniques are readily available in the literature such as [142, 143].

where z_i holds the information regarding K number of indexes in total extending from 0 to $N-1$ that are nulled. Applying FFT on $y(n)$ in order to demodulate the data results in

$$\begin{aligned} Y(m) &= \frac{1}{N}\frac{1}{\sqrt{L}}\sum_{n=0}^{N-1}\sum_{k=0}^{N-1}S(k)\Big[\sum_{l=0}^{L-1}h(l)e^{j2\pi k(n-l)/N} \\ &- \sum_{i=1}^{K}\sum_{l=0}^{L-1}h(l)e^{j2\pi k(z_i-l)/N}\delta(n-z_i)\Big]e^{-j2\pi mn/N} \\ &= \frac{1}{N}\frac{1}{\sqrt{L}}\sum_{l=0}^{L-1}h(l)\sum_{k=0}^{N-1}S(k)e^{-j2\pi kl/N}\sum_{n=0}^{N-1}e^{j2\pi n(k-m)/N} \\ &- \frac{1}{N}\frac{1}{\sqrt{L}}\sum_{l=0}^{L-1}h(l)\sum_{k=0}^{N-1}S(k)e^{-j2\pi kl/N}\sum_{i=1}^{K}\sum_{n=0}^{N-1}e^{j2\pi(z_ik-mn)/N}\delta(n-z_i) \\ &= \frac{N-K}{N}S(m)H(m) - \frac{1}{N}\sum_{i=1}^{K}\sum_{k=0,k\neq m}^{N-1}S(k)H(k)e^{j2\pi z_i(k-m)/N}, \end{aligned} \tag{6.7}$$

If K consecutive samples starting with the sample index x_0 are nulled at the receiver as given in the system model described in Section 6.2, then it is possible to write the obtained signal upon nulling in a more clear expression than (6.7) by using geometric series expansion:

$$\begin{aligned} Y(m) &= \frac{N-K}{N}S(m)H(m) - \frac{1}{N}\sum_{i=1}^{K}\sum_{k=0,k\neq m}^{N-1}S(k)H(k)e^{j2\pi z_i(k-m)/N} \\ &= S(m)H(m) - \frac{1}{N}\sum_{k=0}^{N-1}S(k)H(k)\sum_{z=x_0}^{x_0+K-1}e^{j2\pi z(k-m)/N} \\ &= S(m)H(m) - \frac{1}{N}\sum_{k=0}^{N-1}S(k)H(k)\frac{\sin(\pi(k-m)K/N)}{\sin(\pi(k-m)/N)}e^{j\pi(k-m)(K-1+2x_0)/N} \\ &= \frac{N-K}{N}S(m)H(m) - \frac{1}{N}\sum_{k=0,k\neq m}^{N-1}S(k)H(k)I(k-m), \end{aligned} \tag{6.8}$$

where $I(x) = \dfrac{\sin(\pi xK/N)}{\sin(\pi x/N)}e^{j\pi x(K-1+2x_0)/N}$.

Remark I: Note that nulling some of the samples of the received OFDM symbol gives rise to the following two phenomena: reduction in the power of the useful symbol and the loss of subcarrier orthogonality, hence ICI each weighted with their corresponding channel frequency response (CFR) coefficients. In the analysis given above, noise is considered to be

absent for mathematical clarity. However, it must be incorporated into the analysis while expressing signal-to-interference-plus-noise ratio (SINR). Note that variance of the noise is also changed by nulling and FFT operations. Assume that variance of the complex AWGN affecting $N-K$ time domain samples prior to nulling and FFT operation is N_0. Thus, the instantaneous SINR experienced by the mth subcarrier upon these operations at the receiver is an RV defined by the following ratio:

$$SINR_m = \frac{\left|\frac{N-K}{N}H(m)\right|^2}{\frac{1}{N^2}\sum_{k=0,k\neq m}\left|H(k)\frac{\sin(\pi(k-m)K/N)}{\sin(\pi(k-m)/N)}\right|^2 + \frac{N-K}{N}N_0} \tag{6.9}$$

As a special case, for AWGN channel in which all channel coefficients are equal to unity, SINR at the mth subcarrier is given by

$$SINR_m = \frac{\left(\frac{N-K}{N}\right)^2}{\frac{K(N-K)}{N^2} + \frac{N-K}{N}N_0} = \frac{N-K}{K+NN_0} \tag{6.10}$$

Remark II: Another observation is that the neighboring carriers are expected to play the major role in the ICI that a particular symbol suffers from especially for large values of K/N. This can be verified by looking into average power per carrier contributed to the total ICI that can be computed by averaging the instantaneous ICI power values over channel realizations. So, the contribution coming from kth subcarrier to the mth subcarrier can be expressed as:

$$P(k) = \frac{1}{N^2}\frac{\sin^2(\pi(k-m)K/N)}{\sin^2(\pi(k-m)/N)} \approxeq \frac{\sin^2(\pi(k-m)K/N)}{\pi^2(k-m)^2}, \tag{6.11}$$

Fig. 6.2 shows the ICI contribution coming from subcarriers within an OFDM symbol block for a particular value of m. As can be clearly seen, contribution coming from the neighboring subcarriers becomes more dominant as K increases. For instance, more than 70% of total ICI power stems from the adjacent subcarriers for $K = 25$ when total number of subcarriers N is considered to be 64. It must be emphasized that the ratio K/N plays a

more significant role in the power contribution rather than the sole values of N and K as can be seen from (6.11).

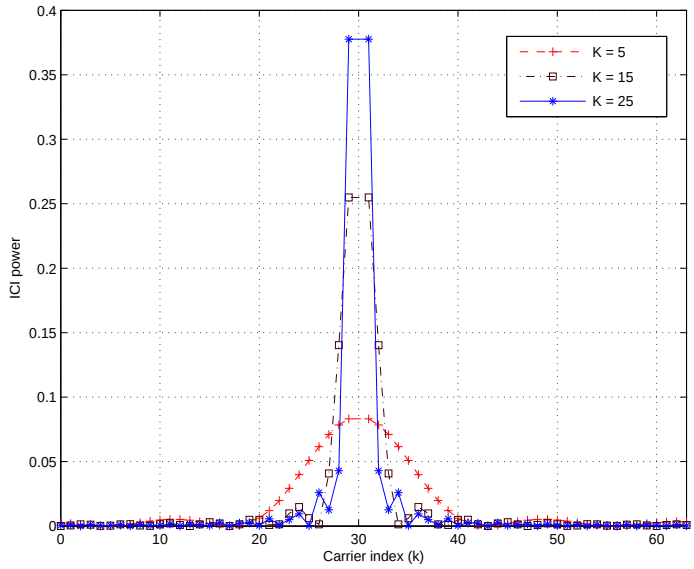

Figure 6.2 ICI power contribution versus carrier index for $N = 64$ with normalized unity power value.

Remark III: Employing matrix representation, (6.8) can be alternatively expressed as:

$$Y = HS, \tag{6.12}$$

where Y is an $Nx1$ vector representing the frequency domain symbols obtained upon nulling, S denotes the $Nx1$ vector of frequency domain transmit symbols, and H is an non–diagonal NxN matrix accounting for the impact of nulling at the receiver as well as the wireless communication channel on S. The first row of H is given below as an example:

$$H(1,:) = \left[\frac{N-K}{N}H(0) \quad -I(1)H(1) \quad \cdots \quad -I(N-1)H(N-1)\right]$$

It is usually believed that the following equality should hold so that every symbol in S can be demodulated.

$$H^H(HH^H)^\dagger H = I, \tag{6.13}$$

where $(\cdot)^\dagger$ and $(\cdot)^H$ are the pseudoinverse and complex conjugate operators, respectively. If H is a full rank matrix, then (6.13) is correct.

With the matrix notation employed for our case, H is a non invertible and *rank deficient* matrix with the rank equal to $N-K$, hence does not satisfy (6.13). In spite of the fact that H is *rank deficient*, each and every symbol $S(k)$, $k \in$ [0,N-1], can still be uniquely demodulated.

We will first show why H is rank deficient and then explain why each symbol is still uniquely identifiable. We adopt AWGN assumption in the remainder of discussion in which $H(k) = 1$, $k \in$ [0,N-1]; however, frequency selective channel case is also applicable. Expressing (6.12) in a more explicit way:

$$Y = HS = FF_z^H S, \tag{6.14}$$

where F is the Fourier matrix and F_z^H refers to the inverse Fourier matrix whose K rows are nulled in order to reject impulsive noise power into the OFDM demodulator. Note that if no impulsive noise is present in the environment, $F_z^H = F^H$ making H an identity matrix. Since F_z^H has K number of its rows equal to 0, it has $N-K$ nonzero singular values, hence a rank of $N-K$. The following equality must hold since F is a full rank matrix:

$$Rank(H) = Rank(FF_z^H) = Rank(F_z^H) \tag{6.15}$$

This proves that H is a rank deficient matrix, hence non invertible with a rank value of $N-K$. However, this fact does not imply the identifiability of only $N-K$ symbols in S. Let us split H into two matrices, H_1 and H_2. H_1 holds the diagonal values of H in its diagonal with all other remaining elements equal 0, whereas H_2 has the remaining values

with $0's$ along its diagonal. So,

$$Y = HS = H_1 S + H_2 S, \tag{6.16}$$

note that the first term holds the information regarding the desired term, whereas the second term in the equation refers to the undesired term, i.e. ICI. ICI term in (6.16) which is seen as a sum of RVs is usually assumed as Gaussian in the literature considering the validity of central limit theorem for large classes of variables especially for large N. It is also worth mentioning that Gaussian assumption as additive noise corresponds to the worst case scenario from channel capacity standpoint [144, page 337]. With this assumption adopted, $H_2 S$ can be thought of an error term, ϵ, defined with zero mean Gaussian RV whose variance is equal to $K(N-K)/N^2$ as can be seen from (6.10). So, our problem turns into identifying N symbols in an AWGN channel as follows:

$$Y = H_1 S + \epsilon, \tag{6.17}$$

since H_1 is invertible and satisfies equalizability condition, each and every $S(k)$, $k \in$ [0,N-1] can be uniquely demodulated with a certain probability that depends on the modulation order and K. This is an important observation considering the applicability of the techniques that are to be discussed subsequently. As a final note for frequency selective channel, symbol identifiability is still applicable given the condition that $H(k) \neq 0$, $k \in$ [0,N-1]. Obviously, this condition is not related to the nulling operation and must be satisfied for any conventional OFDM receiver as pointed out in [145]. Indeed, this observation that relates rank deficiency to unique symbol identifiability was discussed earlier in a different context in the literature as well [146].

The bottom line in this remark is that no symbol is lost at the receiver due to the nulling operation although nulling gives rise to the appearance of a rank deficient channel matrix with a rank value of $N-K$. In spite of the fact that channel matrix H has the rank value of $N-K$, all symbols can still be uniquely demodulated. Although zero forcing equalizer can

not be used to eliminate all ICI at once due to the rank deficiency problem, this does not impose any constraint on the applicability of any other ICI cancellation techniques to be discussed in the forthcoming sections. Implication of this observation is very important in the sense that it is possible to further enhance the receiver performance for a total number of N symbols without any symbol loss if a technique can be employed in order to eliminate the emerging ICI.

In this respect, remainder of the section is dedicated to the discussion of techniques that are used to tackle the emerging ICI as a result of bursty impulsive noise effect. First, we will articulate a technique named "sample replacement based iterative cancellation technique" that was previously proposed in the literature (not in this detail though), next we will discuss our proposed scheme.

6.4 OFDM Receiver Stages After Nulling

6.4.1 Sample Replacement Based Iterative Cancellation Technique

This technique was previously proposed in [138–140]. We will apply this technique to our case and compare its performance with the technique that we propose in the next section. In the first stage of the receiver, samples corrupted with the impulsive noise are nulled. Subsequently, iterative decoding is employed replacing these nulled samples by some values that are obtained upon equalization, demodulation, and modulation processes. The replacement procedure in the absence of noise for the nulled samples can be mathematically expressed as:

$$\begin{aligned} y(n) &= \frac{1}{\sqrt{N}}\frac{1}{\sqrt{L}}\sum_{k=0}^{N-1} S(k)\Big[\sum_{l=0}^{L-1} h(l)e^{j2\pi k(n-l)/N} - \sum_{i=1}^{K}\sum_{l=0}^{L-1} h(l)e^{j2\pi k(z_i-l)/N}\delta(n-z_i)\Big] \\ &+ \sum_{i=1}^{K} r_i\delta(n-z_i), \end{aligned} \tag{6.18}$$

where r_i's correspond to the values replacing the samples of the OFDM symbol that are nulled in the first stage. Applying FFT on $y(n)$ and using the results from Section 6.3,

$$\begin{aligned} Y(m) &= \frac{N-K}{N}S(m)H(m) - \frac{1}{N}\sum_{i=1}^{K}\sum_{k=0,k\neq m}^{N-1} S(k)H(k)e^{j2\pi z_i(k-m)/N} \\ &+ \frac{1}{\sqrt{N}}\sum_{i=1}^{K} r_i e^{-j2\pi z_i m/N}, \end{aligned} \tag{6.19}$$

In the iterative decoding technique considered, r_i's are supposed to correspond to some particular samples (whose indexes are indicated by z_i's) of IFFT of the frequency domain symbols estimated from the nulled received waveform and convolved with the channel response. So,

$$r_i = \frac{1}{\sqrt{N}}\frac{1}{\sqrt{L}}\sum_{l=0}^{L-1}\sum_{k=0}^{N-1}\sum_{i=1}^{K} h(l)\hat{S}(k)e^{j2\pi k(n-l)/N}\delta(n-z_i), \tag{6.20}$$

After plugging this into (6.19), $Y(m)$ becomes

$$\begin{aligned} Y(m) &= \frac{N-K}{N}S(m)H(m) + \frac{K}{N}\hat{S}(m)H(m) \\ &- \frac{1}{N}\sum_{i=1}^{K}\sum_{k=0,k\neq m}^{N-1} \big(S(k)-\hat{S}(k)\big)H(k)e^{j2\pi z_i(k-m)/N}, \end{aligned} \tag{6.21}$$

Note that the ICI term in (6.21) vanishes for the case $\hat{S}(m) = S(m)$ which implies that all the symbols are estimated correctly. Note also that (6.7) is a special case of (6.21) for $\hat{S}(m) = 0$. Similar to the analysis performed in Section 6.3, if the impulsive noise has a bursty nature occupying a certain amount of samples over the OFDM symbol (K samples starting with the sample index x_0), $Y(m)$ in the iterations can be alternatively expressed as

$$Y(m) = S(m)H(m) - \frac{K}{N}E(m)H(m) - \frac{1}{N}\sum_{k=0,k\neq m}^{N-1} E(k)H(k)I(k-m), \tag{6.22}$$

where $E(x) = S(x) - \hat{S}(x)$. It is worth noting that this replacement based technique is analogous to parallel interference cancellation (PIC) since the tentative hard decisions are subtracted from the received symbols simultaneously in parallel [147]. Due to this fact, a number of iterations before attaining the targeted performance merit can be required. In addition, performance is expected to deteriorate significantly especially for high K/N values since it does not consider any ordering among the interfering sources. All of these shortcomings can be addressed by employing the technique that is proposed in the next section. Replacement based technique requires FFT and IFFT algorithms to be run one after another giving a computational complexity of $O(N\log(N))$ for each iteration.

6.4.2 Successive Cancellation Technique

Successive detection technique is widely used in code division multiple access (CDMA) systems for the purpose of multi-user detection in order to achieve higher spectral efficiency [148]. In this section, we will adopt the same approach performing successive symbol decisions. It is more convenient to use matrix notation introduced in (6.12) while explaining this procedure. In successive detection technique, detection order of the symbols has a great influence on the overall performance. Keeping this in mind, the received symbol with the highest signal-to-interference ratio (SIR) is first detected based upon the fact that it is the most reliable one compared to the others as follows:

$$\arg\max_{m} \frac{|\frac{N-K}{N}H(m)|^2}{\sum_{k=0,k\neq m}^{N-1} |\frac{H(k)}{N}\frac{\sin(\pi(k-m)K/N)}{\sin(\pi(k-m)/N)}|^2} \tag{6.23}$$

Suppose that $Y(m)$ has the best SIR and the first symbol to be detected with the corresponding estimated symbol $\hat{S}(m)$. After making hard decision, the received vector Y is updated as

$$Y_{new} = Y_{old} - H\hat{S} \tag{6.24}$$

In other words, interference of the detected symbol, $\hat{S}(m)$, on the other symbols is subtracted. Upon subtraction, the next symbol with the best SIR is determined by using (6.23) and this process is performed successively until all symbols are detected. Detection of the subsequent symbols should be more reliable as long as the hard decisions in the previous steps are correct since smaller number of interferers become effective in the decision process. Considering the computational effort required by the algorithm, each step requires the detection of a symbol and its multiplication by $(N-1)$ number of coefficients along with $(N-1)$ subtractions for interference cancellation. Since this process is performed for each symbol, this requires $N(N-1)$ multiplications and $N(N-1)$ subtractions giving a complexity of $O(N^2)$.

In order to further improve the performance of successive technique, PIC can be employed and the final symbol vector which holds the tentative hard symbol information can be subtracted from the initial received vector after being multiplied with the corresponding coefficients given by (6.8). This procedure can be iterated more than once for enhancing the BER performance. The computational burden that is introduced by the PIC procedure requires additional $O(N^2)$ operations at each iteration. The replacement based technique described in Section 6.4.1 can also be employed instead of PIC for less computational burden.

6.5 Numerical Results

Performance of the detection techniques is tested with computer simulations. An OFDM system employing quadrature phase shift keying (QPSK) symbol mapping with 256 subcarriers is considered. Considering the value of $N = 256$, techniques are initially tested for $K = 25$. Note that the performance of the techniques are dependent on the ratio N/K rather than their sole values. The value $K = 25$ is not arbitrary in this sense. In the literature, it was inspired from the studies that consider the impact of memoryless impulsive noise on the performance of OFDM systems. In these studies, the probability that a sample is corrupted with impulsive noise is given by a certain number denoted by p. The maximum

value of p in most of the studies is equal to 0.1 [141]. This implies that the impulsive noise is expected to occupy 10% of the OFDM symbol duration at most in a variety of studies in a memoryless manner. The choice $K = 25$ which corresponds to approximately 10% of $N = 256$ is based on this observation. For simulating the wireless channel, the normalized delay spread with respect to OFDM symbol duration is assumed to be 1/128 giving rise to a 3 tap channel. A uniform power delay profile (PDP) is assumed with channel taps described by the independently generated complex Gaussian RVs [2]. Sample indexes of the OFDM symbol corrupted with the bursty impulsive noise are assumed to be changing at each simulation step. Figs. 6.3 and 6.4 show the BER performance of replacement based iterative and successive techniques. As can be seen from the figures, both algorithms are successfully able to handle the impact of bursty impulsive noise. However, a number of iterations up to 5 is necessary with replacement based iterative technique in order to have BER values comparable to no ICI case. On the other hand, satisfactory BER performance is obtained within a single cycle of successive detection without any further PIC iterations.

The comparative performance analysis of these techniques can be clearly seen by observing Fig. 6.5. Fig. 6.5 compares the performance of these two techniques for a variety of K values at a specific signal-to-noise ratio (SNR) value of 30dB. It is clearly seen that the performance of the technique that is based on successive symbol detection always outperforms the other especially as K/N goes higher. A single cycle of successive detection is sufficient to keep the BER below 10^{-3} up to $K \approx 40$, whereas the similar performance is observed with sample replacement based iterative technique after 3 iterations at $K \approx 30$. As noted earlier, the contribution of neighboring carriers to the ICI power is expected to become more dominant as K/N goes larger. This behavior brings up the importance of ordering in the detection process especially for high K/N values. By ordering the subcarriers and employing successive detection, the ICI contribution coming from estimated symbols on low SIR carriers are seen immediately leading to a better performance compared to the

[2] We chose not to consider a specific standard communication channel model in the simulations since impulsive noise can be observed in both wireless and PLC based systems. In this respect, an approach similar to [149, 150] was taken in order to avoid drawing channel specific conclusions. Rather, channel time dispersiveness is manipulated and its impact on the techniques are discussed later in the chapter.

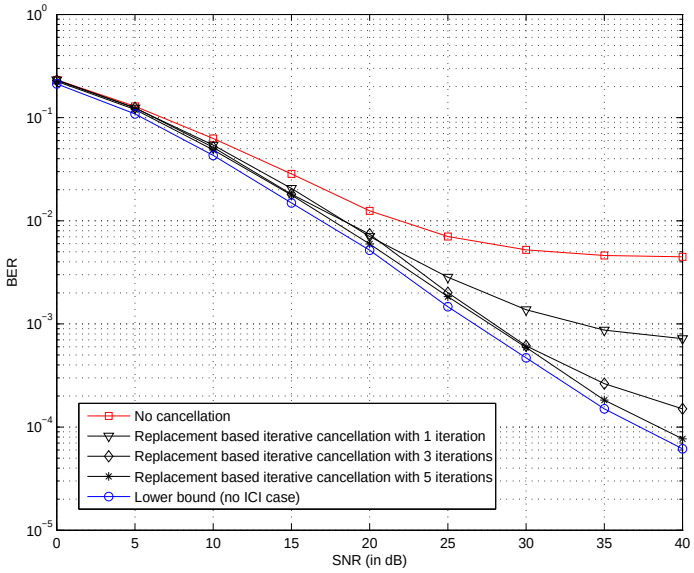

Figure 6.3 BER performance for $N = 256$ and $K = 25$ when replacement based iterative decoding is employed.

replacement based iterative detection technique. It is also observed from the figure that the performance of replacement based iterative decoding technique even after 3 iterations is far from being close to that of successive detection. Implementing a number of additional PIC iterations enhances the BER performance of successive detection even further.

It should also be kept in mind that the performance of both techniques can not be satisfactory even after a particular number of iterations are performed due to the error propagation phenomenon. In order to see this, look at Fig. 6.6 which shows the BER performance of both detection techniques comparatively when K (hence K/N for fixed N) is doubled. It is seen from Fig. 6.6 that even after 3 iterations[3], both techniques do not easily converge to the lower bound, no ICI case. Note again that successive detection provides us with a better BER performance; however, this may not be sufficient for certain communication applications. In order to overcome this convergence problem, ICI that emerges upon nulling needs to be diminished. So, one should ask what measure taken before trans-

[3]Results regarding more number of iterations are not presented since no significant improvement is observed.

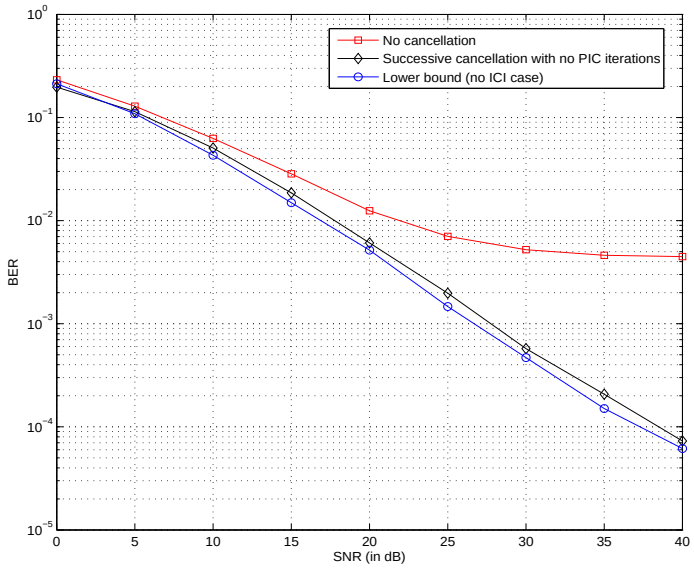

Figure 6.4 BER performance for $N = 256$ and $K = 25$ when successive symbol detection is employed.

mission may lead to a substantial reduction in the emerging ICI power especially as K/N goes larger. Indeed, answer to this question has been implicitly given earlier in Section 6.3. Recall that the ICI contribution coming from neighboring subcarriers become more of an importance as K/N is increased. Thus, a transmission technique that targets the neighboring subcarriers of each subcarrier can be developed. The most straightforward solution is to send no information in subsequent subcarriers. This precaution taken before transmission is expected to lead to a substantial ICI power reduction overcoming the problem observed in Fig. 6.3. However, note that the symbol rate is halved since no subcarrier is neighbored by any other information bearing subcarriers. Figs. 6.7 and 6.8 show the results when this proposed transmission scheme along with the detection techniques of concern are employed. Again a comparable BER performance to no ICI case is achieved with a single cycle of successive detection, whereas a number of iterations are required with replacement based iterative technique. The most important shortcoming of this transmission scheme is the underutilization of the very valuable spectrum. However, one should make a choice between inability to communicate and spectral efficiency for high K/N values. Besides,

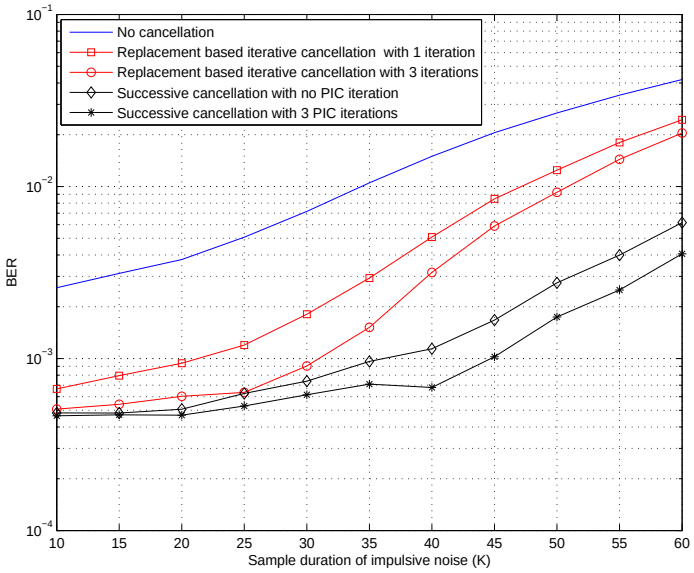

Figure 6.5 BER performance for $N = 256$ and different values of K at $SNR = 30dB$.

this transmission technique employed at the transmitter may lead to new opportunities especially for spectrum sniffing(or opportunistic) transmitters. Note that all these previous simulations are performed by considering a communication channel with a normalized delay spread value of 1/128. Subsequently, dependency of the techniques are tested by changing the normalized delay spread value of the channel with respect to OFDM symbol duration from 1/128 to 1/16. The number of iterations performed at the receiver is assumed to be 3 [4]. Simulation results show that performance of the sample replacement based iterative detection technique slightly degrades for all values of K as the frequency selectivity (or delay spread of the communication channel) becomes larger as can be seen from Fig. 6.9. Successive detection technique exhibits a different trend with the same BER performance compared to the less dispersive case for up to $K \approx 30$. Performance of the successive detection is seen to worsen after $K \approx 30$ when the communication channel becomes more dispersive. Finally, when the two techniques are compared, successive detection outperforms the other regardless of the communication channel time dispersiveness characteristics. Note

[4]This is considered to be the maximum number of iterations that the receiver performs, hence ultimate performance figure.

also that if the BER value of 10^{-3} is taken as reference, successive symbol detection with 3 iterations provides a performance below this reference value for up to $K \approx 35$ even after the normalized delay spread is increased to 1/16.

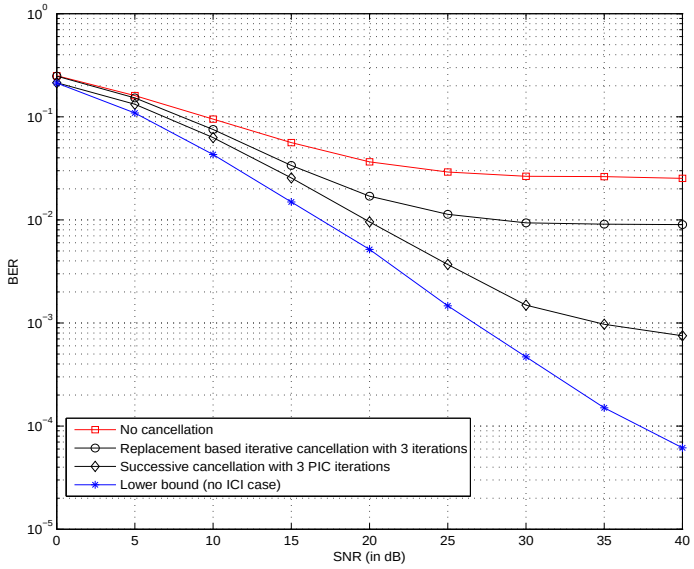

Figure 6.6 BER performance for $N = 256$ and $K = 50$ when replacement based iterative and successive symbol detection techniques are employed with 3 iterations.

6.6 Concluding Remarks

In this letter, a comprehensive study of OFDM receiver under the influence of impulsive noise and multipath communication channel has been carried out. The receiver employs a set of rules for symbol detection followed by nulling the samples corrupted with impulsive noise. We have proposed a successive symbol detection algorithm to mitigate the impact of impulsive noise after elaborating the sample replacement based iterative symbol detection technique that was shown to be equivalent to PIC. A detailed analysis of the nulling operation at the receiver side was initially given to optimally determine the symbol detection order. It was shown that the characteristics of ICI that emerges upon nulling favor the use of successive detection especially for large values of K/N that is the ratio relating impulsive

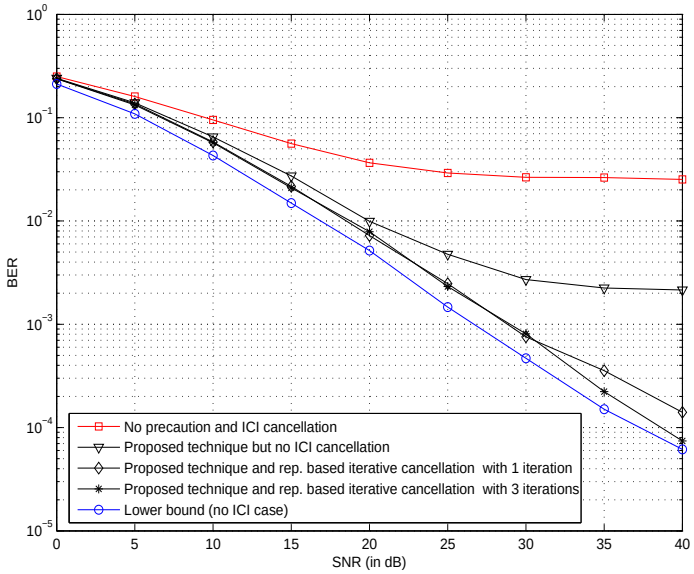

Figure 6.7 BER performance for $N = 256$ and $K = 50$ when replacement based iterative decoding with proposed transmission scheme is employed.

interference duration to OFDM symbol duration. This is because of the fact that weight of interfering subcarriers in the neighborhood becomes more dominant upon nulling as K/N becomes larger. Finally, it was seen that both techniques may fail to become satisfactory as K/N goes even larger as a result of the error propagation phenomenon. A transmission scheme enhancing performance of the receiver in order to overcome this efficiency problem was proposed. It was shown that the techniques proposed in this study can be used with OFDM receivers to combat impulsive noise with bursty structure.

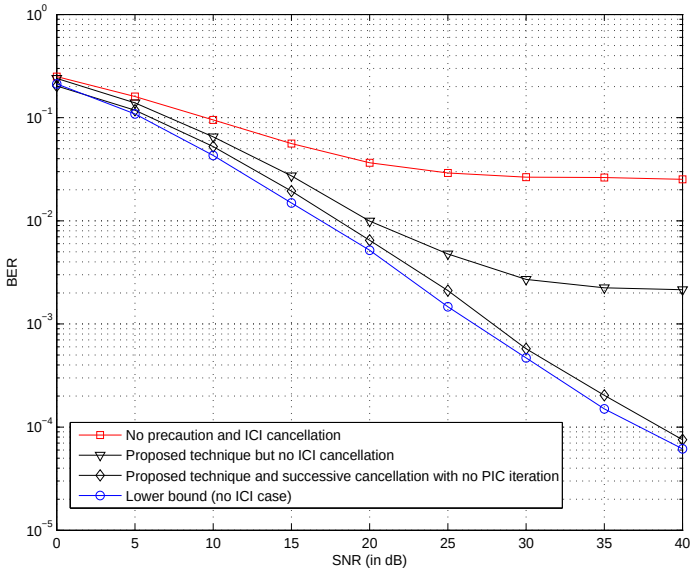

Figure 6.8 BER performance for $N = 256$ and $K = 50$ when successive symbol detection with proposed transmission scheme is employed.

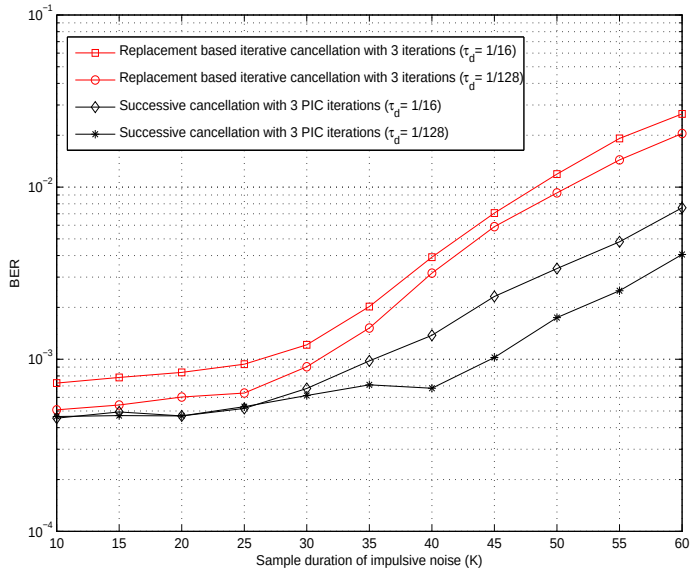

Figure 6.9 BER performance for $N = 256$ with different values of K and normalized delay spread values at $SNR = 30dB$.

CHAPTER 7

CONCLUSION AND FUTURE WORK

This dissertation dealt with various issues regarding the communication channels of smart grid networks. In addition to the investigation of some particular channel characteristics of wireless and power line communication (PLC) environments, some channel models were proposed and discussed. Besides proposing channel models, receiver algorithms were studied and developed aimed at handling some inconveniences that may widely exist in certain wireless and PLC channels of smart grid networks such as impulsive noise. Certain parts of all these research efforts appeared in the literature in the form of publications [1–5]. In the remainder of this section, a list of the specific contributions of the dissertation and possible future directions are given.

7.1 List of Specific Contributions

- A detailed review of wireless and PLC channel characteristics of smart grid networks

  Wireless and PLC channel characteristics of smart grid environments were presented in a very detailed way. Among the communication channel characteristics discussed were path loss and attenuation, time dispersion, time selectivity, path amplitudes and noise characteristics.

- Time selectivity characterization of wireless communication channels

  Doppler spectrum characteristics of wireless channels as well as the factors which define its behavior were investigated through the use of an reverberation chamber (RVC). Operating frequency, speed, and angle of arrival (AOA) were among the factors studied. In conjunction with these factors, a new perspective of mobility in wireless

channels was also given by proposing a concept called motion intensity. Comparison of the experimental results with some vastly used theoretical models was carried out and the reasons of discrepancies between the models and the results were elaborated. In addition, steps for the accurate realization of the theoretical models such as Jakes in RVCs were given.

- Root-mean-squared (RMS) delay spread characteristics of PLC channels

  Impact of the physical attributes and loading of the power line network (PLN) on the RMS delay spread statistics of the communication channel was investigated in detail.

- Path amplitude statistics of PLC channels

  Statistics of the path amplitudes in PLC channels were studied and it was shown that it can be considered to follow a log-Normal distribution.The relationship between the physical attributes of the PLN and the mean and variance of the approximating log-Normal distribution was articulated.

- Mitigating the impact of impulsive noise on orthogonal frequency division multiplexing (OFDM) receivers

  A detailed analysis of the ICI that emerges upon nulling in OFDM receivers operating in impulsive noise environments under the influence of frequency selective channel was given. A detailed performance analysis of the subsequent stages of the OFDM receiver upon nulling was carried out. Mathematical evaluation of the sample replacement based iterative technique in relation to the nulling operation was performed. Alternative to the sample replacement based iterative technique, successive symbol detection technique was applied along with relevant discussions. In case both techniques fail to provide satisfactory performance, a new transmission scheme that is based on ICI reduction was introduced at the expense of reduced data rate (or spectral underutilization).

7.2 Final Comments and Future Work

Smart grid will definitely have its unique challenges related to its communication infrastructure in spite of the fact that these challenges are not well defined so far in the literature. This section is dedicated to the discussion of these future research opportunities.

Smart grid infrastructure can not be isolated from the advances in the radio technology. In this respect, cognitive radio (CR) and its relation to the smart grid applications should be established in a stronger manner. Besides, emergence of electric vehicles (EVs) and their communication and networking requirements in terms of electricity bill charging and the utilization as a back up source of power when needed is likely to lead to very exciting research issues from many aspects. In addition, their impact on the power grid should be given special attention for developing optimum demand scheduling and resource management algorithms. There are also some important research opportunities considering the integration of customers to the smart grid network. For instance, statistics regarding the use of electrical devices is very crucial for the households to monitor their energy usage. One of the most economically convenient ways of collecting these statistics could be to process the noise that these devices emit into the power line conductors. Communication and networking requirements in alternative generation and storage sites are likely to give rise to good research opportunities. Each of these sites will have its unique characteristics affecting the communication systems deployed in different ways. As a specific example, one of the questions requiring further investigation is how the wireless communication is affected by the wind turbine blades in wind power generation stations or what could be the main sources of data errors in these environments for various communication options. Finally, OFDM being the most popular technology for future communication systems was considered in our study. Findings of this dissertation can also be easily extended to some other promising technologies such as single carrier frequency domain equalization (SC-FDE). All of these above-mentioned research issues can lead to another PhD dissertation.

REFERENCES

[1] S. Guzelgoz, H. Arslan, A. Islam, and A. Domijan, "Wireless and plc propagation channel characteristics for smart grid environments," *IEEE Transactions on Smart Grid*, under review.

[2] S. Guzelgoz, S. Yarkan, and H. Arslan, "Investigation of time selectivity of wireless channels through the use of rvc," *Journal of Measurement (by Elsevier)*, vol. 43, no. 10, pp. 1532–1541, December 2010.

[3] S. Guzelgoz, H. Celebi, and H. Arslan, "Articulating factors defining rms delay spread in lv plc networks," *Journal of Computer Systems, Networks, and Communications (by Hindawi)*, vol. 2010, 2010, doi:10.1155/2010/802826.

[4] ——, "Statistical characterization of the paths in multipath plc channels," *IEEE Transactions on Power Delivery*, vol. 26, no. 1, pp. 181–187, January 2011.

[5] S. Guzelgoz and H. Arslan, "Handling bursty impulsive noise in ofdm," *IEEE Communications Letters*, under review.

[6] S. Yarkan, S. Guzelgoz, H. Arslan, and R. Murphy, "Underground mine communications: A survey," *IEEE Communications Surveys Tutorials*, vol. 11, no. 3, pp. 125 –142, 2009.

[7] S. Yarkan, S. Guzelgoz, and H. Arslan, "Statistical wireless channel propagation characteristics in underground mines at 900mhz: A comparative analysis with indoor channels," *IEEE Transactions on Instrumentation and Measurement*, under review.

[8] ——, "Wireless channel propagation characteristics in underground mines: A statistical analysis and a radio controlled robot experiment," in *IEEE ICWCUCA*, ValdOr, Canada, August 2008, accepted for publication.

[9] S. Guzelgoz, H. Celebi, T. Guzel, H. Arslan, and K. Mihcak, "Time frequency analysis of noise generated by electrical loads in plc," in *IEEE ICT*, April 2010.

[10] H. Celebi, S. Guzelgoz, T. Guzel, H. Arslan, and K. Mihcak, "Noise and channel statistics of indoor powerline networks," in *IEEE ICT*, May 2011, accepted for publication.

[11] S. Guzelgoz, H. Celebi, and H. Arslan, "Analysis of a multi-channel receiver: Wireless and plc reception," in *EUSIPCO*, Aalborg, Denmark, August 2010.

[12] S. Guzelgoz and H. Arslan, "A wireless communications systems laboratory course," *IEEE Transactions on Education*, vol. 53, no. 4, pp. 532–541, November 2010.

[13] ——, "Modeling, simulation, testing, and measurements of wireless communication systems: A laboratory based approach," in *IEEE WAMICON*, Clearwater, FL, April 2009.

[14] S. Guzelgoz, A. Hesham, O. Zakaria, and H. Arslan, "An sdr based wireless laboratory: Introducing multi-dimensional signal analysis," in *SDR Forum*, Washington D.C., June 2008.

[15] M. Kuhn, S. Berger, I. Hammerstrom, and A. Wittneben, "Power line enhanced cooperative wireless communications," *IEEE Journal on Selected Areas in Communications*, vol. 24, no. 7, pp. 1401–1410, July 2006.

[16] W. Peng, G. Markarian, and G. Kolev, "A novel hybrid network for hospital environment incorporating ieee 802.16 and homeplug av standards," in *Conference on Wireless, Mobile and Sensor Networks*, December 2007, pp. 1029–1032.

[17] J. Y. Ha, J. Jeon, K. Lee, J. Heo, N. Kim, S. M. Kim, W. H. Kwon, and B. jin Jung, "Design and implementation of convergence sub–layer for a heterogeneous home network," in *IEEE International Symposium on Power Line Communications and Its Applications*, March 2007, pp. 252–256.

[18] H. Kuriyama, H. Mineno, and T. Mizuno, "Evaluation of mutually complementary multichannel sensor network for wireless and power lines," in *IEEE International Symposium on Power Line Communications and Its Applications*, April 1 2009, pp. 223–227.

[19] K. Lee, J. Park, and K. Moon, "Convergence of high-speed powerline communication and wimedia uwb for multimedia home networks," in *IEEE International Symposium on Power Line Communications and Its Applications*, April 2008, pp. 147–151.

[20] J. Mitola, "Cognitive radio: an integrated agent architecture for software- defined radio," Ph.D. dissertation, Royal Institute of Technology (KTH), Stockholm, Sweden, May 2000.

[21] H. Tai and E. Hogain, "Behind the buzz [in my view]," *IEEE Power and Energy Magazine*, vol. 7, no. 2, pp. 92–96, March 2009.

[22] H. Farhangi, "The path of the smart grid," *IEEE Power and Energy Magazine*, vol. 8, no. 1, pp. 18–28, January 2010.

[23] C. Hauser, D. Bakken, and A. Bose, "A failure to communicate: next generation communication requirements, technologies, and architecture for the electric power grid," *IEEE Power and Energy Magazine*, vol. 3, no. 2, pp. 47–55, March 2005.

[24] T. Sauter and M. Lobashov, "End-to-end communication architecture for smart grids," *IEEE Transactions on Industrial Electronics*, vol. PP, no. 99, pp. 1–1, 2010.

[25] V. Sood, D. Fischer, J. Eklund, and T. Brown, "Developing a communication infrastructure for the smart grid," in *IEEE Electrical Power Energy Conference*, October 2009, pp. 1–7.

[26] W. CHU and D. J. H. LIN, "Communication strategies in enabling smart grid development," in *International Conference on Advances in Power System Control, Operation and Management*, November 2009, pp. 1–6.

[27] V. Gungor and F. Lambert, "A survey on communication networks for electric system automation," *Computer Networks*, vol. 50, no. 7, pp. 877–897, May 2006.

[28] M. Qureshi, A. Raza, D. Kumar, S.-S. Kim, U.-S. Song, M.-W. Park, H.-S. Jang, H.-S. Yang, and B.-S. Park, "A survey of communication network paradigms for substation automation," in *IEEE International Symposium on Power Line Communications and Its Applications*, April 2008, pp. 310–315.

[29] A. Sarafi, G. Tsiropoulos, and P. Cottis, "Hybrid wireless–broadband over power lines: A promising broadband solution in rural areas," *IEEE Communications Magazine*, vol. 47, no. 11, pp. 140–147, November 2009.

[30] A. Aggarwal, S. Kunta, and P. Verma, "A proposed communications infrastructure for the smart grid," in *Innovative Smart Grid Technologies*, January 2010, pp. 1–5.

[31] http://smartgrid.ieee.org/standards/approved-ieee-smartgrid standards.

[32] D. Gu and J. Zhang, "Qos enhancement in ieee 802.11 wireless local area networks," *IEEE Communications Magazine*, vol. 41, no. 6, pp. 120–124, June 2003.

[33] D. Chen, D. Gu, and J. Zbang, "Supporting real-time traffic with qos in ieee 802.11e based home networks," in *IEEE Consumer Communications and Networking Conference*, January 2004, pp. 205–209.

[34] A. Mehta, G. Bhatti, Z. Sahinoglu, R. Viswanathan, and J. Zhang, "Performance analysis of beacon-enabled ieee 802.15.4 mac for emergency response applications," in *International Symposium on Advanced Networks and Telecommunication Systems*, December 2009, pp. 1–3.

[35] ——, "A modified beacon-enabled ieee 802.15.4 mac emergency response applications," in *IEEE Symposium on Computers and Communications*, June 2010, pp. 261–267.

[36] I. F. Akyildiz, X. Wang, and W. Wang, "Wireless mesh networks: A survey," *Computer Networks*, vol. 47, no. 4, pp. 445–487, January 2005.

[37] http://www.ieee802.org/15/pub/TG4g.html.

[38] F. Kojima and H. Harada, "Study on multipath characteristics for ieee 802.15.4g sun applications in the frequency band used in japan," in *IEEE International Conference on Communications Workshops*, May 2010, pp. 1–5.

[39] ——, "Long-lived smart utility network management using modified ieee 802.15.4 mac," in *IEEE International Conference on Communications Workshops*, May 2010, pp. 1–5.

[40] http://www.homeplug.org.

[41] DOE, "Communications requirements of smart grid technologies," Department of Energy, Tech. Rep., October 2010.

[42] O. Fatemieh, R. Chandra, and C. A. Gunter, "Low cost and secure smart meter communications using the tv white spaces," in *International Symposium on Resilient Control Systems*, August 2010, pp. 37–42.

[43] A. Neskovic, N. Neskovic, and G. Paunovic, "Modern approaches in modeling of mobile radio systems propagation environment," *IEEE Communications Surveys Tutorials*, vol. 3, no. 3, pp. 2–12, 2000.

[44] A. Microwaves and D. Propagation, "Review on radio propagation into and within buildings," *IEE Proceedings Microwaves, Antennas and Propagation*, vol. 138, no. 1, pp. 61–73, February 1991.

[45] S. Alexander, "Characterising buildings for propagation at 900 mhz," *Electronics Letters*, vol. 19, no. 20, p. 860, September 1983.

[46] A. Committee, "231: Digital mobile radio towards future generation systems final report," Tech. Rep., 1999.

[47] T. S. Rappaport, *Wireless Communications: Principles and Practice*. Upper Saddle River, NJ: Prentice-Hall, 1996.

[48] J. Andersen, T. Rappaport, and S. Yoshida, "Propagation measurements and models for wireless communications channels," *IEEE Communications Magazine*, vol. 33, no. 1, pp. 42–49, January 1995.

[49] ITU–R Rec. ITU–R M. 1225, "Guidelines for evaluation of radio transmission technology for imt–2000," Tech. Rep., 1997.

[50] A. Goldsmith, *Wireless Communications*. Cambridge University Press, 2005.

[51] W. C. Jakes, *Microwave Mobile Communications*. New York:IEEE Press, 1993.

[52] V. C. Gungor, B. Lu, and G. P. Hancke, "Opportunities and challenges of wireless sensor networks in smart grid," *IEEE Transactions on Industrial Electronics*, vol. 57, no. 10, pp. 3557–3564, October 2010.

[53] M. Ibnkahla, *Signal Processing for Mobile Communications Handbook*. CRC Press, 2005.

[54] A. H. Kemp and E. B. Bryant, "Channel sounding of industrial sites in the 2.4 ghz ism band," *Wireless Personal Communications*, vol. 31, pp. 235–248, 2004.

[55] R. Clarke and W. L. Khoo, "3-d mobile radio channel statistics," *IEEE Transactions on Vehicular Technology*, vol. 46, no. 3, pp. 798–799, August 1997.

[56] X. Zhao, J. Kivinen, P. Vainikainen, and K. Skog, "Characterization of doppler spectra for mobile communications at 5.3 ghz," *IEEE Transactions on Vehicular Technology*, vol. 52, no. 1, pp. 14–23, January 2003.

[57] D. Baum, D. Gore, R. Nabar, S. Panchanathan, K. Hari, V. Erceg, and A. Paulraj, "Measurement and characterization of broadband mimo fixed wireless channels at 2.5 ghz," in *International Conference on Personal Wireless Communications*, 2000, pp. 203–206.

[58] S. Thoen, L. Van der Perre, and M. Engels, "Modeling the channel time-variance for fixed wireless communications," *IEEE Communications Letters*, vol. 6, no. 8, pp. 331–333, August 2002.

[59] G. L. Stuber, *Principles of Mobile Communication*, 2nd ed. Boston,MA:Kluwer, 1996.

[60] M. Daoud Yacoub, "Fading distributions and co-channel interference in wireless systems," *IEEE Antennas and Propagation Magazine*, vol. 42, no. 1, pp. 150–160, February 2000.

[61] H. Hashemi, "The indoor radio propagation channel," in *Proceedings of the IEEE*, vol. 81, no. 7, July 1993, pp. 943–968.

[62] K. Blackard, T. Rappaport, and C. Bostian, "Measurements and models of radio frequency impulsive noise for indoor wireless communications," *IEEE Journal on Selected Areas in Communications*, vol. 11, no. 7, pp. 991–1001, September 1993.

[63] O. Batur, M. Koca, and G. Dundar, "Measurements of impulsive noise in broadband wireless communication channels," in *PRIME Research in Microelectronics and Electronics*, April 2008, pp. 233–236.

[64] Q. Shan, S. Bhatti, I. Glover, R. Atkinson, R. Portugues, P. Moore, and R. Rutherford, "Characteristics of impulsive noise in electricity substations," in *European Signal Processing Conference*, August 2009.

[65] A. Shapoury and M. Kezunovic, "Noise profile of wireless channels in high voltage substations," in *IEEE Power Engineering Society General Meeting*, June 2007, pp. 1–8.

[66] S. Zhidkov, "Analysis and comparison of several simple impulsive noise mitigation schemes for ofdm receivers," *IEEE Transactions on Communications*, vol. 56, no. 1, pp. 5–9, January 2008.

[67] D. Fertonani and G. Colavolpe, "On reliable communications over channels impaired by bursty impulse noise," *IEEE Transactions on Communications*, vol. 57, no. 7, pp. 2024–2030, July 2009.

[68] M. Zimmermann and K. Dostert, "Analysis and modeling of impulsive noise in broadband powerline communications," *IEEE Transactions on Electromagnetic Compatibility*, vol. 44, no. 1, pp. 249–258, February 2002.

[69] ——, "A multipath model for the powerline channel," *IEEE Transactions on Communications*, vol. 50, no. 4, pp. 553–559, April 2002.

[70] J. Anatory, N. Theethayi, and R. Thottappillil, "Channel characterization for indoor power-line networks," *IEEE Transactions on Power Delivery*, vol. 24, no. 4, pp. 1883–1888, October 2009.

[71] J. Anatory, N. Theethayi, R. Thottappillil, and N. Mvungi, "A broadband power–line communication system design scheme for typical tanzanian low–voltage network," *IEEE Transactions on Power Delivery*, vol. 24, no. 3, pp. 1218–1224, July 2009.

[72] I. Papaleonidopoulos, C. Capsalis, C. Karagiannopoulos, and N. Theodorou, "Statistical analysis and simulation of indoor single-phase low voltage power-line communication channels on the basis of multipath propagation," *IEEE Transactions on Consumer Electronics*, vol. 49, no. 1, pp. 89–99, February 2003.

[73] Y.-H. Kim, H.-H. Song, J.-H. Lee, and S.-C. Kim, "Wideband channel measurements and modeling for in–house power line communication," in *International Symposium on Power Line Communications and Its Applications*, March 2002.

[74] K. Afkhamie, H. Latchman, L. Yonge, T. Davidson, and R. Newman, "Joint optimization of transmit pulse shaping, guard interval length, and receiver side narrow-band interference mitigation in the homeplugav ofdm system," in *IEEE Workshop on Signal Processing Advances in Wireless Communications*, June 2005, pp. 996–1000.

[75] S. Galli, "A simplified model for the indoor power line channel," in *IEEE International Symposium on Power Line Communications and Its Applications*, April 2009, pp. 13–19.

[76] T. Esmailian, F. R. Kschischang, and P. G. Gulak, "In-building power lines as high-speed communication channels: Channel characterization and a test channel ensemble," *International Journal of Communication Systems*, 2009.

[77] H. Philipps, "Development of a statistical model for powerline com- munication channels," in *International Symposium on Power Line Communications and Its Applications*, 2000, pp. 153–162.

[78] M. Tlich, A. Zeddam, F. Moulin, and F. Gauthier, "Indoor power-line communications channel characterization up to 100 mhzpart ii: Time-frequency analysis," *IEEE Transactions on Power Delivery*, vol. 23, no. 3, pp. 1402–1409, July 2008.

[79] F. Canete, L. Diez, J. Cortes, and J. Entrambasaguas, "Broadband modelling of indoor power-line channels," *IEEE Transactions on Consumer Electronics*, vol. 48, no. 1, pp. 175–183, February 2002.

[80] F. Corripio, J. Arrabal, L. del Rio, and J. Munoz, "Analysis of the cyclic short-term variation of indoor power line channels," *IEEE Journal on Selected Areas in Communications*, vol. 24, no. 7, pp. 1327–1338, July 2006.

[81] S. Barmada, A. Musolino, and M. Tucci, "Response bounds of indoor power-line communication systems with cyclostationary loads," *IEEE Transactions on Power Delivery*, vol. 24, no. 2, pp. 596–603, April 2009.

[82] S. Galli and T. Banwell, "A novel approach to the modeling of the indoor power line channel-part ii: transfer function and its properties," *IEEE Transactions on Power Delivery*, vol. 20, no. 3, pp. 1869–1878, July 2005.

[83] S. Aghajeri, H. Shafiee, and J. Mohammadpour-Velni, "Design of an ofdm system for high rate communication over low voltage power lines," in *Mediterranean Conference on Control and Automation*, July 2002.

[84] I. Papaleonidopoulos, C. loannou, C. Karagiannopoulos, and N. Theodorou, "Branched–bus hf power–delay–profile approach of indoor plc channels," in *International Symposium on Power Line Communications and Its Applications*, April 2005, pp. 147–151.

[85] K. Hoque, L. Debiasi, and F. De Natale, "Performance analysis of mc-cdma power line communication system," in *International Conference on Wireless and Optical Communications Networks*, July 2007, pp. 1–5.

[86] J.-h. Lee, J.-h. Park, H.-S. Lee, G.-W. Lee, and S.-C. Kim, "Measurement, modeling and simulation of power line channel for indoor high-speed data communications," in *International Symposium on Power-Line Communications and Its Applications*, April 2001, pp. 143–148.

[87] O. Hooijen, "On the channel capacity of the residential power circuit used as a digital communications medium," *IEEE Communications Letters*, vol. 2, no. 10, pp. 267–268, October 1998.

[88] M. Arzberger, T. Waldeck, and M. Zimmermann, "Fundamental properties of the low voltage power distribution grid," in *Int. Symp. Power–Line Communications and its Applications (ISPLC)*, March 1997, pp. 45–50.

[89] A. Burr, D. Reed, and P. Brown, "Effect of hf broadcast interference on powerline telecommunications above 1 mhz," in *IEEE Global Telecommunications Conference*, vol. 5, 1998, pp. 2870–2875.

[90] H. Meng, Y. Guan, and S. Chen, "Modeling and analysis of noise effects on broadband power–line communications," *IEEE Transactions on Power Delivery*, vol. 20, no. 2, pp. 630–637, April 2005.

[91] V. Degardin, M. Lienard, A. Zeddam, F. Gauthier, and P. Degauquel, "Classification and characterization of impulsive noise on indoor powerline used for data communications," *IEEE Transactions on Consumer Electronics*, vol. 48, no. 4, pp. 913–918, November 2002.

[92] M. Chan and R. Donaldson, "Amplitude, width, and interarrival distributions for noise impulses on intrabuilding power line communication networks," *IEEE Transactions on Electromagnetic Compatibility*, vol. 31, no. 3, pp. 320–323, August 1989.

[93] J. Abad, A. Badenes, J. Blasco, J. Carreras, V. Dominguez, C. Gomez, S. Iranzo, J. Riveiro, D. Ruiz, L. Torres, and J. Comabella, "Extending the power line lan up to the neighborhood transformer," *IEEE Communications Magazine*, vol. 41, no. 4, pp. 64–70, April 2003.

[94] G. Jee, C. Edison, R. Das Rao, and Y. Cern, "Demonstration of the technical viability of plc systems on medium- and low-voltage lines in the united states," *IEEE Communications Magazine*, vol. 41, no. 5, pp. 108–112, Ma. 2003.

[95] D.-E. Lee, D.-S. In, J.-J. Lee, Y.-J. Park, K.-H. Kim, J.-T. Kim, and S.-G. Shon, "A field trial of medium voltage power line communication system for amr and das," in *Asia and Pacific Transmission Distribution Conference Exposition*, October 2009, pp. 1–4.

[96] M. Schwartz, "The origins of carrier multiplexing: Major george owen squier and at&t," *IEEE Communications Magazine*, vol. 46, no. 5, pp. 20–24, May 2008.

[97] Y. Xiaoxian, Z. Tao, Z. Baohui, N. Xu, W. Guojun, and D. Jiandong, "Investigation of transmission properties on 10-kv medium voltage power lines mdash;part i: General properties," *IEEE Transactions on Power Delivery*, vol. 22, no. 3, pp. 1446–1454, July 2007.

[98] Z. Tao, Y. Xiaoxian, Z. Baohui, C. Jian, Y. Zhi, and T. Zhihong, "Research of noise characteristics for 10-kv medium-voltage power lines," *IEEE Transactions on Power Delivery*, vol. 22, no. 1, pp. 142–150, January 2007.

[99] S. Yarkan and H. Arslan, "Exploiting location awareness toward improved wireless system design in cognitive radio," *IEEE Communications Magazine*, vol. 46, no. 1, pp. 128–136, January 2008.

[100] D. Wu and D. Chang, "The effect of an electrically large stirrer in a mode–stirred chamber," *IEEE Transactions on Electromagnetic Compatibility*, vol. 31, no. 2, pp. 164–169, May 1989.

[101] P. Hallbjorner and A. Rydberg, "Maximum doppler frequency in reverberation chamber with continuously moving stirrer," in *Antennas and Propagation Conference*, April 2007, pp. 229–232.

[102] A. Khaleghi, J. Bolomey, and A. Azoulay, "On the statistics of reverberation chambers and applications for wireless antenna test," in *IEEE Antennas and Propagation Society International Symposium*, July 2006, pp. 3561–3564.

[103] K. Madsen, P. Hallbjorner, and C. Orlenius, "Models for the number of independent samples in reverberation chamber measurements with mechanical, frequency, and combined stirring," *IEEE Antennas and Wireless Propagation Letters*, vol. 3, pp. 48–51, 2004.

[104] J. Valenzuela-Valdes, A. Martinez-Gonzalez, and D. Sanchez-Hernandez, "Diversity gain and mimo capacity for nonisotropic environments using a reverberation chamber," *EEE Antennas and Wireless Propagation Letters*, vol. 8, pp. 112–115, 2009.

[105] P. Hoeher, "A statistical discrete-time model for the wssus multipath channel," *IEEE Transactions on Vehicular Technology*, vol. 41, no. 4, pp. 461–468, November 1992.

[106] C. L. Holloway, D. A. Hill, J. M. Ladbury, P. F. Wilson, G. Koepke, and J. Coder, "On the use of reverberation chambers to simulate a rician radio environment for the testing of wireless devices," *IEEE Transactions on Antennas and Propagation*, vol. 54, no. 11, pp. 3167–3177, November 2006.

[107] E. Genender, C. Holloway, K. Remley, J. Ladbury, G. Koepke, and H. Garbe, "Use of reverberation chamber to simulate the power delay profile of a wireless environment," in *International Symposium on Electromagnetic Compatibility*, September 2008, pp. 1–6.

[108] N. Pavlidou, A. Han Vinck, J. Yazdani, and B. Honary, "Power line communications: state of the art and future trends," *IEEE Communications Magazine*, vol. 41, no. 4, pp. 34–40, April 2003.

[109] S. Galli, A. Scaglione, and K. Dostert, "Broadband is power: internet access through the power line network," *IEEE Communications Magazine*, vol. 41, no. 5, pp. 82–83, May 2003.

[110] Y.-J. Lin, H. Latchman, M. Lee, and S. Katar, "A power line communication network infrastructure for the smart home," *IEEE Wireless Communications Magazine*, vol. 9, no. 6, pp. 104–111, Dec. 2002.

[111] H. Schulze and C. Luders, *Theory and Applications of OFDM and CDMA: Wideband Wireless Communications*. Wiley, 2005.

[112] D. M. Pozar, *Microwave Engineering*. Toronto : John Wiley & Sons,, 1998.

[113] H. He, S. Cheng, Y. Zhang, and J. Nguimbis, "Analysis of reflection of signal transmitted in low-voltage powerline with complex wavelet," *IEEE Transactions on Power Delivery*, vol. 19, no. 1, pp. 86–91, January 2004.

[114] A. Papoulis, *Probability, random variables, and stochastic processes*, 3rd ed. New York:McGraw-Hill Inc., 1991.

[115] D. Anastasiadou and T. Antonakopoulos, "Multipath characterization of indoor power-line networks," *IEEE Transactions on Power Delivery*, vol. 20, no. 1, pp. 90–99, January 2005.

[116] X. Ding and J. Meng, "Channel estimation and simulation of an indoor power–line network via a recursive time–domain solution," *IEEE Transactions on Power Delivery*, vol. 24, no. 1, pp. 144–152, January 2009.

[117] S. Barmada, A. Musolino, and M. Raugi, "Innovative model for time-varying power line communication channel response evaluation," *IEEE Journal on Selected Areas in Communications*, vol. 24, no. 7, pp. 1317–1326, July 2006.

[118] H. Meng, S. Chen, Y. Guan, C. Law, P. So, E. Gunawan, and T. Lie, "Modeling of transfer characteristics for the broadband power line communication channel," *IEEE Transactions on Power Delivery*, vol. 19, no. 3, pp. 1057–1064, July 2004.

[119] L. Tang, P. So, E. Gunawan, Y. Guan, S. Chen, and T. Lie, "Characterization and modeling of in-building power lines for high-speed data transmission," *IEEE Transactions on Power Delivery*, vol. 18, no. 1, pp. 69–77, Jan 2003.

[120] M. Tlich, A. Zeddam, F. Moulin, and F. Gauthier, "Indoor power-line communications channel characterization up to 100 mhzpart i: One-parameter deterministic model," *IEEE Transactions on Power Delivery*, vol. 23, no. 3, pp. 1392–1401, July 2008.

[121] X. Ding and J. Meng, "Channel estimation and simulation of an indoor power-line network via a recursive time-domain solution," *IEEE Transactions on Power Delivery*, vol. 24, no. 1, pp. 144–152, Jan. 2009.

[122] ——, "Characterization and modeling of indoor power–line communication channels," in *Second Canadian Solar Buildings Conference*, June 2007.

[123] J. Anatory, N. Theethayi, R. Thottappillil, M. Kissaka, and N. Mvungi, "The effects of load impedance, line length, and branches in the bplctransmission-line analysis for indoor voltage channel," *IEEE Transactions on Power Delivery*, vol. 22, no. 4, pp. 2150–2155, October 2007.

[124] ——, "The effects of load impedance, line length, and branches in typical low-voltage channels of the bplc systems of developing countries: Transmission-line analyses," *IEEE Transactions on Power Delivery*, vol. 24, no. 2, pp. 621–629, April 2009.

[125] S. Galli and T. Banwell, "A novel approach to the modeling of the indoor power line channel-part ii: transfer function and its properties," *IEEE Transactions on Power Delivery*, vol. 20, no. 3, pp. 1869–1878, July 2005.

[126] D. Sabolic, A. Bazant, and R. Malaric, "Signal propagation modeling in power-line communication networks," *IEEE Transactions on Power Delivery*, vol. 20, no. 4, pp. 2429–2436, October 2005.

[127] N. Mehta, A. Molisch, J. Wu, and J. Zhang, "Approximating the sum of correlated lognormal or, lognormal-rice random variables," in *IEEE International Conference on Communications*, vol. 4, June 2006, pp. 1605–1610.

[128] A. Safak and M. Safak, "Moments of the sum of correlated log–normal random variables," in *IEEE 44th Vehicular Technology Conference*, vol. 1, June 1994, pp. 140–144.

[129] M. Sanchez, L. de Haro, M. Ramon, A. Mansilla, C. Ortega, and D. Oliver, "Impulsive noise measurements and characterization in a uhf digital tv channel," *IEEE Transactions on Electromagnetic Compatibility*, vol. 41, no. 2, pp. 124–136, may 1999.

[130] M. Ghosh, "Analysis of the effect of impulse noise on multicarrier and single carrier qam systems," *IEEE Transactions on Communications*, vol. 44, no. 2, pp. 145–147, February 1996.

[131] D. Middleton, "Statistical-physical models of electromagnetic interference," *IEEE Transactions on Electromagnetic Compatibility*, vol. 19, no. 3, pp. 106 –127, August 1977.

[132] J. Armstrong and H. Suraweera, "Decision directed impulse noise mitigation for ofdm in frequency selective fading channels [dvb-t example]," in *IEEE Global Telecommunications Conference*, vol. 6, november 2004, pp. 3536–3540.

[133] J. Lago-Fernandez and J. Salter, "Modeling impulsive interference in dvb–t – statistical analysis, test waveforms, and receiver performance," BBC Research and Development, Tech. Rep., July 2004.

[134] H. Suraweera and J. Armstrong, "Noise bucket effect for impulse noise in ofdm," *Electronics Letters*, vol. 40, no. 18, September 2004.

[135] S. Zhidkov, "Impulsive noise suppression in ofdm–based communication systems," *IEEE Transactions on Consumer Electronics*, vol. 49, no. 4, pp. 944–948, November 2003.

[136] F. Abdelkefi, P. Duhamel, and F. Alberge, "Impulsive noise cancellation in multicarrier transmission," *IEEE Transactions on Communications*, vol. 53, no. 1, pp. 94–106, January 2005.

[137] J. Haring and A. Vinck, "Iterative decoding of codes over complex numbers for impulsive noise channels," *IEEE Transactions on Information Theory*, vol. 49, no. 5, pp. 1251–1260, May 2003.

[138] H. Matsuo, D. Umehara, M. Kawai, and Y. Morihiro, "An iterative detection for ofdm over impulsive noise channel," in *International Symposium on Power Line Communications and Its Applications*, 2002, pp. 213–217.

[139] T. Hirakawa, M. Fujii, M. Itami, and K. Itoh, "A study on iterative impulse noise reduction in ofdm signal by recovering time domain samples," in *IEEE International Symposium on Power Line Communications and Its Applications*, 2006, pp. 325–330.

[140] J. Radic and N. Rozic, "Reconstruction of the samples corrupted with impulse noise in multicarrier systems," in *IEEE Wireless Communications and Networking Conference*, 5–8 2009, pp. 1–5.

[141] S. Zhidkov, "Performance analysis and optimization of ofdm receiver with blanking nonlinearity in impulsive noise environment," *IEEE Transactions on Vehicular Technology*, vol. 55, no. 1, pp. 234–242, January 2006.

[142] K. Seo, H. Latchman, and K. Afkhamie, "Improved impulse detection in power line communication systems," in *IEEE International Symposium on Power Line Communications and Its Applications*, April 2008, pp. 374 –379.

[143] G. Ndo, P. Siohan, and M.-H. Hamon, "Adaptive noise mitigation in impulsive environment: Application to power-line communications," *IEEE Transactions on Power Delivery*, vol. 25, no. 2, pp. 647–656, April 2010.

[144] R. G. Gallager, *Information Theory and Reliable Communication*. New York:Wiley, 1968.

[145] B. Muquet, Z. Wang, G. Giannakis, M. de Courville, and P. Duhamel, "Cyclic prefixing or zero padding for wireless multicarrier transmissions?" *IEEE Transactions on Communications*, vol. 50, no. 12, pp. 2136–2148, December 2002.

[146] J. Shen and Z. Ding, "Zero-forcing blind equalization based on subspace estimation for multiuser systems," *IEEE Transactions on Communications*, vol. 49, no. 2, pp. 262–271, February 2001.

[147] A. Molisch, M. Toeltsch, and S. Vermani, "Iterative methods for cancellation of intercarrier interference in ofdm systems," *IEEE Transactions on Vehicular Technology*, vol. 56, no. 4, pp. 2158–2167, July 2007.

[148] P. Wolniansky, G. Foschini, G. Golden, and R. Valenzuela, "V-blast: an architecture for realizing very high data rates over the rich-scattering wireless channel," in *International Symposium on Signals, Systems, and Electronic*, September 1998, pp. 295–300.

[149] Y.-S. Choi, P. Voltz, and F. Cassara, "On channel estimation and detection for multicarrier signals in fast and selective rayleigh fading channels," *IEEE Transactions on Communications*, vol. 49, no. 8, pp. 1375 –1387, August 2001.

[150] X. Cai and G. Giannakis, "Bounding performance and suppressing intercarrier interference in wireless mobile ofdm," *IEEE Transactions on Communications*, vol. 51, no. 12, pp. 2047–2056, December 2003.

ABOUT THE AUTHOR

Sabih Güzelgoz received his B.S. degree in Electrical and Electronics Engineering from Osmangazi University, Eskisehir, Turkey, in June 2002, and his M.S. degree in Electronics from the University of York, York, UK, in September 2004. He is a member of the Wireless Communications and Signal Processing Group at the University of South Florida and he is working toward his Ph.D. degree. His research interests include wireless communication channel characterization, power line communication channel characterization, smart grid communications, electrical vehicles and their integration to smart grid, cognitive radio, and OFDM.